Copernicus Marine Service

QUALITY INFORMATION DOCUMENT

Sea Level TAC - DUACS products:

SEALEVEL_GLO_PHY_L3_NRT _008_044

SEALEVEL_GLO_PHY_L4_NRT _008_046

SEALEVEL_EUR_PHY_L3_NRT _008_059

SEALEVEL_EUR_PHY_L4_NRT _008_060

SEALEVEL_GLO_PHY_L3_MY_008_062

SEALEVEL_GLO_PHY_L4_MY_008_047

SEALEVEL_EUR_PHY_L3_MY_008_061

SEALEVEL_EUR_PHY_L4_MY_008_068

SEALEVEL_GLO_PHY_NOISE_L4_STATIC_008_033

Issue: 12.0

Contributors: Maxime Ballarotta , Marie-Isabelle Pujol and SL-TAC team.

Approval date by the CMEMS product quality coordination team: 13/11/2024

CHANGE RECORD

When the quality of the products changes, the QuID is updated and a row is added to this table. The third column specifies which sections or sub-sections have been updated. The fourth column should mention the version of the product to which the change applies.

Issue	Date	§	Description of Change	Author	Validated By
1.0	2019/01/21	All	upgrade for CMEMS VApr2019	G. Taburet	M-I. Pujol
1.1	2019/02/26		Correction after review MO	M-I. Pujol, G. Taburet	M-I. Pujol
1.2	2019/04/15	I,II, V	Upgrade for CMEMS Jul2019	M-I Pujol, G. Taburet	M-I. Pujol
2.0	2019/09/10	I,II, V	Upgrade for CMEMS Nov2019	M-I. Pujol S. Mulet	M-I. Pujol
2.1	2019/10/02	I,II, V	Upgrade of constellation status	G. Taburet	M-I. Pujol
3.0	2020/01/14	I,II, V	Upgrade for SARAL-DP/AL GDR-F change in NRT	M-I. Pujol	M-I. Pujol
4.0	2020/04/03	I,II, V, VI**0**	Correction of temporal period processed by DUACS from the different altimeter (table1) Upgrade for CMEMS Jul2020 release	G. Taburet	M-I. Pujol
4.1	2020/05/11	I,II, V	Correction of some anomalies	M-I. Pujol	M-I. Pujol
4.2	2020/10/13	III, V	Upgrade for CMEMS Dec2020 DT release Upgrade for Jason-3 GDR-F standards changes Upgrade for Cryosat-2 orbit change	G. Taburet	M-I. Pujol
4.3	2021/01/15	III, V	Upgrade for CMEMS May2021 DT & NRT release	G. Taburet	M-I. Pujol
5.0	2021/10/07	All	Upgrade for CMEMS Dec2021 DT & NRT release - Full reprocessing DT-2021 - Upgrade of NRT processing	G. Taburet	M-I. Pujol
5.1	2021/12/16	I,II, V, VI**0**	Change for MY automatic extensions Correction of some references	M-I. Pujol	M-I. Pujol
6.0	2022/03/28	II	- Upgrade of constellation status in NRT conditions: add Sentinel-6A - Correction of some errors	M-I. Pujol	M-I. Pujol
7.0	2022/05/12	I,II, V, VI**0**	- Upgrade of constellation status in NRT conditions: add Jason-3 on interleaved orbit - MAJ some references	M-I. Pujol	M-I. Pujol
			-		
			-		

Issue	Date	§	Description of Change	Author	Validated By
8.0	2022/11/02	All	Upgrade for CMEMS Nov2022 DT & NRT release - Add L3 5 Hz datasets - Change “noise” product - Add temporal extension of MY series - Update of some figures	M-I Pujol	M-I Pujol
8.1	2022/12/08	II.4.5; V.2	- Update Table 9	M-I Pujol	M-I Pujol
8.2	2023/01/16	V	- Updated information for Sentinel-3A L3 MY product quality	M-I Pujol	M-I Pujol
9.0	2023/10/15	All	Use new template Upgrade for CMEMS Nov2023 DT & NRT release - Add L3 5 Hz datasets for global ocean - Add SWOT-nadir mission	M-I Pujol	M-I Pujol
10.0	2024/05/13		MY interim temporal extension	G Taburet	M-I Pujol
11.0	2024/07/01	I.3; II.4; V.3.7; VI.2; VII	Change of the altimeter standards in NRT Add H2B for L3 5Hz production	M-I Pujol	M-I Pujol
12.0	2024/09/23	All	Upgrade for CMEMS Nov2024 DT & NRT release: - full reprocessing of the MY series with DT-2024 version - change of the mapping methodology in NRT - change of the L4 product spatial sampling	M Ballarotta M-I Pujol	K Grassi

TABLE OF CONTENTS

I EXECUTIVE SUMMARY

I.1 Products covered by this document

This document describes the quality of the operational Near Real Time (NRT) and REProcessed/Delayed-Time or Multi-Year (REP/DT or MY) Data Unification and Altimeter Combination System (DUACS) products listed hereafter.

I.1.1 Operational products

I.1.1.1 Along-track products

Product	SEALEVEL_EUR_PHY_L3_NRT_OBSERVATIONS_008_059
Area	Europe
Satellites	Sentinel-6A-HR; Jason-3 interleaved; Sentinel-3A, Sentinel-3B, SARAL-DP/AltiKa; Cryosat-2, HaiYang-2B, SWOT-nadir
Spatial resolution	Along-track 7 km (full 1 Hz resolution) & 1.3 km (5 Hz sampling)
Temporal resolution	10 days to 29 days (variable with satellite); products are stored in 1-day files.

Product	SEALEVEL_GLO_PHY_L3_NRT_OBSERVATIONS_008_044
Area	Global ocean
Satellites	Sentinel-6A-HR; Jason-3 interleaved; Sentinel-3A, Sentinel-3B, SARAL-DP/AltiKa; Cryosat-2, HaiYang-2B, SWOT-nadir
Spatial resolution	Along-track 7 km (full 1 Hz resolution) & 1.3 km (5 Hz sampling)
Temporal resolution	10 days to more than 29 days (variable with satellite); products are stored in 1-day files.

** Dataset included to the catalogue. This dataset will only be supplied in the event of a major anomaly in the existing constellation.*

I.1.1.2 Gridded products

Product	SEALEVEL_EUR_PHY_L4_NRT_OBSERVATIONS_008_060
Area	Europe
Satellites	Merging of the different altimeter measurements available
Spatial resolution	1/16°x1/16° Cartesian grid
Temporal resolution	1 day

Product	SEALEVEL_GLO_PHY_L4_NRT_OBSERVATIONS_008_046
Area	Global ocean
Satellites	Merging of the different altimeter measurements available
Spatial resolution	1/8°x1/8° Cartesian grid
Temporal resolution	1 day

Reanalysis products

The reanalysis products featured in this document cover the period from 1993 to present. The dataset is regularly updated with a nearly 6-month delay. The different production events of the reanalysis products are listed in §V.4.

I.1.1.3 Along-track products

Product	SEALEVEL_EUR_PHY_L3_MY_008_061
Area	Europe
Satellites	Topex-Poseidon; Topex-Poseidon (interleaved orbit); Jason-1; Jason-1 (interleaved orbit); Jason-1 (geodetic orbit); OSTM/Jason-2; OSTM/Jason-2 (interleaved); OSTM/Jason-2 (Long Repeat Orbit Phase); Jason-3; Jason-3 interleaved, Sentinel-6A (LRM), Sentinel-3A&B; ERS-1; ERS-1 (geodetic orbit); ERS-2, Envisat; Envisat (extended phase); Geosat Follow On; Cryosat; SARAL/AltiKa, SARAL-DP/ALtiKa; HaiYang-2A, HaiYang-2A (geodetic orbit), HaiYang-2B, SWOT nadir
Spatial resolution	Along-track 7 km for filtered and unfiltered
Temporal resolution	10 days to 35 days (variable with satellite); products are stored in 1-day files.

Product	SEALEVEL_GLO_PHY_L3_MY_008_062
Area	Global ocean
Satellites	Topex-Poseidon; Topex-Poseidon (interleaved orbit); Jason-1; Jason-1 (interleaved orbit); Jason-1 (geodetic orbit); OSTM/Jason-2; OSTM/Jason-2 (interleaved); OSTM/Jason-2 (Long Repeat Orbit Phase); Jason-3; Jason-3 interleaved, Sentinel-6A (LRM), Sentinel-3A&B; ERS-1; ERS-1 (geodetic orbit); ERS-2, Envisat; Envisat (extended phase); Geosat Follow On; Cryosat; SARAL/AltiKa, SARAL-DP/ALtiKa; HaiYang-2A, HaiYang-2A (geodetic orbit), HaiYang-2B, SWOT nadir
Spatial resolution	Along-track 7 km for filtered and unfiltered
Temporal resolution	10 days to 35 days (variable with satellite); products are stored in 1-day files.

I.1.1.4 Gridded products

Product	SEALEVEL_EUR_PHY_L4_MY_008_068
Area	Europe
Satellites	Merging of the different altimeter measurements available
Spatial resolution	1/16°x1/16° Cartesian grid
Temporal resolution	1 day

Product	SEALEVEL_GLO_PHY_L4_MY_008_047
Area	Global ocean
Satellites	Merging of the different altimeter measurements available
Spatial resolution	1/8°x1/8° Cartesian grid
Temporal resolution	1 day

The number of altimeter data processed by the system varies with time, according to satellites availability. Table 1 summarizes the periods during which the datasets for each mission are available. Figure 4 and Figure 5 present it in a schematic form.

Table 1: Temporal period processed by DUACS system for the different products/datasets. These periods are necessarily shorter than the L2P availability presented in Table 12.

Altimeter Mission[1]	NRT		REP	
	Begin date	End date	Begin date	End date
al	2019/11/09 (Global) 2019/04/01 (Europe)	YYYY/MM/DD[2]	2013/03/14	2015/03/31
alg	2019/11/09 (Global) 2019/04/01 (Europe)	YYYY/MM/DD[2]	2015/03/31	nearly 6-month delay compared to NRT[1]
c2			2010/07/16	2020/07/31
c2n	2020/10/09	YYYY/MM/DD[2]	2020/08/01	nearly 6-month delay compared to NRT[1]
j3	2019/11/09 (Global) 2019/04/01 (Europe)	2022/04/05	2016/05/26	2022/02/09
J3n	2022/05/03	YYYY/MM/DD[2]	2022/04/28	nearly 6-month delay compared to NRT[1]
s6a	2022/03/16	YYYY/MM/DD[2]	2022/02/10	nearly 6-month delay compared to NRT[1]
s3a	2019/11/09 (Global) 2019/04/01 (Europe)	YYYY/MM/DD[2]	2016/03/01	nearly 6-month delay compared to NRT[1]
s3b	2019/11/09 (Global) 2019/04/01 (Europe)	YYYY/MM/DD[2]	2018/11/27	nearly 6-month delay compared to NRT[1]
h2b	2020/06/17	YYYY/MM/DD[2]	2019/12/20	nearly 6-month delay compared to NRT[1]
swonc			2023/01/16	2023/07/20
swon	2023/11/10	YYYY/MM/DD[2]	2023/07/21	nearly 6-month delay compared to NRT[1]
e1[3]			1992/10/23	1995/05/15
e1g			1994/04/10	1995/03/21
e2			1995/05/15	2002/05/14
en			2002/05/17	2010/10/18
enn			2010/10/26	2012/04/08
g2			2000/01/07	2008/09/07
h2a			2014/04/12	2016/03/15
h2ag			2016/03/31	2020/06/09
j1			2002/04/24	2008/10/19
j1n			2009/02/10	2012/03/03
j1g			2012/05/07	2013/06/21
j2			2008/10/19	2016/05/26
j2n			2016/10/17	2017/04/03
j2g			2017/07/11	2017/09/14
tp			1992/10/03	2002/04/24
tpn			2002/09/20	2005/10/08
merged	2017/04/13	YYYY/MM/DD[2]	1993/01/01	nearly 6-month delay compared to NRT[1]

[1] Description of each abbreviation in Section I.9 - CMEMS-SL-PUM-008-032-068.pdf

[2] Global Ocean Along Track L 3 Sea Surface Heights Nrt | Copernicus Marine Service - Those dates are regularly updated (three to four times per year for REP; daily for NRT)

[3] ERS-1: Geodetic phases (E-F) are included. No ERS-1 data between December 23,1993 and April 10, 1994 (ERS-1 phase D - 2nd ice phase)

I.1.1.5 Mesoscale (CMEMS) vs Climate (C3S) dedicated products

Two types of sea level altimetric gridded products generated by the DUACS production system are currently available:

- Global and regional (European seas) gridded products disseminated via the CMEMS project.
- Global gridded products distributed via the Copernicus Climate Change (C3S) project.

This section aims at presenting the particularities of these sea level gridded datasets produced for two distinct applications:

- The retrieval of mesoscale signals in the context of ocean modelling, and the analysis of the ocean circulation at global or regional scale. This requires the most accurate sea level estimation at each time step with the best spatial sampling of the ocean. Such dataset is produced within the Copernicus Marine Service (CMEMS).
- The monitoring of the long-term evolution of the sea level for climate applications and the analysis of Ocean/Climate indicators (such as the global and regional Mean Sea Level evolution). This requires a homogeneous and stable sea level record. Such dataset is produced within the Copernicus Climate Service (C3S).

The level 2 altimeter standards used to compute the sea level anomalies in the CMEMS and C3S products are currently identical. The main differences between the Copernicus Marine Service and C3S altimeter sea level products are the following:

- **the number of altimeters used in the satellite constellation**: all available altimeters are included in the CMEMS products whereas a steady number (two) of altimeters are included in the C3S products. Previous studies Dibarboure et al., (2011); Pascual et al., (2006) underscored the necessity of a minimum of a two-satellite constellation for the retrieval of mesoscale signals. Within the production process, the long-term stability and large-scale changes are built upon the records from the reference missions (TOPEX-Poseidon, Jason-1, Jason-2, Jason-3 and Sentinel-6A) used in both CMEMS and C3S products. The additional missions (e.g., between four and five additional missions from 2016; Figure 5) are homogenized with respect to the reference missions. These missions contribute to improve the sampling of mesoscale processes, provide a high-latitude coverage and increase the product accuracy. However, the total number of satellites strongly varies during the altimetry era and some biases may appear with the introduction of new satellites flying on a drifting orbit, which may affect the stability of the global and regional Mean Sea Level (MSL). The spatial sampling is reduced with less satellites but also the risk of introducing such anomaly is reduced, whereas the stability is improved in the C3S products, since only two altimeters are used. In the CMEMS products, the stability is ensured by the reference missions. In these products, the mesoscale errors are reduced due to the improved ocean surface sampling thanks to the use of all satellites available in the constellation.

– **The reference used to compute the Sea Level Anomalies**: this reference is either a Mean Sea Surface (MSS) for all missions in the C3S products or a mean profile of sea surface heights used along the theoretical track of the satellites with a repetitive orbit in the CMEMS products. These mean profiles increase the local accuracy of the sea level estimates. However, the combined use of both MSS and mean profiles for successive missions in the CMEMS merged products can be at the origin of some biases affecting the sea level stability. Even if this has a minor impact at global scale, the stability of the regional MSL can be affected, and particularly in the Mediterranean Sea and Black Sea (not showed here). Therefore, the systematic use of the MSS for all missions contributes to ensure the MSL stability in the C3S products. The

accuracy of the CMEMS products is increased with the use of the mean profiles for repetitive missions.

- **The mapping methods:** the Copernicus Marine Service DT-2024 L4 production is now based on the Multiscale Inversion of Ocean Surface Topography algorithm Ubelmann et al., (2021a) while the C3S L4 production is based on an Optimal Interpolation described in Le Traon et al., (1998a). The spatial and temporal correlation scales differ slightly between these two systems, reflecting the increased number of altimeters in the Copernicus Marine Service configuration. This adjustment results in enhancing the resolution of mesoscale signals and significantly improved performance in regions with high ocean variability, particularly for scales ranging from 65 to 500 km.

In conclusion, with the best spatial sampling, the all-satellite CMEMS gridded merged products should be preferred for oceanic mesoscale applications and data-assimilation while the C3S two-satellite gridded merged products should be used for climate applications including mean sea level change, variability and oceanic circulation.

In the future, additional differences may be introduced between these two multi-mission sea level products related to specific processing of some missions. For example, Low-Resolution Mode (LRM) and Synthetic Aperture Radar (SAR) modes of the Jason-CS/Sentinel-6 mission could contribute to differentiate the CMEMS and C3S products.

I.1.2 Time invariant Product

This product gives the spatial pattern of the residual measurement noise (uncorrelated) errors observed on the “sla_unfiltered” variable given in the L3 products. The values of the map are normalized. Values given in the Table 2 can be used to retrieve the absolute noise level pattern for each mission (see PUM[4] for details).

Table 2: Residual measurement noise (uncorrelated) errors product characteristics.

Product	SEALEVEL_GLO_PHY_NOISE_L4_STATIC_008_033
Area	Global
Satellites	-
Spatial resolution	1/4°x1/4° Cartesian grid
Temporal resolution	Static

[4] https://catalogue.marine.copernicus.eu/documents/PUM/CMEMS-SL-PUM-008-032-068.pdf

I.2 Summary of the results

The quality of the MY/DT DUACS products has been assessed by comparison with independent measurements (*in situ* and satellite) and in coordination with other projects (Copernicus C3S[5] and CNES SALP[6]). The NRT products are assessed by routine validation and by comparison with MY/DT products. The results are summarized below. **Sea Leavel Anomaly (SLA) and Absolute Dynamic Topography (ADT):**

The sea level long-term/climatic trend signal can be monitored with MY/DT products. The uncertainty in the global mean sea level trend since 1993 is estimated to be ± 0.30 mm/yr with a confidence interval of 90% (1.65 sigma) Guérou et al., (2022). On a regional scale, the averaged local sea level trend uncertainty during 1993–2019 is 0.86 mm/yr with local values ranging from 0.80 to 1.30 mm/yr Prandi et al., (2021). Nevertheless, due to the specific processing applied, it is recommended to use the C3S products for climatic applications (specialty MSL trends; see section I.1.1.5). **NRT products should not be used for such long-term signal analysis due to frequent constellation and platforms events that can induce jumps, discontinuities and/or drifts in the time series.**

Sea level Errors for mesoscales vary between 1 cm² in low variability areas, over18 cm² in high variability areas. This estimation is based on a 4-satellite constellation in DT conditions. Degraded results can be observed when only two altimeters are available, since they use minimal altimeter sampling. The estimated error during these periods is up to ~40% larger in high variability areas compared to ~5% to the computation with 4-altimeter constellation (. Unlike Delayed-Time (DT) products, which use both past and future observations in the interpolation process, Near Real-Time (NRT) products rely solely on past observations, as future data is not yet available. As a result, the NRT product quality is reduced. Four altimeters are required in NRT conditions to reach the 2-altimeter DT capabilities Dibarboure et al.,(2011); Pascual et al.,(2006). On global average, effective resolution with gridded products is nearly 180 km and 33 days.

Along-track SLA/ADT fields also include residual measurement noise (uncorrelated) errors that are spatially and temporally variable (correlated with wave heights) and differ from one altimeter to another, and from one frequency to another. Characteristic mean noise values over the global ocean vary between 2.0-3.6 cm Root Mean Square (RMS) for raw 1 Hz measurements, and 0.85-1.53 cm for filtered products. The presence of this measurement noise limits the observability of wavelengths shorter than ~65 km (global mean value) with the 1 Hz product. For the higher resolution 5 Hz product, the mean noise values vary between 1.5 and 3.6 cm RMS for raw measurement. The observability of the wavelengths shorter than 40 to 55 km over the North East Atlantic area remains limited with this 5 Hz product.

Geostrophic currents:

Geostrophic currents derived from altimeter gridded products are usually underestimated when compared to the *in situ* observations. Errors on geostrophic currents have been estimated to range between 9 and 16 cm/s depending on the ocean surface variability. As for SLA field, NRT products quality is reduced and more sensitive to the constellation changes compared too MY product.

The geostrophic currents derived from along-track products are sensitive to the residual noises and the noise reduction strategy applied on SLA. At short wavelengths, the kinetic energy can be higher than expected due to possible residual noises, then fall drastically due to the reduction of the signal induced by the low pass filtering applied on SLA. The wavelength limit is around 100 km, with geographical variations but also with variations from one altimeter to the other.

[5] https://cds.climate.copernicus.eu/about-c3s
[6] https://www.aviso.altimetry.fr/en/home.html

I.3 Estimated Accuracy Numbers

The Estimated Accuracy Numbers (EAN) are representative of the signature of different error signals on the products, including both uncorrelated (i.e., noise) and correlated (spatial and temporal scale) error signals.

Measurement noise:

The measurement noise error (i.e., uncorrelated error) was specifically estimated at regional scale. It is presented in §IV.1.1.2.1. A Synthesis is given in .

Table 3: Mean noise measurement of the SLA L3 1 Hz and 5Hz over the Global Ocean. The estimation is done for the different altimeters. Noise for raw (bold) and filtered -low-pass filtering- SLA (in parenthesis) are indicated. Units: centimetres root mean square (cm rms).

Altimeter Mission	1 Hz	5 Hz
Sentinel-3A	**2.0** (0.85)	**3.0** (0.3)
Sentinel-3B	**2.0** (0.85)	**3.0** (0.3)
Sentinel-6A HR	**1.6** (0.68)	**2.2** (0.15)
Sentinel-6A LR	**2.3** (0.98)	-
Jason-3	**2.6** (1.11)	**4.3** (0.55)
Jason-2	**2.6** (1.11)	-
Cryosat-2	**2.6** (1.11)	-
SARAL/AltiKa	**2.0** (0.85)	-
HaiYang-2A	**2.6** (1.11)	-
HaiYang-2B	**2.6** (1.11)	**4.7** (0.67)
Topex/Poseidon	**2.6** (1.11)	-
Jason-1	**2.6** (1.11)	-
Envisat	**2.6** (1.11)	-
ERS-1	**3.6** (1.53)	-
ERS-2	**3.6** (1.53)	-
Geosat Follow On	**3.0** (1.27)	-
SWOT-nadir	**1.6 (0.68)**	**3.5 (0.4)**

The annual mean regional pattern of the noise is given in the “008_033” product. Values given in the previous table can be used to retrieve the absolute noise level pattern for each mission (see PUM[7] for details).

[7] https://catalogue.marine.copernicus.eu/documents/PUM/CMEMS-SL-PUM-008-032-068.pdf

MSL trend & climatic scales:

The errors at climatic scales were estimated within the ESA SL_CCI project (see §IV.1.1.2.2; synthesis given in).

Table 4: Estimated errors at climatic scales observed on sea level DUACS DT products (L3 & L4). (Guérou et al., 2022; Prandi et al., 2021).

Spatial scales	Temporal scales	Altimetry errors
Global MSL	Long-term evolution (25 years)	< 0.30 mm/yr
	Inter-annual signals (< 5 years)	< 2 mm over 1 year
	Annual signals	< 1 mm
Regional MSL	Long term evolution (> 10 years)	< 1.22 mm/yr [8]

Mesoscale:

For merged maps (L4 products), EAN were estimated using the results of comparisons between maps and independent along-track data. They represent a nominal version of the reprocessed product quality. Indeed, they were estimated considering a 4-altimeter constellation (Jason-1, Cryosat-2, HaiYang-2A, Sentinel-3A) available for the merged gridded product computation. Results are summarized in and (see also §IV.1.2.2).

*Table 5: Variance of the differences between gridded (L4) DT2024 all-sat-merged products (one altimeter was kept independent for validation) and independent SARAL-DP/AltiKa (ALG) along-track measurements over the period (2018-01-01, 2018-12-31) for different geographic selected areas (i.e., areas selected by oceanic regime and covering the entire globe, except for the reference area which is a region of the South Atlantic corresponding to a region with very low oceanic variability). Units: cm². In parenthesis: variance reduction (as %) compared with the results obtained with the DT2021 products. Statistics are presented for wavelengths ranging between 65-500 km and after latitude selection (|LAT| < 60°). *The reference area is defined by 330, 360°E; -22, -8°N and corresponds to a very low-variability area in the South Atlantic subtropical gyre where the observed errors are small*

Selection criteria	Independent data: ALG (year 2018)
Reference area* (South Atlantic)	1.0 (-2.37%)
Low variability (<200 cm²) & offshore (distance coast >200 km) areas	2.2 (-3.06%)
High variability (>200 cm²) & offshore (distance coast >200 km) areas	10.21 (-8.18%)
Coastal areas (distance coast < 200 km)	4.92 (-6.82%)

[8] Only the uncertainty related to the instrumental observing system has been considered.

Table 6: Variance of the differences between gridded (L4) DT2024 regional Europe product and SARAL-DP/ALtika independent along-track measurements over the period (2018-01-01, 2018-12-31). Units: cm². In parenthesis: variance reduction (as %) compared with the results obtained with the DT2024 Global product.

	ALG (2018)
Black Sea	18.05 (-0.93%)
Mediterranean Sea	14.76 (-20.56%)
Atlantic	18.16 (-9.70%)

Geostrophic current:

EAN on geostrophic current are deduced from comparisons between altimeter L4 products and drifter measurements (see Pujol et al. 2016 for a full description of the methodology). Synthesis is presented in (see also §IV.3).

Table 7: RMS of the differences between DUACS DT2024 geostrophic current (L4) products and independent drifter measurements. Units: cm/s. In parenthesis: mean square reduction (as %) compared with the results obtained with the DT2021 products. Statistics are presented after latitude selection (5° <|LAT| < 60°).

Selection criteria	**Zonal**	**Meridional**
Global excluding equatorial band (±5°N)	11.4 (-0.87%)	10.5 (-0.75%)
High variability areas (>200 cm²)	16.18 (-1.76%)	15.73 (-2.96%)
Low variability areas (<200 cm²)	10.84 (-0.64%)	9.89 (-0.20%)

Observable wavelengths:

The along-track (L3) products are delivered with a 1 Hz (~7 km) and 5 Hz (~1 km) along-track sampling. Gridded (L4) products are delivered on a 0.125° x 0.125° regular grid for global and 0.0625° x 0.0625° for regional products. Nevertheless, this spatial sampling is not representative of the effective spatial resolution of the products. Along-track product is affected by measurement noise that limit the observation of the small scales as discussed in §IV.1.1.2.1. Gridded products resolution capability is directly linked to the altimeter constellation state and mapping methodology as discussed in §IV.1.2.2. The effective resolution capability of the products is summarized in and , and is fully discussed in Ballarotta et al., (2019).

Table 8: Effective mean spatial and temporal resolution of the DUACS DT-2024 global products (L3 & L4) over global ocean for mid-latitudes. In parenthesis: reduction (as %) compared with the results obtained with the DT2021 products. Negative reduction means that the DT-2024 product resolves smaller spatial scales than the previous DT-2021 product.

	L3 products (1 Hz)	**L4 global products**
Spatial Wavelengths observable (km)	> ~65 (-0%)	> ~180 (-5%)
Temporal Wavelengths observable (days)	-	~33 (-3%)

Table 9: Effective mean spatial and temporal resolution of the DUACS DT-2024 European products (L3 1 Hz & L4) over Mediterranean Sea and Black Sea. In parenthesis: reduction (as %) compared with the results obtained with the DT2021 products. Negative reduction means that the DT-2021 product resolves smaller spatial scales than the previous DT-2021 product.

	L3 products	**L4 regional-Europe products over Mediterranean Sea**	**L4 regional-Europe products over BlackSea**
Spatial Wavelengths observable (km)	> ~40 (-0%)	>~120 (-0%)	> ~125 (-10%)

Table 10: Effective mean spatial resolution of the DUACS NRT L3 5 Hz: Mean value for the North-Eastern Atlantic Area (estimated over the period April-June 2022) and global ocean (estimated over the period October 2022-August 2023).

	Sentinel-6A HR	**Sentinel-3A/B**	**Jason-3**	**Swot-nadir**	**HaiYang-2B**
Spatial Wavelengths observable in the North-Eastern Atlantic Area (km)	40	48	55	55	55
Mean spatial Wavelengths observable in the global ocean (km)	40	48	57	57	63

II PRODUCTION SYSTEM DESCRIPTION

II.1 Production center name

SL-CLS-TOULOUSE-FR

II.2 Operational system name

Data Unification and Altimeter Combination System (DUACS)[9]

II.3 Introduction to the altimeter measurement

The altimeter measures the 'Altimeter Range' which is the distance between the centre of mass of the satellite to the surface of the Earth (see Figure 1). This allows computing the 'Sea Surface Height' (SSH) which is the sea surface height above the reference ellipsoid. The 'Satellite Altitude' refers to the distance of the centre of mass of the satellite above a reference point. The reference point will usually be either on the reference ellipsoid or on the centre of the Earth.

$$SSH = Satellite\ Altitude - Altimeter\ Range - Corrections \qquad Equation\ 1$$

The 'Corrections' due to environmental conditions need to be applied in order to retrieve the correct 'Sea Surface Height' (Eq. 1). They are listed in Table 14 (for NRT), and Table 15 (for DT).

The Mean Sea Surface (MSS_P) is the temporal mean of the SSH over a period P (Eq. 2). It is a mean surface above the reference ellipsoid and it includes the Geoid.

$$MSS_P = \langle SSH \rangle_P \qquad Equation\ 2$$

Note that the MSS used in DUACS products (see Table 14, and Table 15 for DT products) is not distributed by CMEMS but is available via the Aviso+ website[10] (after registration):

The Sea Level Anomaly (SLA_P) is the anomaly of the signal around the mean component. It is deduced from the SSH and MSS_P:

$$SLA_P = SSH - MSS_P \qquad Equation\ 3$$

The Mean Dynamic Topography (MDT_P) is the temporal mean of the SSH above the Geoid over a period P.

$$MDT_P = MSS_P - Geoid \qquad Equation\ 4$$

The Absolute Dynamic Topography (ADT) is the instantaneous height above the Geoid. The geoid is a gravity equipotential surface that would correspond with the ocean surface if ocean was at rest (i.e., with no currents under only the gravity field). Then, when the ocean is also influenced by wind, differential heating and precipitation and other sources of energy, the ocean surface moves from the geoid. Thus, the departure from the geoid provides information on the ocean dynamics.

The ADT is the sum of the SLA_P and MDT_P:

$$ADT = SLA_P + MDT_P = SSH - MSS_P + MDT_P \qquad Equation\ 5$$

The reference period P considered can be changed as described in Pujol et al. (2016).

[9] https://duacs.cls.fr/

[10] http://www.aviso.altimetry.fr/en/data/products/auxiliary-products/mss.html

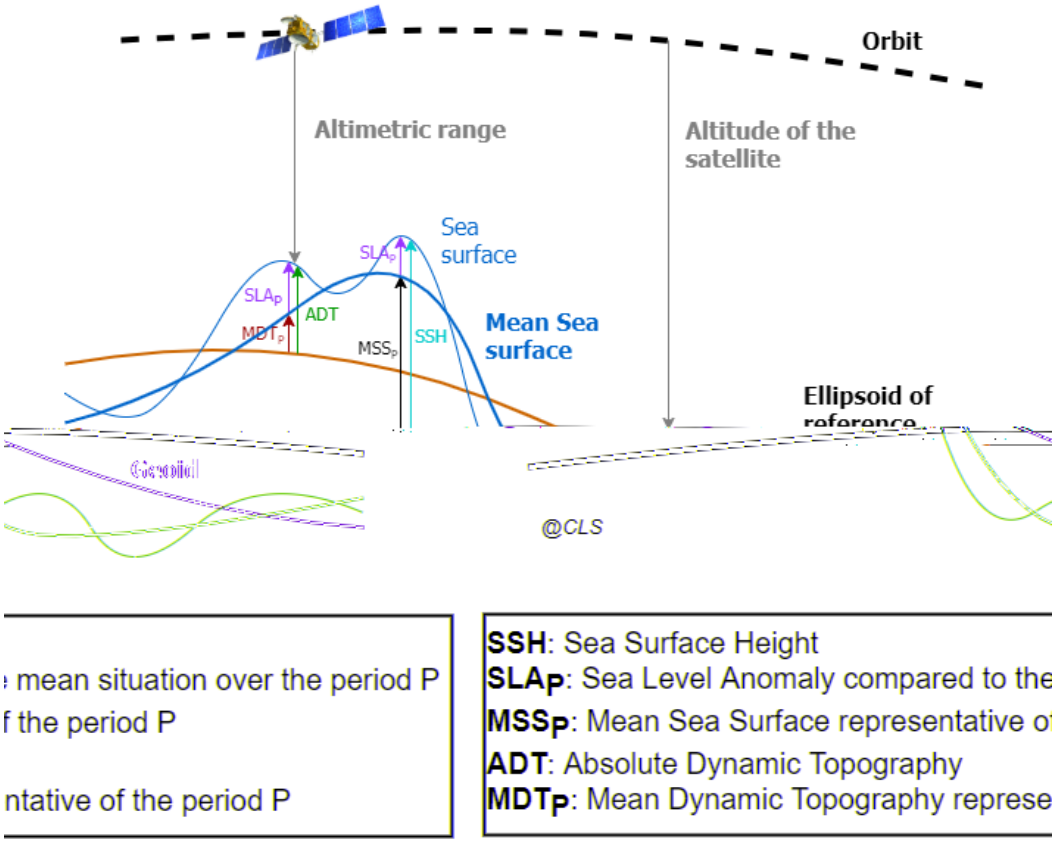

Figure 1: Different measures related to the sea surface height used in altimetry (Credits CLS).

II.4 Production centre description for the version covered by this document

II.4.1 Introduction

The DUACS system comprises of two components: Near Real Time (NRT) and Delayed-Time (DT also named REP or MY).

In NRT, the system's primary objective is to provide operational applications with directly usable high-quality altimeter data from all missions available. Since November 29th 2023, the DUACS system has been upgraded in order to process both L3 1Hz and 5Hz products:

In DT, the primary objective is to maintain a consistent and user-friendly altimeter database using the state-of-the-art recommendations from the altimetry community. The DT products/datasets are extended in time on a quarterly basis. Therefore, these datasets cover 1993 up to five-nine months before present. These datasets benefit from the highest quality altimeter measurements and geophysical corrections, and are produced with a unique system (no changes in time in the set up, extended in time using the same system) to minimize the risk of quality loss or spurious signals appearing over time.

Figure 2 provides an overview of the system, where processing sequences can be divided into seven main steps:

- **A.** Acquisition
- **B.** Input data quality control
- **C.** Multi-mission cross-calibration
- **D.** Along-track SLA computation
- **E.** Along-track product generation
- **F.** Merged products generation
- **G.** Final quality control

The processing is similar for NRT and DT components. Below, we set out a description of the different steps of the processing. The reader can also see Pujol et al., (2016, 2023) for complementary details.

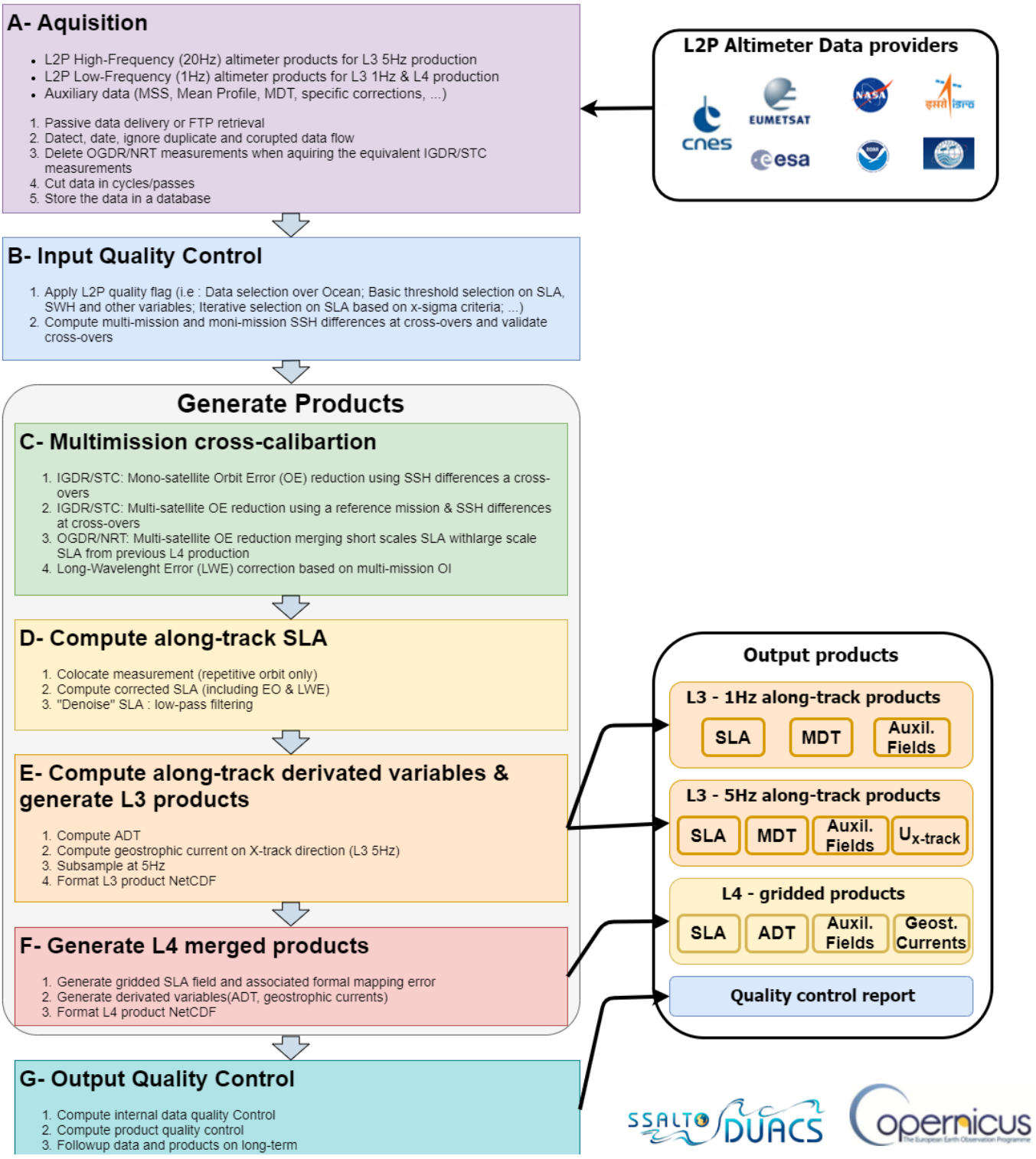

Figure 2: Overview of the DUACS system processing.

II.4.2 Altimeter Input data description

The altimeter measurements used as input of the DUACS system consist of a majority of Level 2p products from different missions that are available in three forms, with different availability times:

- Fast delivery or Near Real Time products (OGDR or NRT). These products do not always benefit from precise orbit determination, nor from some external model-based corrections (Dynamic Atmospheric Correction –(DAC)-, Global Ionospheric Maps –(GIM)-).
- The Intermediate or Slow Time Critical products (IGDR or STC) that are the latest high-quality altimeter data produced in near-real-time.
- Delayed Time or Non-Time Critical product (GDR or NTC).

Details on the sources of the different L2p altimeter products and on their delays in availability are given in . OGDR/NRT and IGDR/STC are both used in the operational system while GDR/STC are involved in the delayed time processing.

Table 11: Sources and delays in availability of the different altimeter data used as inputs of the DUACS system.

Altimeter mission	Type of product	Source	Delay in availability
Sentinel-3A	NRT	ESA/EUMETSAT	~3 h
	STC		~48 h
	NTC		~1 month
Sentinel-3B	NRT	ESA/EUMETSAT	~3 h
	STC		~48 h
	NTC		~1 month
Sentinel-6A	NRT	ESA/EUMETSAT	~3 h
	STC		~48 h
	NTC		~1 month
Jason-3	OGDR	EUMETSAT/NOAA	~3 to 5 h
	IGDR	CNES	~24h
	GDR	CNES	~3 months
Cryosat-2	NOP	ESA/CNES	~7 h
	IOP		~48 h
	GOP	ESA	~3 month
Saral/AltiKa	OGDR	ISRO/EUMETSAT	~3 to 5 h
	IGDR	CNES	~48 h
	GDR	CNES	~2 months
SWOT-nadir	OGDR	CNES	~3 to 5 h
	IGDR	CNES	~48 h
HaiYang-2C	IGDR	NSOAS	~48h
HaiYang-2B	IGDR	NSOAS	~48 h
	GDR	NSOAS	Best effort
HaiYang-2A	GDR	NSOAS	Best effort
Topex/Poseidon	GDR	CNES	Reprocessing only
Jason-1	GDR	CNES	Reprocessing only
Jason-2	GDR	CNES	Reprocessing only
Envisat	GDR	ESA	Reprocessing only
ERS-1	GDR	ESA	Reprocessing only
ERS-2	GDR	ESA	Reprocessing only
Geosat Follow On	GDR	NOAA	Reprocessing only

L2P products with two different frequencies are used:

- The low frequency 1 Hz (~7 km). This frequency corresponds to the historical sampling used from the start of the DUACS production. It is used as input of the L3 1 Hz production when higher frequency is not available.
- The high frequency 20 Hz (~350 m). This frequency allows a better observation of the fine scale structures and near coast area. It however presents a higher level of measurement noise compared to the conventional 1 Hz and thus requires specific processing and/or corrections to extract the useful short wavelength signal. It is used for producing the L3 products with a final 5 Hz sampling (~1 km) frequency.

The following table (Table 12) gives relevant information about the characteristics of the different altimeters used.

Table 12: Characteristics of the altimetric missions and L2p products availability period (continues).

Altimetric mission	Cycle duration (days)	Latitude range (°N)	Number of tracks in the cycle	Inter-track distance at equator (km)	Sun-synchronous	Dual-frequency Altimeter	Radiometer on board	Input (L2p) data availability Start-End dates
Sentinel-3A	27	±81.5	770	~100	Yes	Yes	Yes	2016/03/01 (cycle 1) Ongoing
Sentinel-3B	27	±81.5	770	~100	Yes	Yes	Yes	2018/11/23 (cycle 19; interleaved orbit) Ongoing
Sentinel-6A	10	±66.0	254	~315	No	Yes	Yes	2020/11/30 (cycle 1) Ongoing
SWOT-nadir (Calval phase)	1	±77.6	28	~1500	No	Yes	Yes	2023/01/17 (cycle 403) 2023/07/20 (cycle 588)
SWOT-nadir (science phase)	21	±77.5	584	~140				2023/07/21 (cycle 1) Ongoing
Jason-3	10	±66.0	254	~315	No	Yes	Yes	2016/02/12 (cycle 1) 2022/04/07 (cycle 226)
Jason-3 Interleaved	10	±66.0	254	~315	No	Yes	Yes	2022/04/25 (cycle 300) Ongoing
Jason-2	10	±66.0	254	~315	No	Yes	Yes	2008/07/12 (cycle1) 2016/10/02 (cycle 303)
Jason-2 Interleaved	10	±66.0	254	~315				2016/10/13 (cycle 305) 2017/05/17 (cycle 327)
Jason-2 Long Repeat Orbit	9.86	±66.0	254	-				2017/07/11 (cycle 500) 2018/11/13 (cycle 612)
Cryosat-2	29 (sub cycle)	±88.0	840	~98	No	No	No	2010/07/16 (cycle 7) 2020/07/31 (cycle133)
Cryosat-2 New Orbit	25 (sub-cycle)	±88.0	724	~98	No	No	No	2020/08/01 (cycle 200) Ongoing
Saral/AltiKa	35	±81.5	1002	~80	Yes	No	Yes	2013/03/14 (cycle 1) 2015/03/31 (cycle 24)
SARAL-DP/AltiKa	35	±81.5	1002	-				2015/03/31 (cycle 24) Ongoing
HaiYang-2A	14	±81.0	386	~210	Yes	Yes	Yes	2014/04/12 (cycle 67) 2016/03/15 (cycle 117)
HaiYang-2A geodetic	9 (sub cycle)	±81.0	248	-				2016/03/30 (cycle 118) 2020/06/09 (cycle 289)

Table 12: (continued) Characteristics of the altimetric missions and L2p products availability period.

Altimetric mission	Cycle duration (days)	Latitude range (°N)	Number of tracks in the cycle	Inter-track distance at equator (km)	Sun-synchronous	Dual-frequency Altimeter	Radiometer on board	input (L2P) data availability Start-End dates
HaiYang-2B	14	±81.0	386	~210	Yes	Yes	Yes	2019/11/15 (cycle 27) Ongoing
Topex/Poseidon	10	±66.0	254	~315	No	Yes	Yes	1992/09/25 (cycle 1) 2002/04/23 (cycle 353)
Topex/Poseidon Interleaved	10	±66.0	254	~315				2002/04/24 (cycle 354) 2005/10/08 (cycle 481)
Jason-1	10	±66.0	254	~315	No	Yes	Yes	2002/01/15 (cycle 1) 2009/01/26 (cycle 259)
Jason-1 Interleaved	10	±66.0	254	~315				2009/02/10 (cycle 262) 2012/03/03 (cycle 374)
Jason-1 Geodetic	10.91	±66.0	280	-				2012/05/07 (cycle 500) 2013/06/21 (cycle 537)
Envisat	35	±81.5	1002	~80	Yes	Yes (S-band lost after cycle 65)	Yes	2002/05/14 (cycle 6) 2010/10/19 (cycle 94)
Envisat-New Orbit	30	±81.5	862	-				2010/10/26 (cycle 95) 2012/04/08 (cycle 113)
ERS-1	35	±81.5	1002	~80	Yes	Yes	Yes	1992/10/23 (cycle 15) 1993/12/20 (cycle 27) & 1995/03/24 (cycle 41) 1996/06/02 (cycle 53)
ERS-1 geodetic	168	±81.5	1002	-				1994/04/10 (cycle 30) 1995/03/21 (cycle 40)
ERS-2	35	±81.5	1002	~80	Yes	Yes	Yes	1995/05/15 (cycle 1) 2003/08/11 (cycle 86)
Geosat Follow On	17	±72	488	~165	No	No	Yes	2000/01/07 (cycle 37) 2008/09/07 (cycle 222)

II.4.3 Acquisition processing

The acquisition process is two-fold:

- straightforward retrieval and reformatting of altimeter data
- synchronization process.

The measurements ([O/I]GDR or equivalent) from different altimeters are retrieved. The DUACS system takes as input L2p altimeter products.

In NRT processing, the acquisition step uses two different data flows: the OGDR/NRT flow (within a few hours), and the IGDR/STC flow (within a few days). The acquisition software detects, downloads and processes incoming data as soon as they are available on remote sites (external database, FTP site). Data are split into passes if necessary. This processing step delivers "raw" data that have been divided into cycles and passes, and ordered chronologically.

For each OGDR/NRT input, the system checks that no equivalent IGDR/STC entry is available in the data base before acquisition; for each IGDR/STC input, the system checks and deletes the equivalent OGDR/NRT entry in the data base. These operations aim to avoid duplicates in the DUACS system. This processing is summarized in Figure 3**.**

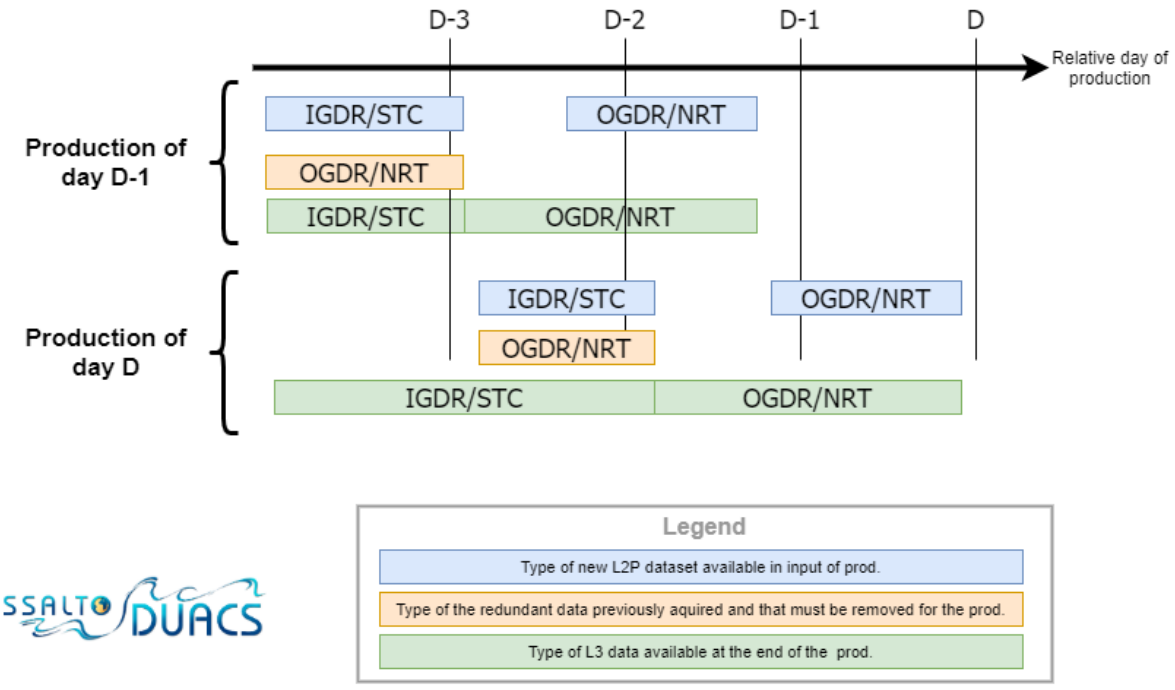

Figure 3: Overview of the near real-time system data flow management.

In the NRT system, full-rate (typically 20Hz) altimeter measurements are acquired when available, Otherwise, low-rate (1Hz) measurements are considered. The following table (Table 13) lists the sampling-rate used for the different altimeters.

Table 13: Sampling-rate of the different altimeters used in the NRT L3 production.

Altimeter mission	NTC(IGDR)/NRT(OGDR) Sampling-rate used (Hz)
Sentinel-6A	20
Sentinel-3A/B	20
Jason-3	20
Cryosat-2	1
SARAL-DP/AltiKa	1
SWOT-nadir	20
HaiYang-2B	20

In DT system, the GDR/NTC data flow, with the 1Hz posting rate, is used. The acquisition is activated specifically before each DT production.

The number of altimeters processed varies with time as summarized in Figure 4 and Figure 5.

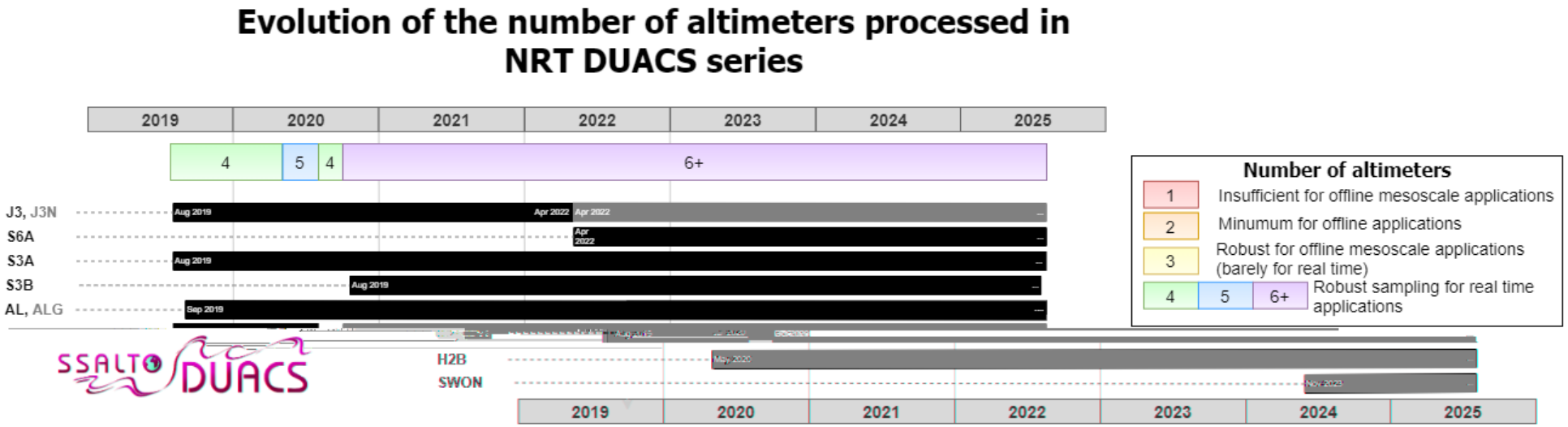

Figure 4: Evolution of the number of altimeters processed in NRT conditions. See for details.

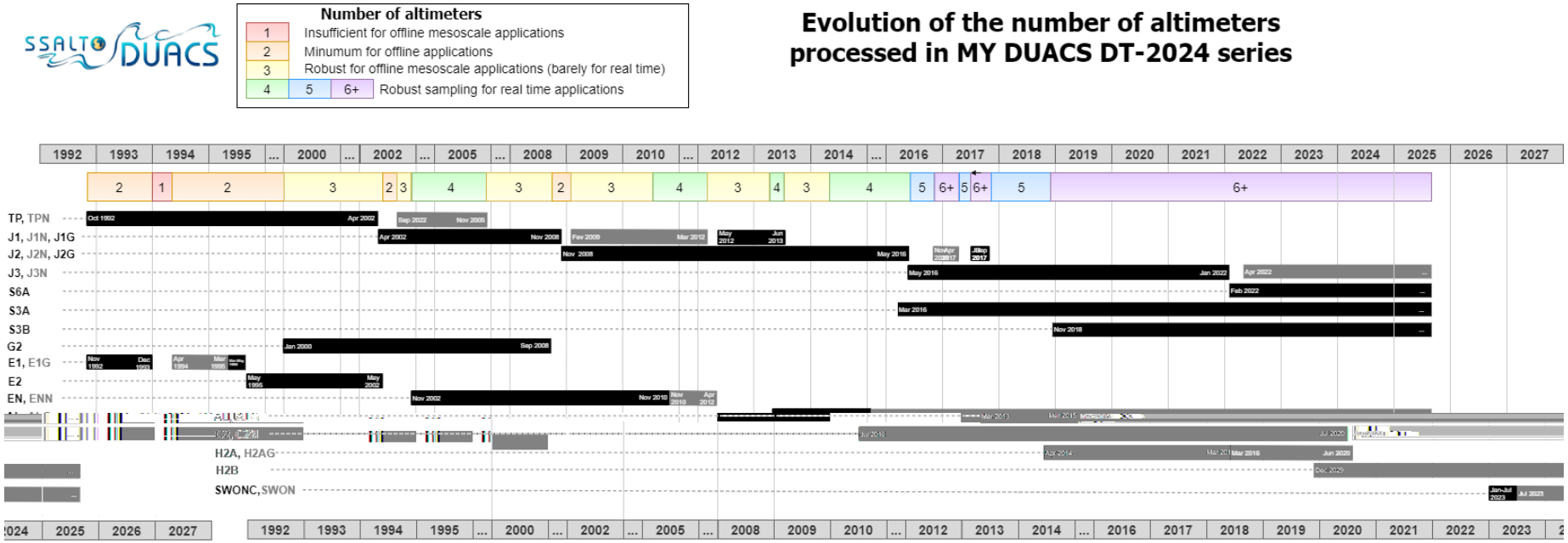

Figure 5: Evolution of the number of altimeters processed for the MY DT-2024 series. See for details.

II.4.4 Input data quality control

The L2 Input Data Quality Control is a critical process applied to guarantee that DUACS uses only the most accurate altimeter data. DUACS system is supplied with L2p altimeter products that include a quality flag for each measurement. The valid data selection is directly based on this quality flag. Thanks to the high quality of current missions, this process rejects only a small percentage of altimeter measurements, but this small amount of erroneous data could be the cause of a significant quality loss.

The L2p quality control is based on various indicators: (i) relies on standard raw data editing with quality flags or parameter thresholds; but also (ii) on complex data editing algorithms based on the detection of erroneous artifacts; (iii) mono and multi-mission crossover validation; and (iv) macroscopic statistics to edit out large data flows that do not meet the system's requirements. Details of threshold editing can be found in the handbook of each altimeter mission (e.g., Aviso+, 2020, 2022).

II.4.5 Homogenization and cross-calibration

Homogenization and cross-calibration are done at different steps of the processing.

The first homogenization step consists of acquiring altimeter and ancillary data from the different altimeters that are *a priori* as homogeneous as possible. The DUACS processing is based on the altimeter standards given by L2p products. They include the most recent standards recommended for altimeter global products by the different agencies and expert groups such as OSTST, ESA Quality Working groups. Each mission is processed separately as its requirements vary depending on the input data. When available, a specific standard recommended for regional processing can be applied by DUACS. The list of corrections and models currently applied in NRT processing is provided in Table 14. The list of corrections and models currently applied in REP/DT processing is provided in Table 15.

Input L2p products include a first cross-calibration processing that consists of ensuring mean sea level continuity between the altimeter reference missions. This step, crucial for climate signals, is done as accurately as possible in REP/DT conditions, taking into account both the global and regional biases, as presented in Pujol et al.,(2016). In NRT conditions, the accuracy of this cross-calibration step is reduced due to the temporal variability of the orbit solutions. Only the global bias between the reference mission is usually corrected.

Nevertheless, they are not always coherent at large regional scales due to various sources of geographically correlated errors (instrumental, processing, orbit residuals errors). Consequently, the DUACS multi-mission cross-calibration algorithm aims to reduce these errors in order to generate a global, consistent and accurate dataset for all altimeter constellations. This processing step consists of applying the Orbit Error Reduction (OER) algorithm. This process consists of reducing orbit errors through a global minimization of the crossover differences observed for the reference mission, and between the reference and other missions also identified as complementary and opportunity missions Le Traon and Ogor, (1998). Multi-satellite crossover determination is performed on a daily basis. All altimeter fields (measurement, corrections and other fields such as bathymetry, MSS, etc.) are interpolated at crossover locations and dates. Crossovers are then appended to the existing crossover database as more altimeter data become available. This crossover dataset is the input of the OER method. Using the precision of the reference mission orbit (Topex/Jason series), an accurate orbit error can be estimated. This processing step is applied on GDR/NTC as well as on IGDR/STC measurements, except for some missions that present a high error level at long wavelengths (e.g., H2C). It does not concern either OGDR/NRT measurements. Specifically, to the OGDR measurements and [I]GDR measurements processing for some specific missions, the DUACS system includes SLA filtering. The reduced quality of the orbit solution indeed limits the use of the long-wavelength signal with these products. The DUACS processing extracts from these data sets the short scales (< ~900 km) which are useful to better describe the ocean variability in real time, and merges this information with a fair

description of large-scale signals provided by the multi-satellite observation (i.e., L4 product) in near real time. Finally, a "hybrid" SLA is computed. This specific processing is summarized in Figure 6.

The last step consists of applying the long wavelength error (LWE) reduction algorithm. It is based on multiscale mapping method Ubelmann et al., (2021a). This process reduces geographically correlated errors between neighbouring tracks from different sensors. This optimal interpolation based empirical correction also contributes to reduction of the residual high frequency signal that is not fully corrected by the different corrections that are applied (mainly the Dynamic Atmospheric Correction and Ocean tides).

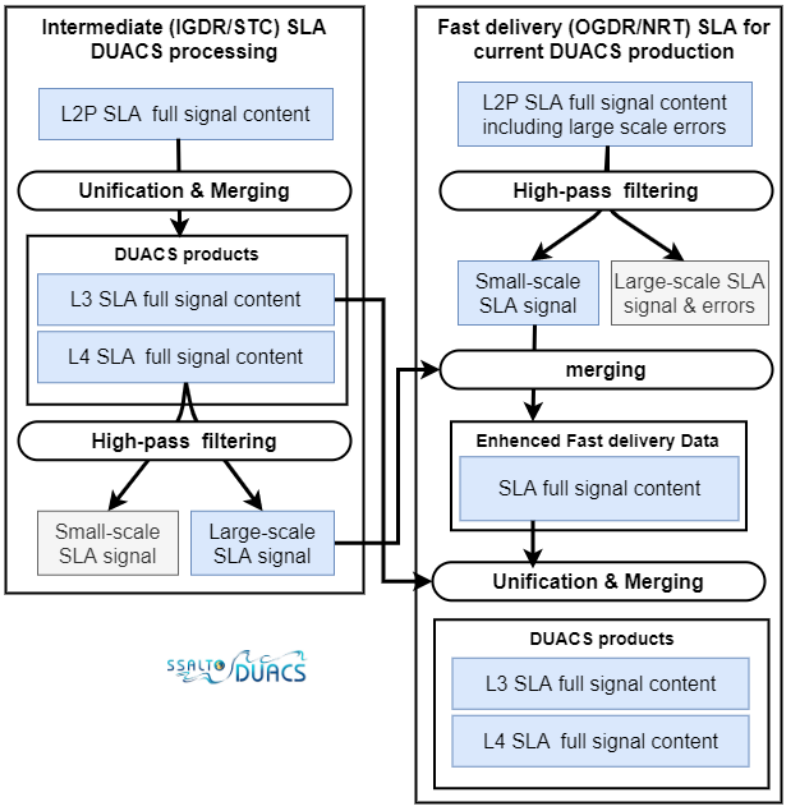

Figure 6: Overview of the cross-calibration processing for fast delivery (OGDR/NRT) measurements.

Table 14: Standards of the different corrections applied on altimeter measurements in L3 1Hz and 5Hz NRT processing.

	Sentinel-3A	Sentinel-3B	Sentinel-6A	Jason-3 [Interleaved]	SWOT-nadir	HaiYang-2B	Cryosat-2	SARAL-DP/AltiKa
Product standard ref	L2P products (Aviso+, 2022)		L2P products (Aviso+, 2022) HR mode used	GDR-F	GDR-F	NSOAS	NOP/IOP baseline	GDR-T version, Patch 2 up to 2020/01/27; GDR-F after
Retracking	SAMOSA		NR	MLE4 (Amarouche et al., 2004)	MLE4	MLE4	"Ocean MLE4" retracking MLE4 fit from 2nd order Brown analytical model: MLE4 simultaneously retrieves the 4 parameters that can be inverted from the altimeter waveforms: Epoch (tracker range offset)⇒altimeter range Composite Sigma⇒SWH Amplitude⇒Sigma0 Square of mispointing angle "Ice OCOG" retracking Geometrical analysis of the altimeter waveforms, which retrieves the following parameters: Epoch (tracker range offset)⇒altimeter range Amplitude⇒Sigma0	MLE4 (Amarouche et al., 2004) and LUT correction
Orbit	MOE for STC Navigator for NRT			MOE-F mixt (DORIS+GPS)	MOE-F		NOP: DORIS Navigator IOP: DORIS Preliminary Orbit-GDR-E	POE-F
Ionospheric	Dual-frequency altimeter range measurements; filtered				GIM model computed from vertical Total Electron Content maps (Chou et al., 2023) rescaled on the orbit altitude with IRI95 model (https://irimodel.org/)			
Dry troposphere	Model computed from ECMWF Gaussian grids (new S1 and S2 atmospheric tides are applied)							
Wet troposphere	From Sentinel Microwave radiometer			AMR radiometer	Model computed from ECMWF Gaussian grids		Model computed from ECMWF Gaussian grids	ALTIKA_RAD radiometer GDR-T patch2 up to 2020/01/27; GDR-F patch-4 after
DAC	MOG2D High Resolution forced with ECMWF pressure and wing fields (S1 and S2 were excluded) + inverse barometer computed from rectangular grids. (Carrère and Lyard, 2003)							
Ocean tide	FES2014b (S1 and S2 are included) (Carrere et al., 2015) before 2024/07/07; FES2022b (Loren Carrère et al., 2023) after							
Internal tide	(Zaron, 2019)(HRETv8.1 tidal frequencies: M2, K1, S2, O1)							
Pole tide	(Desai et al., 2015) & Mean Pole Location, 2017							
Solid earth tide	Elastic response to tidal potential (Cartwright and Edden, 1973; Cartwright and Tayler, 1971)							
Loading tide	FES2014 (Carrere et al., 2016)							

	Sentinel-3A	Sentinel-3B	Sentinel-6A	Jason-3 [Interleaved]	SWOT-nadir	HaiYang-2B	Cryosat-2	SARAL-DP/AltiKa
Sea State Bias	Non-parametric SSB (Tran et al., 2012) from J2 GDR-D		Non-parametric SSB from J3 GDR-F (Bignalet-Cazalet et al., 2021)	Non-parametric SSB (Tran, 2011)	Non-parametric SSB from J3 GDR-F (Bignalet-Cazalet et al., 2021)	NSOAS	Empirical solution from Cryosat-2 Ocean Baseline-B data in LRM Mode	Hybrid SSB (Scharroo et al., 2013) up to 2020/01/27; 3D SSB (Tran, 2019) after
High Frequency Adjustment	-		-	(Tran et al., 2021)	(Tran et al., 2021) from J3 GDR-F	-	-	-
Mean Profile/ Mean Sea Surface	Hybrid MSS (SIO,CNES/CLS15,DTU15) before 2024/07/07; Hybrid MSS (SIO; CNES/CLS22; DTU21) (Laloue et al., 2024a) after Referenced to the 1993-2012 period							
Mean Dynamic Topography	Before 2024/11/06: MDT_CNES_CLS18 (Mulet et al., 2021), combined with MDT_CMEMS_2020_MED and MDT_CMEMS_2020_BLK (Jousset et al., 2022; Jousset and Mulet, 2020) over the Mediterranean and Black Sea. Consistent with the 20-year reference period used for the SLA. From 2024/11/06: Global ocean: MDT_CNES_CLS22 (Jousset et al., 2023), combined with MDT_CMEMS_2020_MED and MDT_CMEMS_2020_BLK (Jousset et al., 2022; Jousset and Mulet, 2020) over the Mediterranean and Black Sea. Consistent with the 20-year reference period used for the SLA; Europe area: MDT Europe CMEMS_2024 (Jousset et al, in prep)							
GIA	The DUACS products are not corrected from Glacial Isostatic Adjustment (GIA) effects							

Table 14: (continued) Standards of the different corrections applied on altimeter measurements in L3 1Hz and 5Hz NRT processing.

Table 15: Standards of the different corrections applied on altimeter measurements in DT-2024 processing (Kocha et al., 2023). Bold text indicates the standards that evolved compared to the previous product version (DT-2021; Lievin et al., 2020).

	Topex / Poseidon	**Jason 1**	**Jason 2**	**Jason 3**	**ERS-1**	**ERS-2**	**ENVISAT**	**SARAL**	**Sentinel-6A**	**Sentinel 3A**	**Sentinel 3B**	**Geosat FO**	**Cryosat 2**	**HY 2A**	**HY-2B**	**SWON C/SWON**
Product standard ref	**GDR-F**	GDR-D	GDR-F	GDR-F					**F09**	**BC05**						
RETRACKING	**MLE3**	MLE4	MLE4	MLE4	OPR	OPR	MLE-3 (OCE-1)	MLE4	**Numerical LRM**	**SAMOSA**		GFO retracker	SAMOS A2.3	MLE4	MLE4	MLE4
ORBIT	GSFC STD18	**POE-F**	**POE-F**		Reaper		**POE-F**	POE-F	**POE-F**	**POE-F**		GSFC	POE-F	POE-D	POE-F	POE-F
IONOSPHERIC	**Filtered dual-frequency altimeter range measurements** (Ablain and Legeais, 2010) **on Topex ; DORIS on Poseidon**	Filtered dual-frequency altimeter range measurements (Guibbaud et al., 2015)	Filtered dual-frequency altimeter range (Guibbaud et al., 2015) (from SSB C-band)	**Filtered dual-frequency altimeter range measurements GDR-F ;** (Nencioli et al., 2022)	Reaper NIC09 model (Scharroo and Smith, 2010)	GIM (Iijima et al., 1999)	Filtered from L2; c>65 : GIM (Iijima et al., 1999) corrected for 8mm bias	GIM (Iijima et al., 1999)	**Filtered dual-frequency altimeter range** (Guibbaud et al., 2015)	**Filtered dual-frequency altimeter rangefrom L2**		GIM (Iijima et al., 1999)			GIM (Iijima et al., 1999)	Filtered dual-freq altimeter range (Guibbaud et al., 2015)
SEA STATE BIAS	**2D Non parametric** (Putnam et al., 2023) **on Topex**; BM4 on Poseidon	2D Non parametric (Tran, 2015)	Non parametric (Tran et al., 2012)	**2D Non parametric** (Bignalet-Cazalet et al., 2021)	BM3 (Gaspar and Ogor, 1994)	Non parametric (Mertz et al., 2005)	2D Non parametric (Tran, 2017)	Non parametric (Tran, 2019)	**Non Parametric** (Bignalet-Cazalet et al., 2021) **J3 MLE4 GDR-F**	**Non parametric** (Tran,et al 2021)		Non parametric (Tran et al., 2010)	2D Non parametric (baseline C) (Tran, 2018) Baseline C	Non parametric from J3 MLE4 (Bignalet-Cazalet et al., 2021)	From L2 product	Non parametric from J3 MLE4 (Bignalet-Cazalet et al., 2021)

	Topex / Poseidon	Jason 1	Jason 2	Jason 3	ERS-1	ERS-2	ENVISAT	SARAL	Sentinel-6A	Sentinel 3A	Sentinel 3B	Geosat FO	Cryosat 2	HY 2A	HY-2B	SWON C/SWON
WET TROPOSPHERE	**TMR GDRF radiometer reprocessing**	JMR (FCDR) radiometer	**AMR radiometer GDR-F**		GPD+ (Fernandes et al., 2015)		MWR radiometer reprocessed	Neuronal Network (5 entries) V4	**AMR radiometer**	**GPD+** (Fernandes and Lázaro, 2016)		GFO Radiometer and ECMWF model	GPD+ (Fernandes and Lázaro, 2016)	ECMWF model	ECMWF model	ECMWF model
DRY TROPOSPHERE	ERA5 (1-hour) model based															
DYNAMICAL ATMOSPHERIC CORRECTION	**TUGO High frequencies forced with analysed ERA5 pressure and wind field before S6A era and ECMWF field after + inverse barometer LF**															
OCEAN TIDE	**FES22b** (Loren Carrère et al., 2023)															
POLE TIDE	(Desai et al., 2015); Mean Pole Location 2017 (Ries and Desai, 2017)															
SOLID TIDE	Elastic response to tidal potential (Cartwright and Edden, 1973; Cartwright and Tayler, 1971)															
INTERNAL TIDE	(Zaron, 2019) (HRETv8.1 tidal frequencies: M2, K1, S2, O1)															
MEAN SEA SURFACE	**MP for repetitive orbit phases; Hybrid_2023 MSS (SIO,CNES/CLS22,DTU21)** (Laloue et al., 2024a) **for geodetic/LRO phase**				**Mean profile**		**MP for repetitive orbit phases Hybrid_2023 MSS (SIO,CNES/CLS22,DTU21)** (Laloue et al., 2024a) **for geodetic phase**		**Mean profile**		**Mean profile**	**Hybrid_2023 MSS (SIO,CNES/CLS22,DTU21)** (Laloue et al., 2024a)				
MEAN DYNAMIC TOPOGRAPHY	**Global: MDT_CNES_CLS22** (Jousset et al., 2023) merged with regional MDT CMEMS_2020 Mediterranean and Black Sea (Jousset et al., 2022; Jousset and Mulet, 2020) **Europe: MDT Europe CMEMS_2024 (Jousset et al, in prep)**															
GIA	The DUACS products are not corrected from GIA effects															

Table 15: (continued) Standards of the different corrections applied on altimeter measurements in DT-2024 processing (Kocha et al., 2023). Bold text indicates the standards that evolved compared to the previous product version (DT-2021; Lievin et al., 2020).

II.4.6 Along-track (L3) products generation

II.4.6.1 SLA computation

The Sea Level Anomalies (SLA) are used in oceanographic studies. They are computed from the difference of the instantaneous SSH minus a temporal reference. This temporal reference can be either a Mean Profile (MP), in the case of repeat track, or a gridded Mean Sea Surface (MSS), when the repeat track cannot be used. Table 16 gives the MPs and MSS used for the MY 1 Hz SLA processing. The NRT 1Hz and 5 Hz SLA processing is based on a gridded MSS only.

The errors affecting the SLAs, MPs and MSS have different magnitudes and wavelengths. The computation of the SLAs and their associated errors are detailed in Pujol et al. (2016) and Taburet et al. (2019). Errors of the MSS are described in Pujol et al. (2018). Both MP and MSS are referenced to the same reference period as specified in Table 16. The methodology applied to shift the reference period is presented in Pujol et al. (2016).

Table 16: Mean Profiles (MPs) and Mean Sea Surface (MSS) used for the 1 Hz SLA computation along the different altimeters.

Altimeter mission	1 Hz MP description
Topex/Poseidon, Jason-1, OSTM/Jason-2, Jason-3 Sentinel-6A	MY: 1 Hz MP computed with Topex/Poseidon (January 1993, April 2002; cycles 11 to 353), Jason-1 (April 2002, October 2008; cycles 10 to 249); Jason-2 (October 2008, May 2016; cycles 10 to 290), Jason-3 (May 2016, December 2021; cycles 11 to 217) and Sentinnel-6A (December 2021, August 2023; cycles 42 to 103) measurements. Referenced to the (1993, 2012) period. NRT before 2022/11/10: 1 Hz MP computed with Topex/Poseidon (January 1993, April 2002; cycles 11 to 353), Jason-1 (April 2002, October 2008; cycles 10 to 249); Jason-2 (October 2008, May 2016; cycles 10 to 290) and Jason-3 (May 2016, March 2020; cycles 11 to 150) measurements. Referenced to the (1993, 2012) period. NRT after: gridded MSS is used as described in Section II.4.5, corrected with long wavelengths of the 1 Hz MP
ERS-1/ERS-2, Envisat,SARAL/AltiKa	1 Hz MP computed with ERS-2 (May 1995, January 2000; cycles 1 to 49), Envisat (May 2002, October 2010; cycles 6 to 94) and SARAL/Altika (Mars 2013, Mars 2015; cycles 1 to 22) measurements. Referenced to the 1993-2012 period.
Topex/Poseidon interleaved, Jason-1 interleaved, OSTM/Jason-2 interleaved, Jason-3 interleaved	MY:1 Hz MP computed with Topex/Poseidon interleaved (September 2002, October 2005; cycles 368 to 481), Jason-1 interleaved (February 2009, March 2012; cycles 262 to 374), Jason-2 interleaved (October-2016; March-2017; cycles 305 to 322).and Jason-3 interleaved (April 2024, August 2023; cycles 300 to 350) measurements. Referenced to the (1993, 2012) period NRT before 2022/11/10: 1 Hz MP computed with Topex/Poseidon interleaved (September 2002, October 2005; cycles 368 to 481) and Jason-1 interleaved (February 2009, March 2012; cycles 262 to 374), Jason-2 interleaved (October-2016; March-2017; cycles 305 to 322). measurements. Referenced to the (1993, 2012) period NRT after: gridded MSS is used as described in Section II.4.5, corrected with long wavelengths of the 1 Hz MP
Geosat Follow-On	1 Hz MP computed with Geosat Follow On (January 2000, September 2008; cycles 37 to 222) measurements. Referenced to the (1993, 2012) period.
Sentinel-3A	MY: 1 Hz MP computed with Sentinel-3A (June 2016, August 2023; cycles 6 to 103). NRT before 2022/11/10: 1 Hz MP computed with Sentinel-3A (March 2016, August 2020; cycles 1 to 61). NRT after: gridded MSS is used as described in Section II.4.5, corrected with long wavelengths of the 1 Hz MP
Sentinel-3B	MY: 1 Hz MP computed with Sentinel-3B (November 2018, August 2023; cycles 19 to 83). NRT: MSS is used as described in Section II.4.5, corrected with long wavelengths of the 1 Hz MP
ERS-1 geodetic phase	No MP available for these missions. A gridded MSS is used as described in Section II.4.5
Envisat new orbit	
Jason-1 geodetic, Jason-2 Long Repeat Orbit Phase	
Cryosat-2	
SARAL-DP/AltiKa	
HaiYang-2A	
HaiYang-2B	
SWOT-nadir	

II.4.6.2 Along track (L3) noise filtering

The filtering processing consists in removing from along-track measurements the noise signal and short wavelength affected by this noise.

For the 1 Hz SLA, this processing consists in a low-pass filtering with a cut-off wavelength of 65 km over the global ocean. This cut-off wavelength comes from the study by Dufau et al. (2016) and is discussed in Pujol et al. (2016). It represents the minimum wavelength associated with the dynamical structures that altimetry would statistically be able to observe with a signal-to noise ratio greater than 1. The cut-off is reduced for regional products to preserve as much as possible the short wavelength signal. The different cut-off wavelength used are summarized in . No subsampling is applied in the SLA 1 Hz processing.

Table 17: Filtering and subsampling parameters used for L3 1 Hz products.

Region	Product considered	Filtering cut-off wavelength (km)	Distance between two points (km)
Global	Filtered and not-subsampled	~65	~7
	Not-filtered and not-subsampled	-	~7
Europe	Filtered and not subsampled	~40	~7
	Not-filtered and not-subsampled	-	~7

For the 5 Hz SLA construction, two different filtering/subsampling are applied on the upstream 20 Hz measurements:

For the raw (“unfiltered”) SLA 5 Hz computation, a filtering on the raw 20 Hz measurement is applied in order to filter the measurement noise at the 5 Hz Nyquist frequency (i.e., ~2,5 km). Then a subsampling is applied to extract the 5 Hz positions.

For the filtered SLA 5 Hz computation, as for the 1 Hz processing, the short wavelength dominated by the measurement noise is reduced by a low pass filtering. Then, a subsampling is applied to extract the 5 Hz positions. The cut-off wavelength used for the filtering varies from one altimeter to the other, according to their observing capability estimated on the upstream full rate (i.e., 20 Hz) measurement. For the processing over the European area, it was estimated over the North Atlantic area over a reduced temporal period (April-June 2022) and thus could be revised in the future. Currently, the cut of wavelength varies from 40 km for the Sentinel-6A HR mission to 55 km for the Jason mission (0).

For the processing over the global ocean, the observing capability of the different altimeters was estimated over a nearly 1-year period (October 2022-August 2023), considering possible geographical variations. The Figure 7 illustrates the results obtained for Sentinel-6A (SAR mode measurement) and Jason-3 (LRM mode measurement). The cut-off wavelengths can vary from 20 km (Sentinel-6A, West Pacific, to 120 km (HaiYang-2B, South-Est Pacific area). The mean observable wavelength over the global ocean is close to the one observed in the North-East Atlantic area (see).

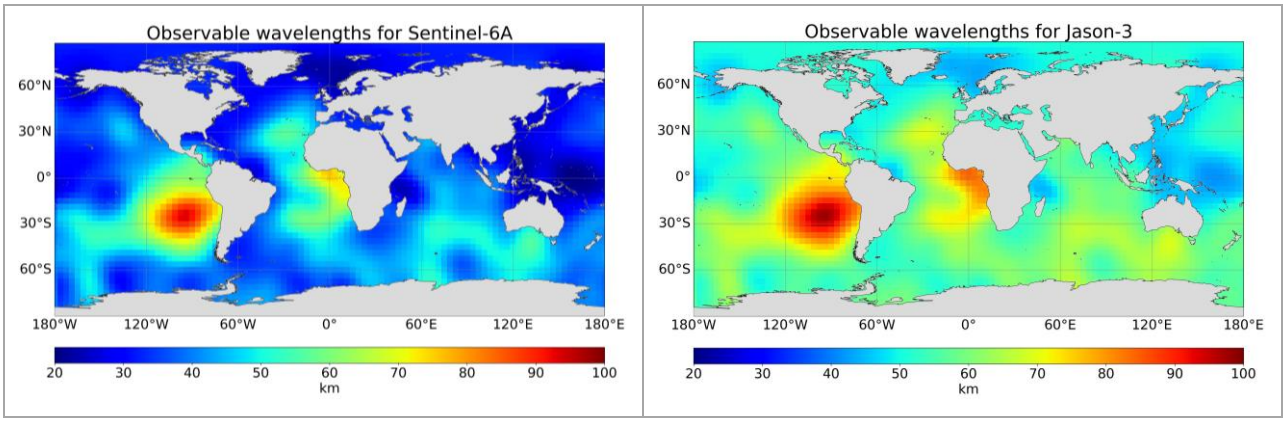

Figure 7: Spatial distribution of the cut-off wavelength used for the 5Hz "sla filtered" processing. Sentinel-6A (left) and Jason-3 (right).

II.4.6.3 Derived variables generation (for L3 5 Hz)

The L3 derived variables consist of geostrophic currents (absolute and anomalies) in the across-track direction. This processing is applied only for the final L3 5 Hz production.

The geostrophic current is computed using a finite difference of maximal order 5 in open ocean. The order is progressively reduced when approaching the coast or a gap with no valid measurement. This processing is applied on SLA, after filtering of the short wavelengths dominated by noises (see section II.4.6.2), to retrieve the anomaly of the geostrophic current. It is also applied on MDT, to retrieve the mean component of the geostrophic current. This processing is applied on high resolution upset (20 Hz) measurements. The estimation of the geostrophic current in the equatorial band is not available.

The MDT field is obtained by interpolating the Mean Dynamic Topography (MDT) on along-track positions. The MDT used in the DUACS reprocessing is described in section II.4.5.

II.4.6.4 Measurement subsampling

For the L3 5 Hz production, a subsampling is applied on along-track measurement in order to reach the final 5 Hz sampling. Indeed, the previous processing steps are applied using the upstream measurement sampling, i.e., 20 Hz sampling. This subsampling is thus applied on the different variables delivered in the L3 5 Hz products (e.g., SLA, currents).

No subsampling is applied in the L3 1 Hz processing.

II.4.7 SLA Gridded (L4) products generation

The processing methodology for the L4 product generation consists of an optimal interpolation processing for the C3S product described in Pujol et al. (2016). The L4 CMEMS product generation is based on the Multiscale Inversion of Ocean Surface Topography (MIOST) mapping approach, as described in Ubelmann et al., (2021a, 2022). This method is able to account for various modes of variability of the ocean surface topography (e.g., geostrophic, barotrope, equatorial waves dynamic, etc.) by constructing several independent components within an assumed covariance model. In these products, we focused only on the geostrophic mode to depict the geostrophically balanced evolution of sea surface height (SSH).

The computation of L4 products uses the upstream 5Hz L3 SLA field, filtered and subsampled.

In the REP/DT processing, the products can be computed optimally with a centred computation time window of ±6 weeks around the date of the map to be computed.

In the NRT processing, contrary to the REP/DT case, the products cannot be computed with a centred computation time window: indeed, as the future data are not available yet, the computation time window is not centred. Only data over the period the last 7 weeks to D ([D – 7 weeks, D]) are used, where D is the date of the production considered. For each day of NRT production, three merged maps are produced daily and delivered to the users (Figure 8):

- A 0-day delay (i.e., map centred on day D), which represents a preliminary map production
- A 3-day delay (i.e., map centred on day D - 3 days), which represents an intermediate map production. When available, this map replaces the 0-day delay map
- A 6-day delay (i.e., map centred on day D - 6 days), which represents a final NRT map production. When available, this map replaces the 3-day delay map

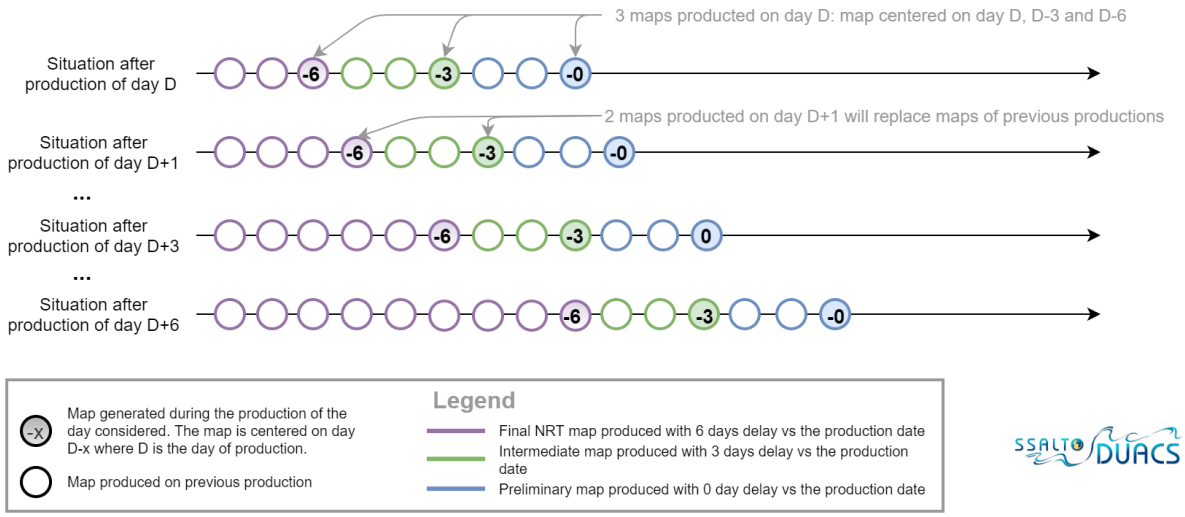

Figure 8: L4 product generation, NRT production. Three merged maps are produced daily and delivered to the users: final map (D - 6: 6-day delay), intermediate map (d-3: 3-day delay) and preliminary map (d0: 0-day delay).

Both for the REP/DT and NRT, the maps are centred on midnight.

Note however that the spatial and temporal scales of the variability that is resolved in the DUACS merged products data set are imposed by the temporal correlation function used in the mapping procedure, as described in Pujol et al. (2016) and Ubelmann et al., (2021).

It's important to note that, in the polar regions, the sea-level anomaly provided by the MIOST mapping algorithm is derived through extrapolation, as no local altimeter data from leads are used to constrain the maps. Therefore, users should disregard gridded data in these areas and instead rely on the sea-ice mask included in the products.

II.4.7.1 Number of satellites to compute the maps

Both in REP/DT and NRT processing, the maps are computed with all the satellites available. This allows an improved signal sampling when more than two altimeters (corresponding to the minimal

constellation) are available. The mesoscale signal is indeed more accurately reconstructed during these periods Pascual et al., (2006), when omission errors are reduced by the altimeter sampling. The all-sat-merged series is however not homogeneous in time due to the evolutions of the altimeter constellation (see Figure 4 and Figure 5).

II.4.7.2 Formal mapping error

The formal mapping error does not represent the precision of the SLA gridded products, but it represents an excellent indicator of the consistency of the grid. The formal error variance should correspond to a local minimum in the least squares sense (i.e. minimizing deviations from the mean). However, due to the computational cost and the wavelet-based formulation of the MIOST mapping approach, the error estimation method had to be revised for MIOST to deliver a global estimation of the formal error. In the MIOST products, the formal mapping error is determined using an ensemble approach. Specifically, an ensemble of 20 gridded product members is generated, each with a perturbed covariance model and observations. The standard deviation of the sea level anomaly (SLA) estimations across these ensemble members represents the formal mapping error.

In practice, the formal mapping error obtained depends on the constellation sampling capability (i.e. spatial distribution and density of the data used in the suboptimal estimation) and its consistency with the spatial/temporal scales and sea surface variability considered. But also on the noise budget for the different measurements used. The formal mapping error is usually low under the tracks of the different altimeters used in the mapping. It is higher within the inter-track diamonds. Higher formal mapping error is also observed over high variability areas.

The formal error for geostrophic currents is directly deduced from the SLA formal error matrix, by linearly combining diagonal and non-diagonal terms, follows the centred finite difference discretization.

II.4.7.3 L4 derived variables generation.

The L4 derived variables consist of the Absolute Dynamic Topography (ADT) (maps and along-track) and maps of geostrophic currents (absolute and anomalies).

The ADT variable is obtained by adding a Mean Dynamic Topography (MDT) to the SLA field. The MDT used in the DUACS reprocessing is described in section II.4.5.

The anomaly of the geostrophic current disseminated to users is derived from gridded SLA field. It is computed using a 3-point stencil width methodology Arbic et al., (2012) for latitudes outside the ± 5°N band. In the equatorial band, the Lagerloef methodology Lagerloef et al., (1999) introducing the β plane approximation is used. The absolute geostrophic current is obtained by adding to this anomaly the mean geostrophic current associated with the MDT field previously used.

II.4.8 L3 and L4 Quality control

The production of homogeneous products with high-quality data and within a short time period is the key feature of the DUACS processing system. But some events (failure on payload or on instruments, delay, maintenance on servers), can impact the quality of measurements or the data flows. A strict quality control on each processing step is indispensable to appreciate the overall quality of the system and to provide the best user services.

The Quality Control is the final process used by DUACS before product delivery. In addition to daily automated controls and warnings to the operators, each production delivers a large QC Report composed of detailed logs, figures and statistics of each processing step. An overview of the diagnostics used is given in section III. Altimetry experts analyse these reports twice a week (only for internal validation, thus those reports are not disseminated).

III VALIDATION FRAMEWORK

The validation aims to check the quality of the external products and the performance of the key processing steps. Three different points are assessed during the validation process:

- the data availability and spatial/temporal coverage
- the multi-mission homogenization processing
- the ocean signal consistency

Table 18 lists the different metrics that are used. They mainly consist of an analysis of the SLA field at different steps of the processing; check consistency of the SLA along the tracks of different altimeters and between gridded and along-track products; and comparison of the different variable fields (SLA, ADT, geostrophic current) with external *in situ* measurements.

Assessment of the DUACS products is also completed by specific studies (for reference papers, please see references in section IV), done in coordination with other projects (e.g., C3S[11], CNES SALP[12]) that aim to characterize the errors observed on specific fields, wavelengths and timescales.

[11]https://cds.climate.copernicus.eu/about-c3s
[12] https://www.aviso.altimetry.fr/en/home.html

Table 18: List of the metrics used for the operational validation of DUACS products.

Name	Description	Ocean parameter	Supporting reference dataset	Quantity
SLA_L2-NC—AVAIL	Number of altimeter measurement available/rejected	Sea Level Anomaly	None	Missing/valid/invalid data are identified over the data flow processed Temporal evolution on the number of measurements on a daily basis and/or along each track of the altimeter considered
SLA_L2-NC-ALT—MEAN	SLA differences at mono- and multi-missions crossover positions	Sea Level Anomaly	None	Mean difference between two SLA measurements corresponding to altimeter tracks cross-over positions The statistic is averaged over 7 days The performance of the product before and after Orbit Error correction are compared
SLA_L2-NC-ALT-STD				Standard deviation of the difference between two SLA measurements corresponding to altimeter tracks cross-over positions The statistic is averaged over 7 days The performance of the product before and after Orbit Error correction are compared
SLA_L2-NC-ALT-AVAIL				Number of SLA measurements corresponding to altimeter tracks cross-over positions The statistic is averaged over 7 days The performance of the product before and after Orbit Error correction are compared
SLA_LWENC-VAR	Variance of the Long Wavelength Error (LWE) correction applied on SLA products	LWE correction	None	Variance of the LWE correction averaged over the last 49 days
SLA_LWE—NC-DIFFVAR	Difference of variance of the SLA with and without LWE correction applied	Sea Level Anomaly	None	Difference of the variance of the SLA with and without LWE correction applied Statistics averaged over the last 49 days
SLA_SW-NC-VAR	Variance of the short wave SLA signal	Sea Level Anomaly; measurement noise	None	Variance of the short-wave signal (<65 km) filtered from along-track products Temporal daily statistics evolution Regional mean statistics computed over the last 49 days
SLA-D-NC-MEAN-<REGIONS>	SLA signal monitoring	Sea Level Anomaly	None	Mean of the along-track SLA (L3) over different regions averaged on a daily basis
SLA-D-NC-STD-<REGIONS>				Standard deviation of the along-track SLA (L3) over different regions averaged on a daily basis
SLA-D-NC-AVAIL-<REGIONS>				Number of along-track SLA (L3) over different regions averaged on a daily basis
SLA-NC-PSD-<REGIONS>	SLA signal spectral content	Sea Level Anomaly	None	Spectral decomposition of the SLA signal over different regions

Table 18: (continues) List of the metrics used for operational validation of the DUACS products

Name	Description	Ocean parameter	Supporting reference dataset	Quantity
SLA-D-NC-ALT-MEANDIFF-<REGIONS>	Difference between two SLA map products	Sea Level Anomaly	None	Mean difference between two SLA map products: Map of days D0 and Day D-7 Map of day D0 merging all the altimeters available and only one altimeter Map of day D0 computed over global ocean and regional area
SLA-D-NC-MEAN-<REGIONS>	SLA signal monitoring	Sea Level Anomaly	None	Mean of the map SLA (L4) over different regions averaged on a daily basis
SLA-D-NC-STD-<REGIONS>				Standard deviation of the map SLA (L4) over different regions averaged on a daily basis
SLA-D-NC-AVAIL-<REGIONS>				Number of grid node defined by the map SLA (L4) over different regions averaged on a daily basis
SLA-D-NC-MERR-<REGIONS>	Formal Mapping Error (ERR) monitoring	Formal Mapping Error	None	Mean of the ERR associated to the map SLA (L4) over different regions averaged on a daily basis
MKE-D-SURF-NC-MEAN-<REGIONS>-3MONTHLY	EKE monitoring	Eddy Kinetic Energy	None	Mean of the EKE deduced from the map SLA (L4) over different regions averaged on a daily basis Regional mean over the last 3 months
SLA-D-NC-DFS_MEAN	Contribution of the different altimeters to the map product	DFS	None	Mean contribution of the different altimeters available to the merged SLA map product
DHA_2000m-SURF-CLASS4-PROF-MEAN	DHA comparison with *in situ* Temperature/Salinity profiles estimation	Dynamic Height Anomalies	ARGO Temperature/Salinity profiles	Monitoring of the differences between Altimetry and T/S DHA estimation, at global and regional scales
SLA-D-CLASS2-TG-RMSD	SLA comparison with *in situ* Tide Gauges measurements	SLA	Tide Gauges measurements (PSMSL & GLOSS CLIVAR)	Map of the variability of the differences between altimetry and TG measurements
SLA-D-CLASS4-ALT--RMSD	SLA comparison with independent altimeter along-track measurements	SLA	Altimeter measurements non-used in map products construction	Map of the variability of the differences between altimetry and independent along-track measurements
UV-SURF-D-CLASS4--BUOY-RMSD	U&V geostrophic current comparison with *in situ* drifters' measurements	geostrophic current	Drifters' measurements (AOML)	Map of the variability of the differences between altimetry and drifters' measurements

IV VALIDATION RESULTS

IV.1 Variable SLA

IV.1.1 Level-3 along-track

IV.1.1.1 Main sources of errors

The along-track SLA product is affected by different errors:

- Instrumental errors: they characterise the precision of the instruments and accuracy of the altimeter pointing. They are also representative of the quality of the retracking processing.

  Different corrections are included in the data processing in order to minimize as much as possible these errors:

  - Mispointing correction: it allows to take into account possible mis-pointing of the altimeter measurement with respect to the nadir direction
  - Doppler effect correction that takes into account the motion of the satellite
  - The tracking bias that allows to take into account the imprecision of the different algorithms
  - The correction of the Ultra Stable Oscillator (USO) that correct the drift of the instrument
  - The internal calibration that takes into account the transit time of the data in the antenna.

  In spite of these different corrections, part of the instrumental errors remains in the along-track product. They are mainly characterized by uncorrelated measurement noise, discussed in §IV.1.1.2.1.

- Environmental and sea state errors: the path of the electromagnetic signal that goes through the atmosphere influences the measurement. In the same way, the sea state bias (presence and shape of the waves and roughness at the surface) also introduces an error on the measurement.

  Different corrections are used in the data processing in order to correct the measurement from atmospheric and sea surface effects:

  - The dry and wet troposphere corrections that correct the path delay effects linked to the presence of dry gases and water vapor in the atmosphere.
  - The ionospheric correction that allows to take into account the effect of the ions present in the atmosphere.
  - The sea state bias correction that corrects the effects of the sea surface state on the reflection of the altimeter signal on the surface.

  In spite of these different corrections, part of the environmental errors can still be observed in the along-track SLA signal. They can be spatially and temporally correlated.

- Geophysical errors: They mainly involve subtracting from the measurement any physical signal that cannot be accurately sampled with the altimeter (due for instance to the inconsistency between the temporal sampling of the altimeter and the temporal scales characteristic of the

signal considered) or which is not of interest for the study of the dynamic signal. In that way, different geophysical corrections are applied on the altimeter measurement (geoid, ocean tide, inverse barometer and high frequency wind and pressure effects, etc.). See Table 14 and Table 15 for the details of these corrections.

The quality of the different corrections, that depends on numerical models, can lead to uncertainty in the different geophysical corrections applied. They are considered as errors on the SLA product, and most of them are correlated in space and time.

IV.1.1.2 REP/MY product errors description

IV.1.1.2.1 Uncorrelated errors or measurement noise and mesoscale observability

The measurement noise is mainly induced by instrumental (altimeter) measurement errors. It can be mitigated with specific processings and corections (e.g. Moreau et al., 2021; Tran et al., 2021) and thus strongly depend on the altimeter data processing and standards applied.
The measurement noise is quantified by an analysis of the wavenumber spectra of the SLA (Figure 9). Indeed, the uncorrelated measurement error is the noise level estimated as the mean value of energy at high wavenumbers (wavelengths smaller than ~5 km). It follows the same trend as in the instrumental white-noise linked to the Surface Wave Height. **For the conventional radar altimeter measurement (e.g., LRM mode), the inhomogeneity of the sea state within the altimeter footprint also induces an error visible as a "hump" in the wavenumber spectra of the SLA**. As it also limits the short wavelenght signal observation, the noise error associated to the conventional radar measurement is estimated using the wavelenght range of the hump. The full understanding of this hump of spectral energy Dibarboure et al., (2014) remains to be achieved. This issue is strongly linked with the development of new retracking, new editing strategy or new technology. For the SAR measurement, part of the high frequency signal is characterized by a correlated signal (Figure 9). This signal still needs to be fully explained. At this time, it is considered as an additional unknown signal that is assumed to be a "red noise" error considering the ocean geostrophic signal.

The mean 1 Hz and 5 Hz measurement noise observed for the different altimeters is summarized in . The product SEALEVEL_GLO_PHY_NOISE_L4_STATIC_008_033 gives the normalized **spatial variation of this noise, mainly correlated with high/low wave heights areas**. It was defined using one year of SARAL/Altika measurement and following the spectral decomposition methodology described in Vergara et al. (2019). Note that this product gives an annual mean status of the noise level. It does not take into account the temporal variability of the wave height that modulate the noise, as discussed in Dufau et al. (2016) and Vergara et al. (2019). The spatial distribution of the noise level for each mission is retrieved using the global mean noise amplitude given in (see PUM[13] for details). Figure 10 shows the example for the Jason-3 mission with 1 Hz sampling.

The presence of measurement noise on along-track products limits the observability of the shorter mesoscales. The SLA power spectrum density analysis was used to determine the wavelength where signal and error are on the same order of magnitude (Figure 9). It represents **the minimum wavelength associated with the dynamical structures** that altimetry would statistically be able to observe with a signal-to-noise ratio greater than 1. This wavelength has been found to be variable in space and time (Dufau et al., 2016; Vergara et al., 2022).

The mean observable wavelength with the conventional 1 Hz measurement **was found to be nearly 65 km**. It was defined with a single year of Jason-2 measurements over the global ocean, excluding latitudes

[13] https://catalogue.marine.copernicus.eu/documents/PUM/CMEMS-SL-PUM-008-032-068.pdf

between 20°S and 20°N (mainly due to the limit of the underlying surface quasi-geostrophic turbulence in these areas).

The mean observable wavelength over the Europe area, observed with the regional Europe L3 5 Hz SLA, was found to range between 55 km (Jason-3) to 40 km (S6A) (). These last values were obtained taking into account the unbalanced motion signal as described in Vergara et al. (2022), and using only few months of measurements (April-June2022).

The mean observable wavelength over the global ocean, observed with the Global L3 5Hz SLA, is in the same order as the one observed over the European area (). However, a clear regional pattern is underscored, as shown in Figure 7, and locally the observable wavelength range between ~20 km (Sentinel-6A) and ~more than 100km (HY2B). These values were obtained over the period covering October 2022-July 2023, considering only the dynamical balanced motion and the measurement noise as described in Dufau et al., (2016).

The Observable wavelength will evolve in the future, depending on advances in the determination method and the availability of longer data series.

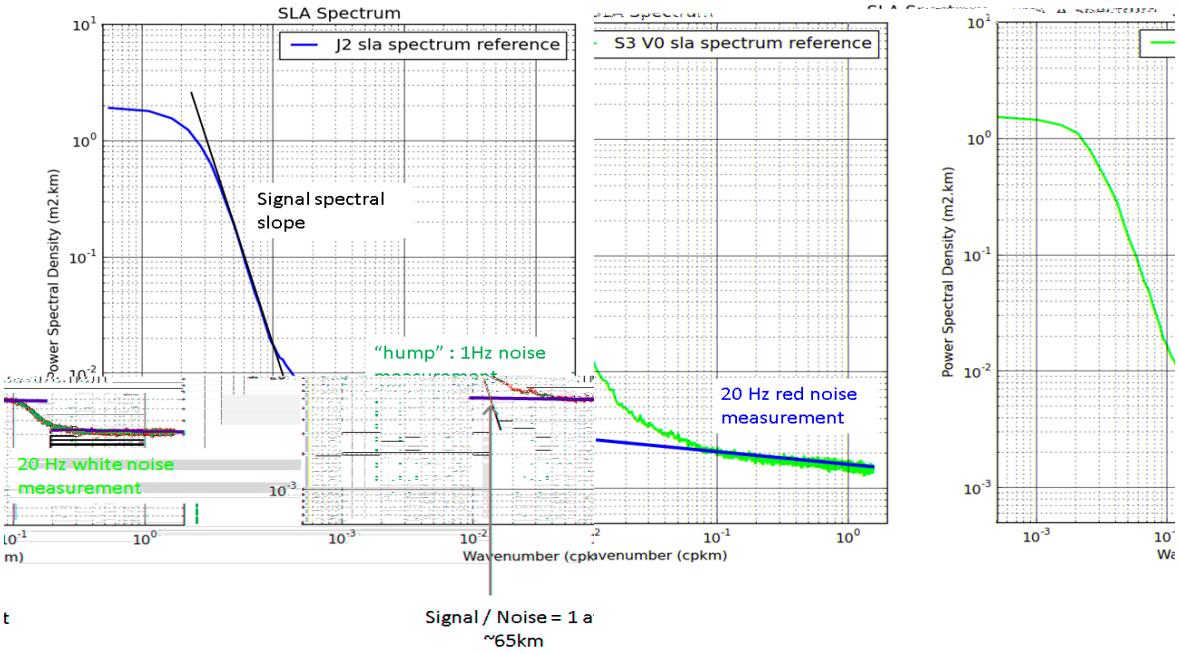

Figure 9 : Mean wavenumber Spectra of Jason-2 (left) and Sentinel-3A (right) SLA over the global ocean. x-axis: Wavenumber (cpkm); y-axis: Power Spectral Density (m^2.km).

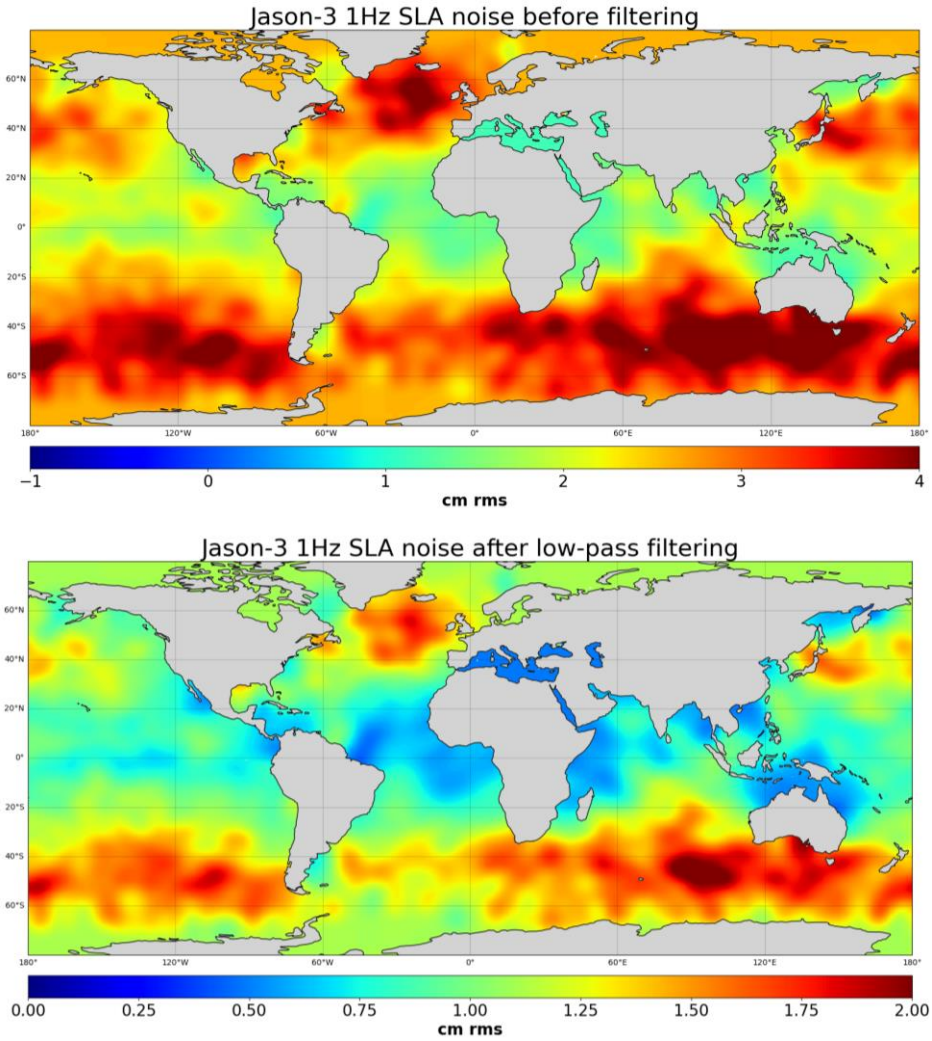

Figure 10: The 1 Hz measurement noise observed along Jason-3 tracks before (top) and after (bottom) along-track filtering processing. Note that the scales are different in each panel; units : root mean square (cm rms).

IV.1.1.2.2 Errors at climatic scales

In the framework of the ESA SL-CCI project, the altimeter measurement errors at climatic scales have been estimated using the Topex/Poseidon, Jason-1, Jason-2 and Jason-3 missions. Details on the error budget estimation at climatic scale can be found in Ablain et al.,(2019) and Guérou et al., (2022). Results are summarized in .

All the parameters/algorithms involved in the altimeter measurement processing can induce errors at climatic scales. However, some parameters contribute more strongly than others. The largest sources of errors for Global Mean Sea Level trend estimation have been identified. They concern i) the radiometer wet tropospheric correction with a drift uncertainty in the range of 0.2~0.3 mm/yr Legeais et al., (2014), ii) the orbit error Couhert et al., (2015) and iii) the altimeter parameters (range, sigma-0, SWH) instabilities Ablain et al., (2012), with additional uncertainty of the order of 0.1 mm/yr over the whole altimeter period, and slightly more over the first decade (1993-2002; Ablain, (2013). Errors of multi-mission calibration (see §II.4.5) also contribute to the Global Mean Sea Level (GMSL) trend error of about 0.15 mm/yr over the 1993-2010 period Zawadzki and Ablain, (2016). All sources of errors described

above also have an impact at the inter annual time scale (< 5 years) close to 2 mm over a 2-5 years period.

The regional sea level trend uncertainty has an average estimate of 0.83 mm/yr with local values ranging from 0.78 to 1.22 mm/yr depending on the regions. These values are only related to the errors of the altimeter instrumental observing system Prandi et al., (2021). The orbit solution remains the main source of the error Couhert et al., (2015) with large spatial patterns at hemispheric scale. Furthermore, errors are higher during the first decade (1993-2002) where the Earth gravity field models are less accurate. Additional errors are still observed, e.g., for the radiometer-based wet tropospheric correction in tropical areas, other atmospheric corrections in high latitudes, and high frequency corrections in coastal areas.

IV.1.1.3 NRT vs REP products

The NRT along track L3 products are usually less accurate than the DT ones. The main sources of divergence come from the different quality of the L2p altimeter products used in input as detailed below:

- The Orbit estimation is usually more precise in delayed time conditions due to more precise environmental model (pole position, solar activity) and different techniques (DORIS; GPS) used in real time or delayed time conditions. This can induce differences of a few centimetres in the Sea level.
- The quality of the Dynamic Atmospheric Correction is improved in DT thanks to a better centring of the filtering windows. For some period, the input atmospheric model can also be improved (ERA Interim reanalysed fields).
- The measurement calibrations (radiometer, altimeter, …) processing are usually more accurate in DT conditions. It is the case for example for the radiometer measurement that can be impacted by drift or significant jump induced by inaccurate NRT calibration processing. Additionally, possible altimeter standard changes in the altimeter L2p products used as inputs of the DUACS processing can induce jump in the SLA field. The management of these jumps, necessary to ensure a seamless transition for the users, is more precise in DT processing.

Additionally, part of the DUACS processing is also less performant in NRT conditions:

- The multi-mission cross-calibration processing (e.g., Orbit Error Reduction (EOR) and Long Wavelengths Error -LWE-; see §II.4.5) is more accurate when using a centred temporal window. This is not possible in NRT processing since measurements in the future are not available.

For these reasons, we do not recommend to use NRT products for climatic scale signal studies (e.g., MSL trend).

IV.1.2 Level-4 gridded

IV.1.2.1 The main sources of errors

The quality of the merged L4 products directly depends on the quality of the L3 products used as input in the L4 processing. Nevertheless, the main source of error comes from the sampling capability of the altimeter constellation. The more altimeters are available, the best is the mesoscale sampling, as discussed in §II.4.7. Another source of error for L4 products is directly linked to the methodologies and parameters applied for SLA interpolation on a regular grid. Optimal Interpolation (see §II.4.7) or the

MIOST mapping approach used in DUACS processing does not allow the restitution of the full dynamical spectrum, limiting the capability of retrieving small mesoscale in L4 products Chelton et al.,(2011, 2014).

IV.1.2.2 Global gridded products

The quality of the global gridded SLA products was estimated by comparison with independent altimeter along-track and tide gauge measurements, with focus on mesoscale signal and coastal signal, respectively. The methodology is fully discussed in Pujol et al., (2016) and Taburet et al., (2019). Here we only summarize the main outcome obtained during the validation of the DT-2024 product version.

Figure 11a presents the RMS of the difference between DUACS-DT2024 sea level anomaly gridded product and independent SARAL-DP/ALtiKa along-track measurements over the period from 2018-01-01 to 2018-12-31 . It illustrates the inhomogeneity of the SLA gridded product error for the mesoscale signal, particularly between low and high variability areas. The SLA gridded product errors for the mesoscale signal () in the open ocean varies between ~1 cm^2, in low variability areas, and up to ~10 cm^2 in high variability areas, where the altimeter sampling does not allow a full observation of the SLA variability. Figure 11b compares the mapping error between the DT2024 and DT2021 reprocessing. A blue pattern indicates a reduction in mapping error, while a red pattern means an increase of mapping error in the new DT2024 reprocessing. Overall, the new reprocessing reduces error except in the inter-tropical band. Compared to the previous version of the products (i.e., DT-2021), this error is significantly reduced (up to 8% in high variability areas). The SLA gridded product errors in the coastal areas (< 200 km) are estimated at 5 cm^2, with higher values in high variability coastal areas. This error is globally reduced by7% compared to the previous version of the products.

It is important to keep in mind that these results are representative of the quality of the gridded products when three to four altimeters are available (see section II.4.3 for the evolution of the altimeter constellation). Degraded results can be observed when only two altimeters are available, since they use minimal altimeter sampling for mesoscale mapping. The comparison with results obtained considering the C3S “two-altimeters” maps over the same period, underscores higher errors at mesoscale for this last product: the additional error reaches nearly 6% in low variability area and up to 40% in high variability areas.

a)

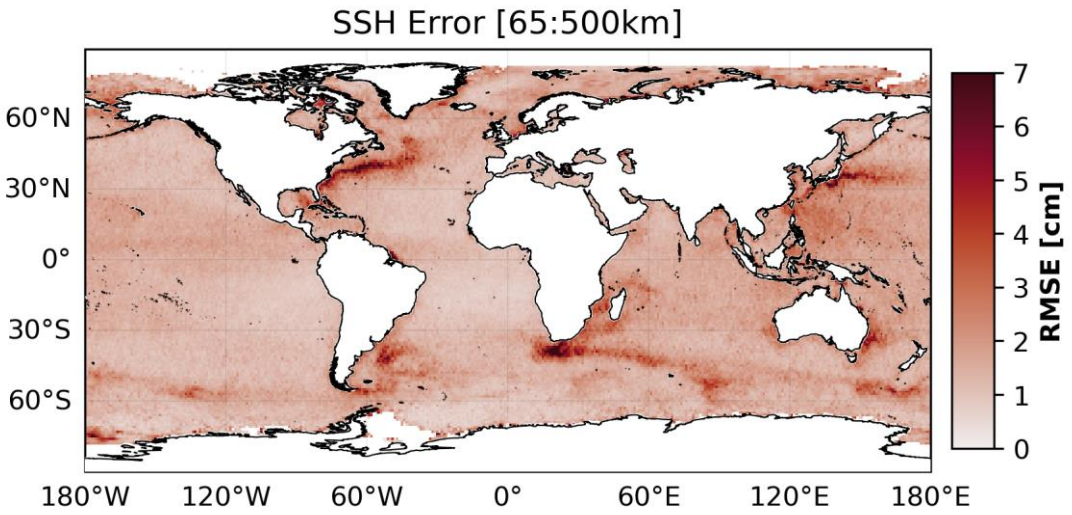

b)

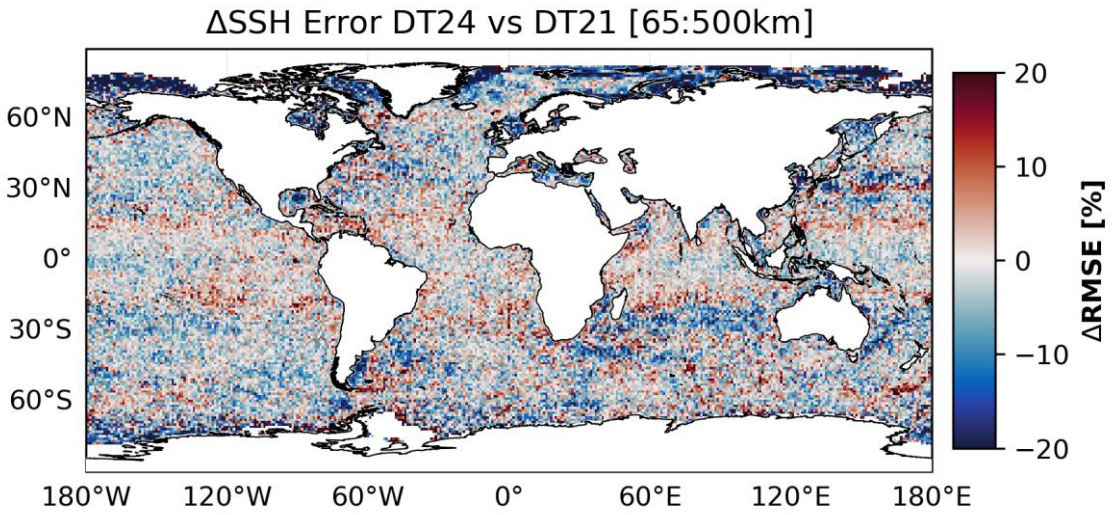

Figure 11: a) RMS of the difference between global gridded DUACS DT-2024 sea level anomaly and independent SARAL-DP/AltiKa along-track measurements over the period 2018-01-01 to 2018-12-31 (units: cm); and b) difference in RMSE (as percentage) between DUACS-DT2024 and DUACS-DT2021 global gridded products. Negative values (i.e., blue colour) indicates a reduction in the error of DUACS-DT2024 products.

Tide Gauges (TG) from the GLOSS/CLIVAR network have been used for SLA gridded products validation over the Global Ocean and for the period 1993-2020. Figure 12a presents the RMS of the difference between DUACS-DT2024 sea level anomaly gridded product and independent TG dataset. It also illustrates the inhomogeneity of the SLA gridded product error in coastal area. The SLA gridded product errors vary between ~1 cm to more than 10 cm. The comparison of altimeter SLA and independent TG measurement shows improved results when the altimeter product DT-2024 version is considered rather than the previous one (DT-2021) (Figure 12b). The variance of the differences between altimetry and TG is especially reduced in western coasts (US, EU,), part of the European coasts and main part of island coasts in the different oceans. In those regions, the reduction in the variance of the differences between altimetry and TGs ranges between 0.2% to more than 5 % of the TG signal. In some other coastal areas,

degradation is however observed. This is the case along the US eastern coast, where the differences between altimetry and TG reaches less than 1% of the TG signal.

a)

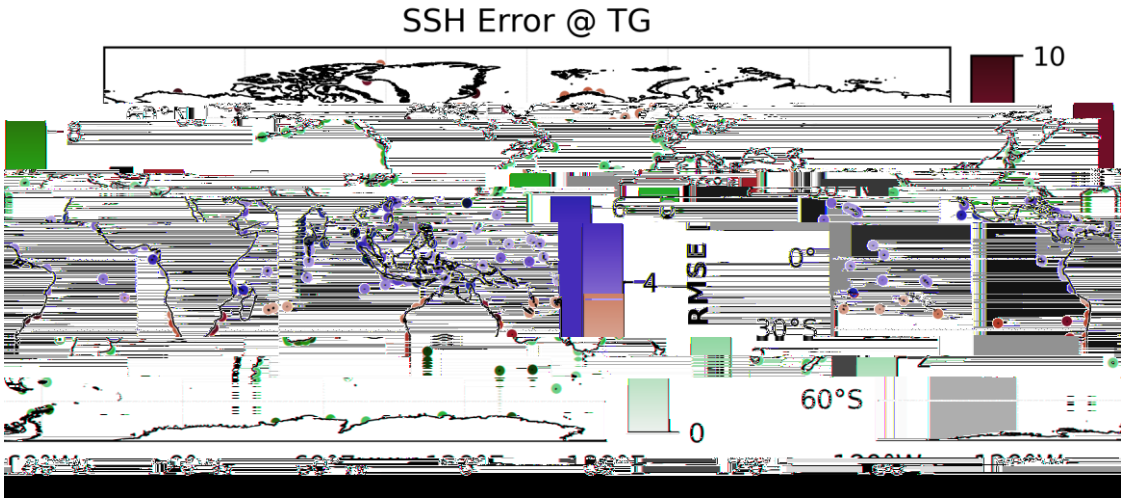

b)

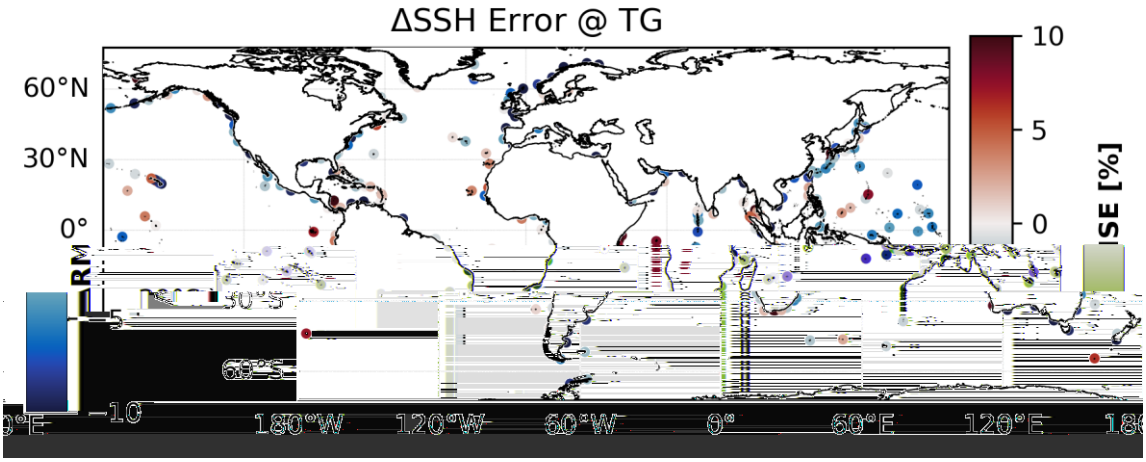

Figure 12: a) RMS of the difference between global gridded DUACS DT-2024 sea level anomaly and independent tide gauge measurements over the period 1993 to 2020 (units: cm); and b) difference in RMSE (as percentage) between DUACS-DT2024 and DUACS-DT2021 global gridded products. Negative values (i.e., blue colour) indicates a reduction of error in DUACS-DT2024 products

The errors observed on mesoscales also highlight the L4 product spatial resolution capability. As discussed in Pujol et al. (2016), the SLA gridded product effective resolution is constrained by the altimeter sampling capability and mapping methodology used. In order to estimate the spatial resolution of the gridded products, an evaluation has been carried out based on a spectral approach. Full description of this approach can be found in Ballarotta et al. (2019).

Figure 13a) shows the global map of the effective spatial resolution of the DT-2024 global maps computed over the period from 2018-01-01 to 2018-12-31, where Saral/AltiKa data were used as an independent dataset. The resulting mean spatial resolution of the global gridded SLA is slightly less than

200 km at mid-latitudes (see Estimated Accuracy Number in Section I.3), with larger values near the Equator (~500km) and finer values at the poles (~100km) The comparison with the spectral content computed from full-resolution Saral/AltiKa 1 Hz along-track measurements (not reported here) shows that a large part of the energy observed in along-track measurements at wavelengths ranging from 200 to 65 km is missing in the SLA gridded products. The loss reaches nearly -40% at wavelength 200 km and rapidly increase at shorter wavelengths. It is important to note that this evaluation has been made using from four to five satellites (Jason-3, Jason-2, Cryosat-2, Sentinel-3A, and HY-2A). Depending on the time period, the number of altimeters in the constellation evolved and so as the spatial resolution. The comparison of the performances with a two-satellites merged map series (i.e., C3S product line) shows that the observable wavelengths are globally increased by 10-12% when the constellation is reduced. Overall, the DT2024 SLA gridded products are finer (up to 10% finer) than the DT2021 reprocessing as illustrated in Figure 13b.

a)

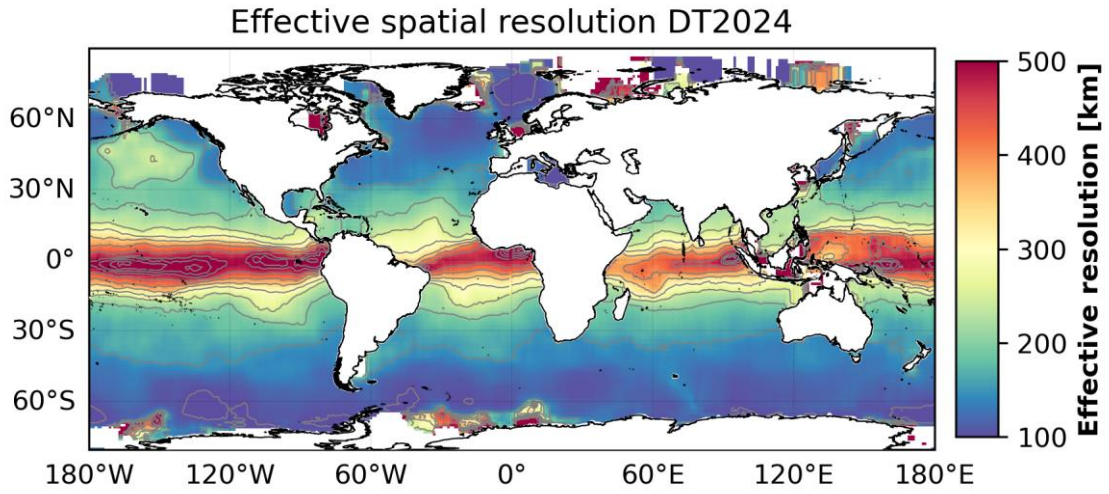

b)

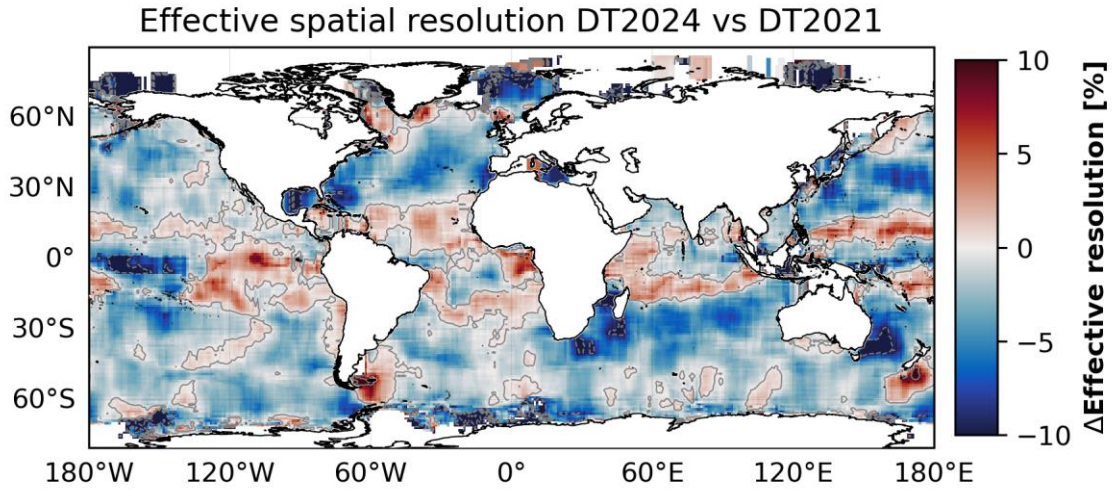

Figure 13: a) Effective spatial resolution (wavelength in km) of the DUACS-DT2024 global maps; and b) Gain(-)/loss(+) of effective resolution between DUACS-DT2024 and DUACS-DT2021 gridded products. Negative values (i.e., blue colour) means finer resolution in DUACS-DT2024 than in DUACS-DT2021.

IV.1.2.3 Regional gridded products

The quality of the regional gridded SLA products was estimated by comparison with independent altimeter along-track data. The methodology is fully discussed in Pujol et al. (2016). We summarize here the main outcomes.

presents the SLA gridded DT-2024 product errors for the total signal in Europe. This error is estimated through the variance of the SLA differences between the gridded product and independent along-track measurements. It reaches around 15-18 cm² in the three different areas considered (i.e., areas covering the three main basins that are considered for the European Sea products): Black Sea, Mediterranean Sea and Atlantic Ocean (see Figure 14a for the regional pattern of the error). It appears that, compared to the previous regional version (DT-2021), the error remains nearly constant over the Black Sea whereas the errors are reduced over the Mediterranean Sea (~20%) and the Atlantic basin (~10%). The regional pattern of the reduced error variance is illustrated in Figure 14b. The regional gridded product has been tuned for mesoscale in the Mediterranean Sea compared to the global one. Figure 15 shows the SLA difference variance reduction between gridded and independent along-track product when comparing regional and global grid performance. The error is reduced by nearly 5% over the Mediterranean Sea.

As presented in the previous chapter, the SLA gridded product effective resolution is constrained by the altimeter sampling capability and mapping methodology used. An evaluation, based on a spectral approach, has been carried out to evaluate the spatial resolution of the regional gridded product. A full description of this approach can be found in Ballarotta (2019). Figure 15 shows the effective spatial resolution of the DT-2024 regional-Europe gridded product computed over the period 1 January 2018–31 December 2018, where AltiKa data were used as an independent dataset. The resulting mean spatial resolution of the regional-Europe gridded SLA is slightly less than 150 km (120 km for the Mediterranean Sea and 125 km for the Black Sea, see Estimated Accuracy Number in Section I.3). Although the DT2024 and DT2021 regional-Europe maps have similar mean effective spatial resolution, regional investigation highlights ∼10 % improved resolution in DT2024 in the Atlantic basin and central Mediterranean Sea. Degradation is found in the Black Sea region.

It is important to note that this evaluation has been made using from four to five satellites (Jason-3, Jason-2, Cryosat-2, Sentinel-3A, and HY-2A). Depending on the time period, the number of altimeters in the constellation evolved as well as the spatial resolution

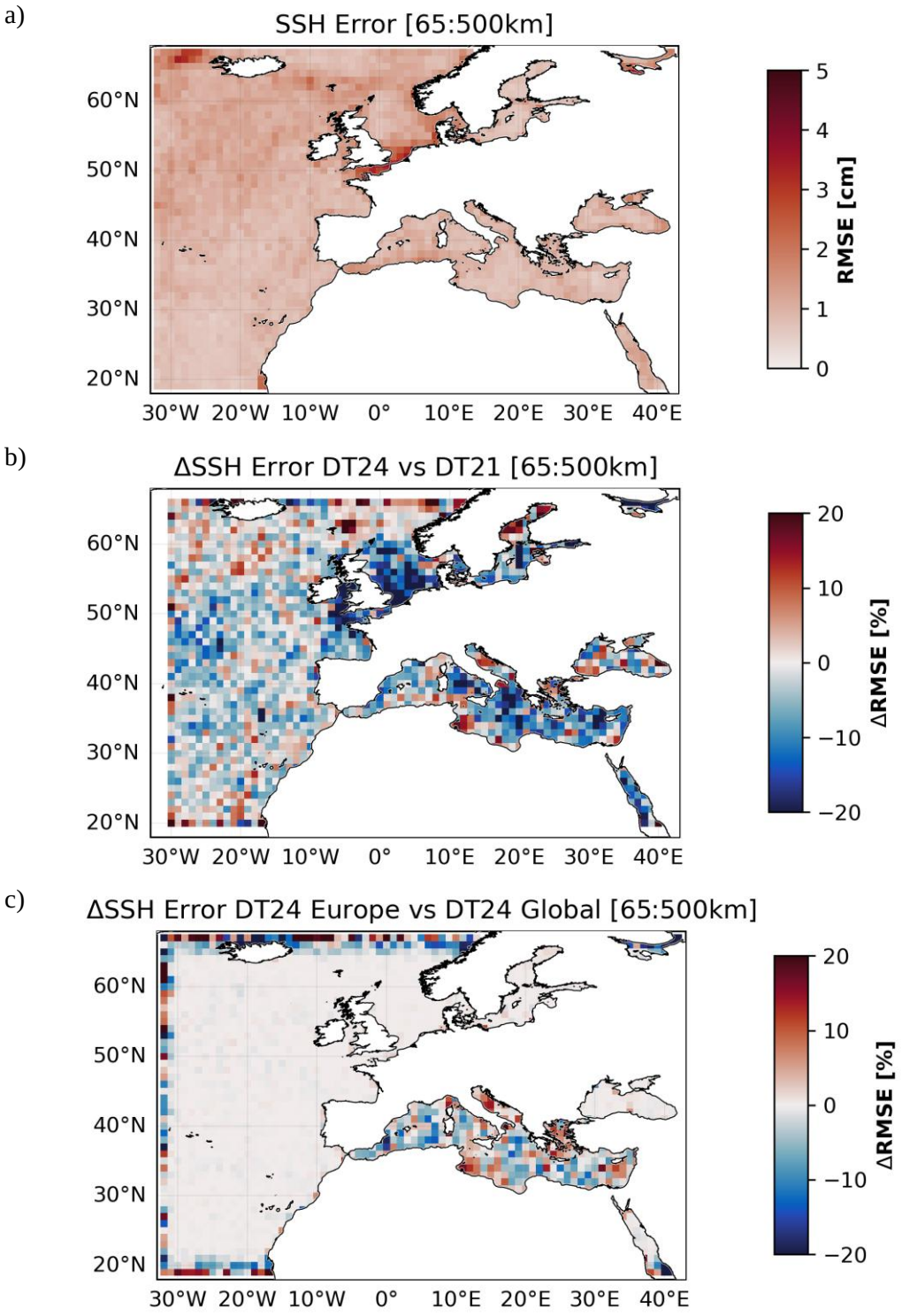

Figure 14: a) RMS of the difference between regional gridded DUACS DT-2024 sea level anomaly and independent SARAL-DP/AltiKa along-track measurements over the period 2018-01-01 to 2018-12-31 (units: cm); b) Difference of RMSE between DUACS-DT2024 and DUACS-DT2021 regional gridded products. Negative values (i.e., blue colour) indicates a reduction of error in DUACS-DT2024 products; and c) Difference in RMSE between DUACS-DT2024 regional and global gridded products. Negative values (i.e., blue colour) indicates a reduction of error in DUACS-DT2024 regional products (continues in next page).

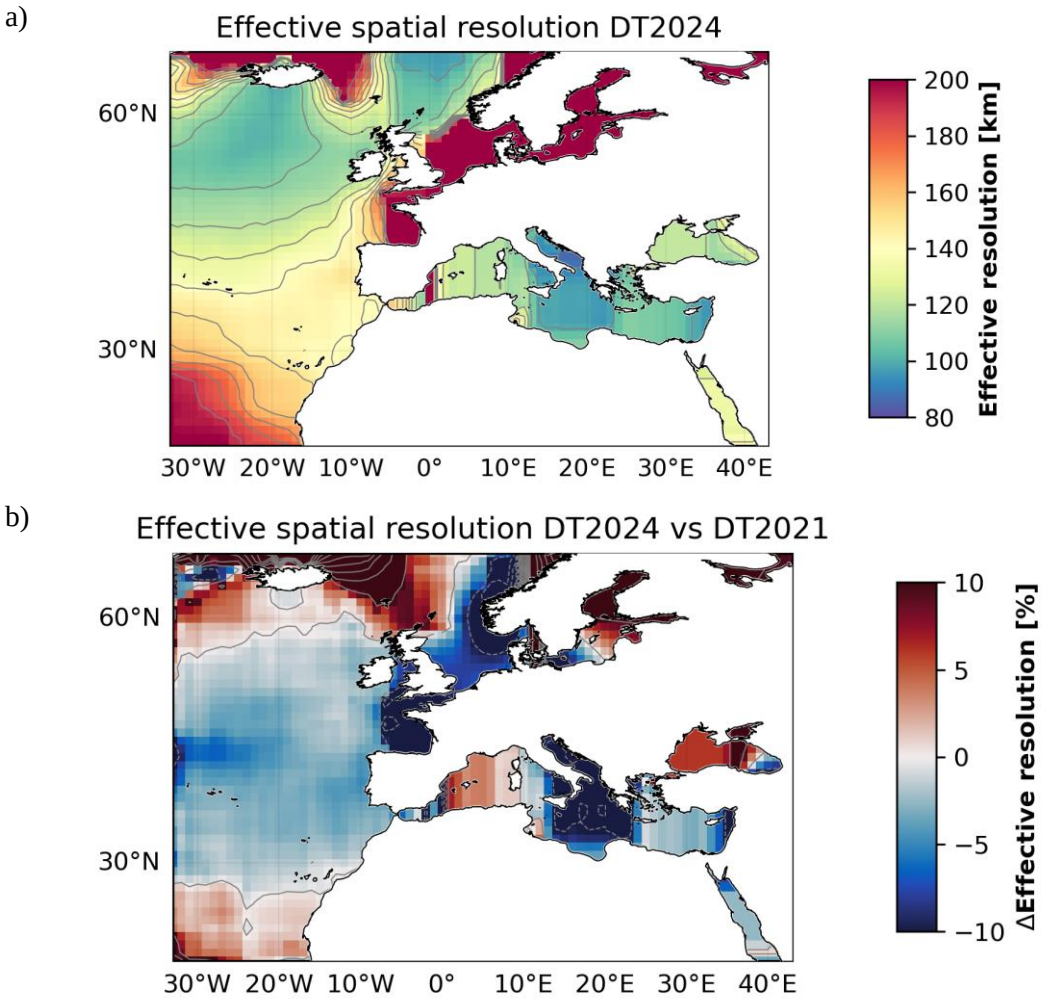

Figure 15 : a) Effective spatial resolution (wavelength in km) of the DUACS-DT2024 regional-Europe gridded product; and b) Gain(-)/loss(+) of effective resolution between DUACS-DT2024 and DUACS-DT2021 gridded products. Negative values (i.e., blue colour) means finer resolution in DUACS-DT2024 compared to DUACS-DT2021.

IV.1.2.4 NRT vs REP products

The NRT gridded L4 product are usually less accurate than the DT one. Different factors explain this degradation:

- The reduced accuracy of the different parameter and corrections applied for SLA computation as discussed in §IV.1.1.3
- The availability of altimeter measurements, potentially reduced in NRT condition due to problems on platforms or ground segment, usually retrieved in DT conditions.
- The uncentred temporal window used in NRT L4 processing, since measurements in the future are not available, reducing the amount of data by a factor of the order of 2, compared to the DT conditions.

The last one is considered as the main source of errors for mesoscale signal reconstruction in L4 NRT products as discussed in Pascual et al. (2006). These authors showed that at least four altimeters are required in NRT conditions to retrieve the same accuracy as the DT products generated with only two altimeters.

IV.2 Variable ADT=SLA+MDT

The quality of the ADT field is directly depending on the quality of the SLA and MDT fields (see §II.3). The SLA error budget is described in the previous chapter. The quality of the MDT fields used in the DUACS processing is described in MDT specific QUID document [14] for products 008-063, 008-066 and 008-067.

IV.3 Variable UV

The absolute surface currents in the product are calculated using the principle of geostrophy from gridded SLA/ADT products (see §II.4.7.3 for instance). The quality of these products strongly depends on the quality of the SLA/ADT field and on the methodology used to estimate the derivate.

IV.3.1 Level-3 along-track

The geostrophic currents defined in the across-track direction were validated using a qualitative comparison with gridded fields (Level-4) and by analysing the spectral content of the stream. The qualitative comparison shows a good agreement between the current deduced from Level-3 and Level-4 products, especially at large and medium scales. Some differences are observed at small mesoscales, that are not accurately reproduced by Level-4 product. Qualitative comparison with independent sea surface temperature a/o chl-a concentration shows that some of the small structures observed in the L3 product seem to correspond to the signature small mesoscale structures (see an example in Figure 16).

a) b)

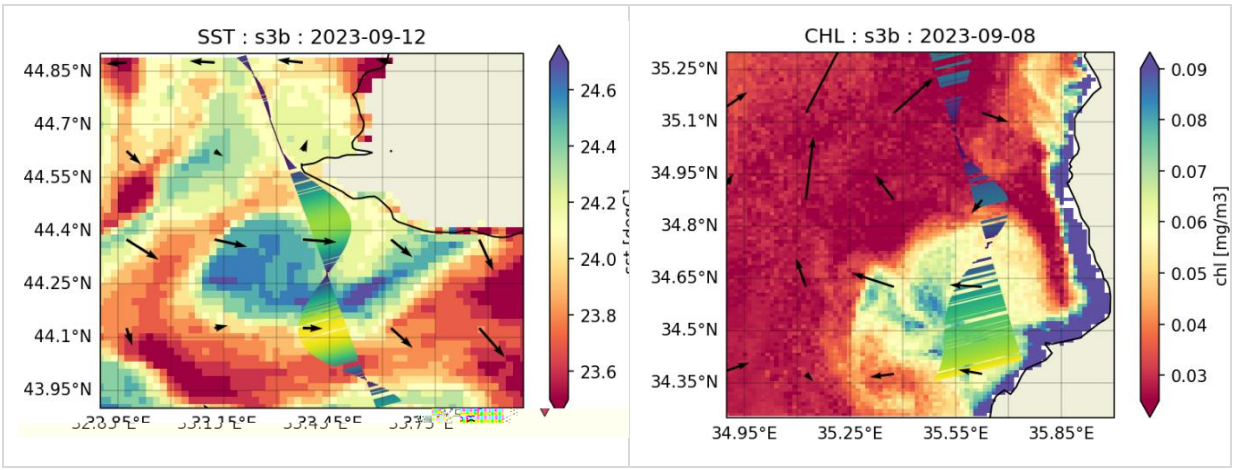

Figure 16: Example of small mesoscale (< 50km diameter) structure underlined with a) Sea Surface Temperature (SST) in the Black Sea; and b) Chl-a field (background map) in the East Mediterranean Sea, and geostrophic current defined along the L3 5Hz track (coloured bars) of Sentinel-3B. Black arrows correspond to the geostrophic current defined in the L4 product.

[14] https://catalogue.marine.copernicus.eu/documents/QUID/CMEMS-SL-QUID-008-063-066-067.pdf

The spectral content of the current in the across-track direction clearly shows the dynamical signal at mesoscale (Figure 17). In the mid-latitudes area, the spectral slope observed is around K^{-2} , that it is consistent with the Surface Quasi Geostrophic (SQG) theory Held et al., (1995). This dynamic dominates at wavelengths up to ~100km. Down to this wavelength, the quality of the geostrophic current is degraded. Indeed, another spectral slope, in the order of $K^{+0.2}$ to $K^{+0.6}$ appears. The content of the currents at these wavelengths is still under investigation. However, this positive spectral slope may be interpreted as the signature of residual measurement noises are still significant at these wavelengths and then affect the estimation of the current. Nevertheless, the spectral slope observed is too low to be explained only by measurement noise. At small wavelengths, the kinetic energy falls drastically. This is induced by the low-pass filtering applied on SLA before geostrophic current estimation (see section II.4.6). The wavelengths impacted depending on the area and mission considered.

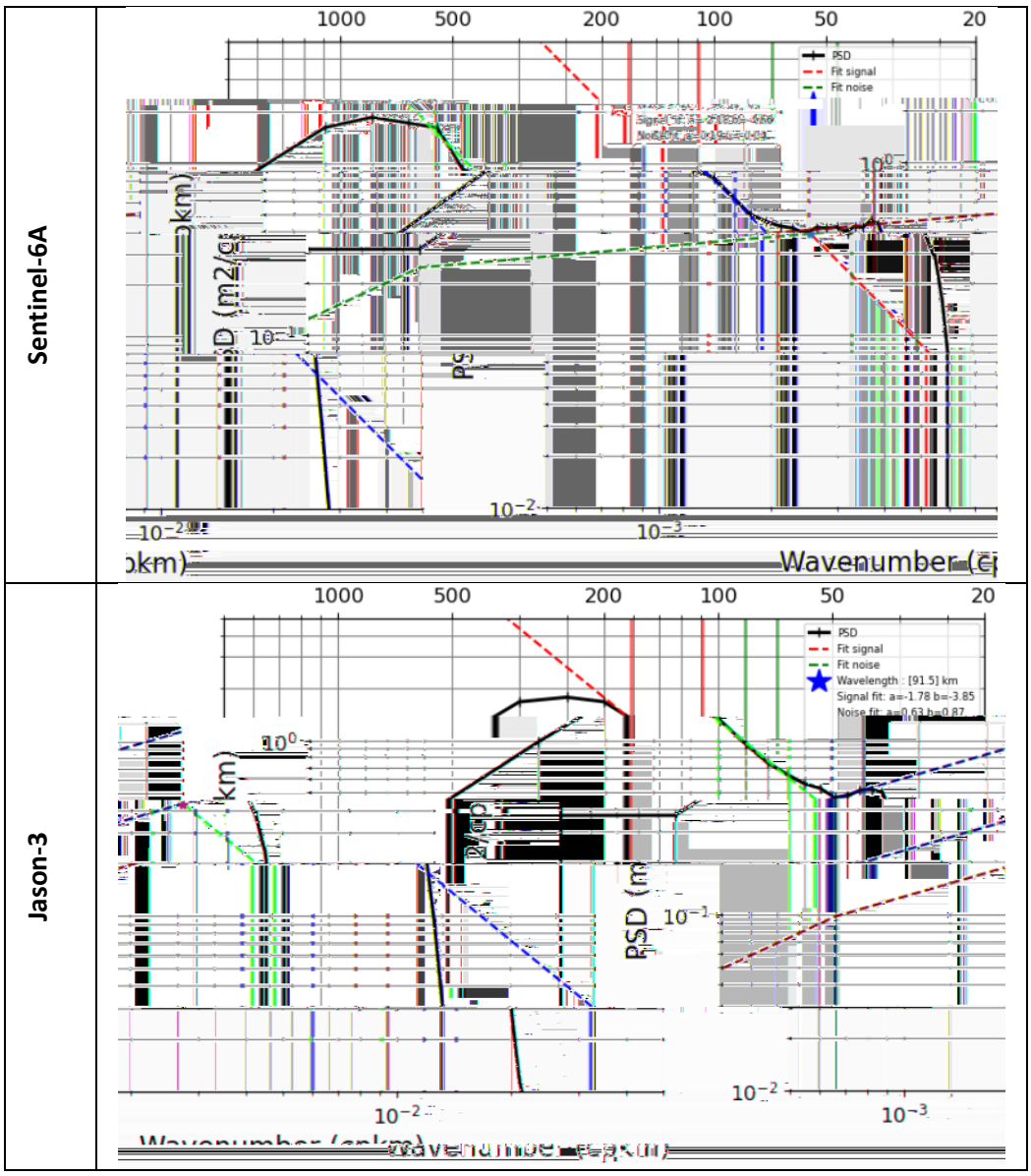

Figure 17: Power Spectral Density (PSD)of the geostrophic current in the across-track direction over the north-east Atlantic area for Sentinel-6A (top) and Jason-3 (bottom).

IV.3.2 Level-4 gridded

IV.3.2.1 REP/DT products error description

IV.3.2.1.1 Global product

The comparison with drifter measurements gives an indication of the errors on geostrophic current products. The methodology used for this comparison is described in Pujol et al., (2016).

The distribution of the speed of the current (not provided in this document) shows a global underestimation of the current in the altimeter products compared to the drifter observations, especially for currents with medium and strong intensities (> 0.2 m/s). Figure 18 shows the zonal and meridional RMS differences in 5°x5° grid cells between AOML drifters and absolute geostrophic current products over the period 1993-2020. The equatorial band was excluded from the analysis since the geostrophic approximation do not lead to an accurate estimation of the currents in this area. Elsewhere, the RMS of the differences is around 11cm/s (11.4 cm/s for zonal, 10.7 cm/s for meridional components, respectively). Locally, the RMS of the differences is higher and it reaches more than 15 cm/s over high variability areas.

The difference with the previous version of the products (DT2021 standards) is shown in Figure 19. A reduction of the error is found mainly at mid-latitude (5-10%), while larger error are found in the inter-tropical area.

a)

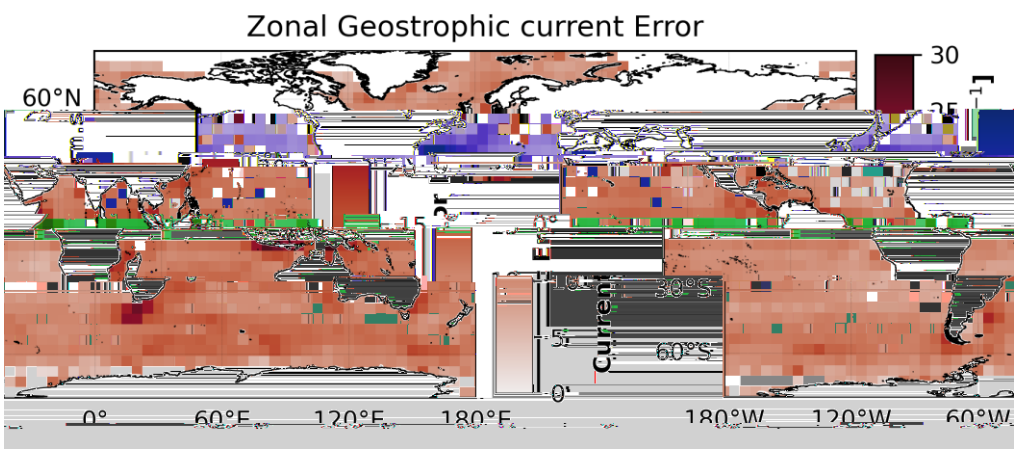

b)

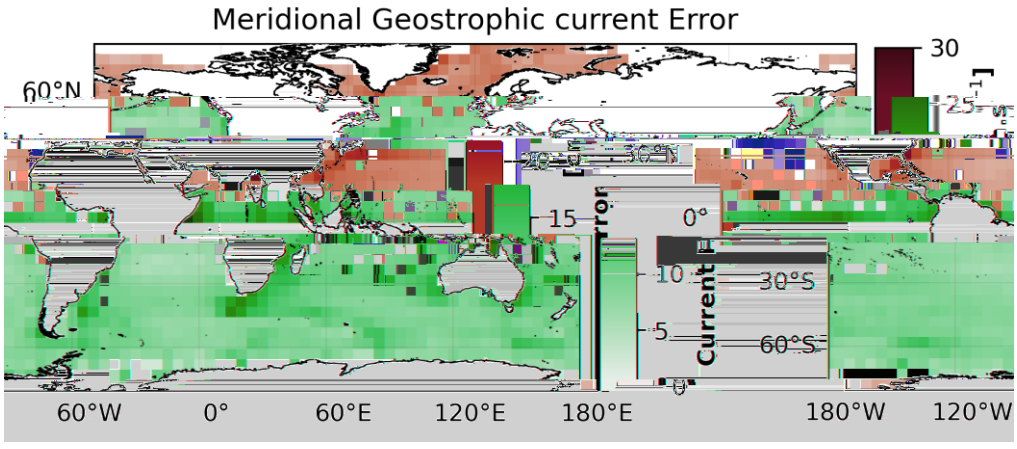

Figure 18: a) Zonal and b) meridional RMS of the difference between DUACS-DT2024 geostrophic current and drifter's measurements over the period 1993-2019 (units: cm/s).

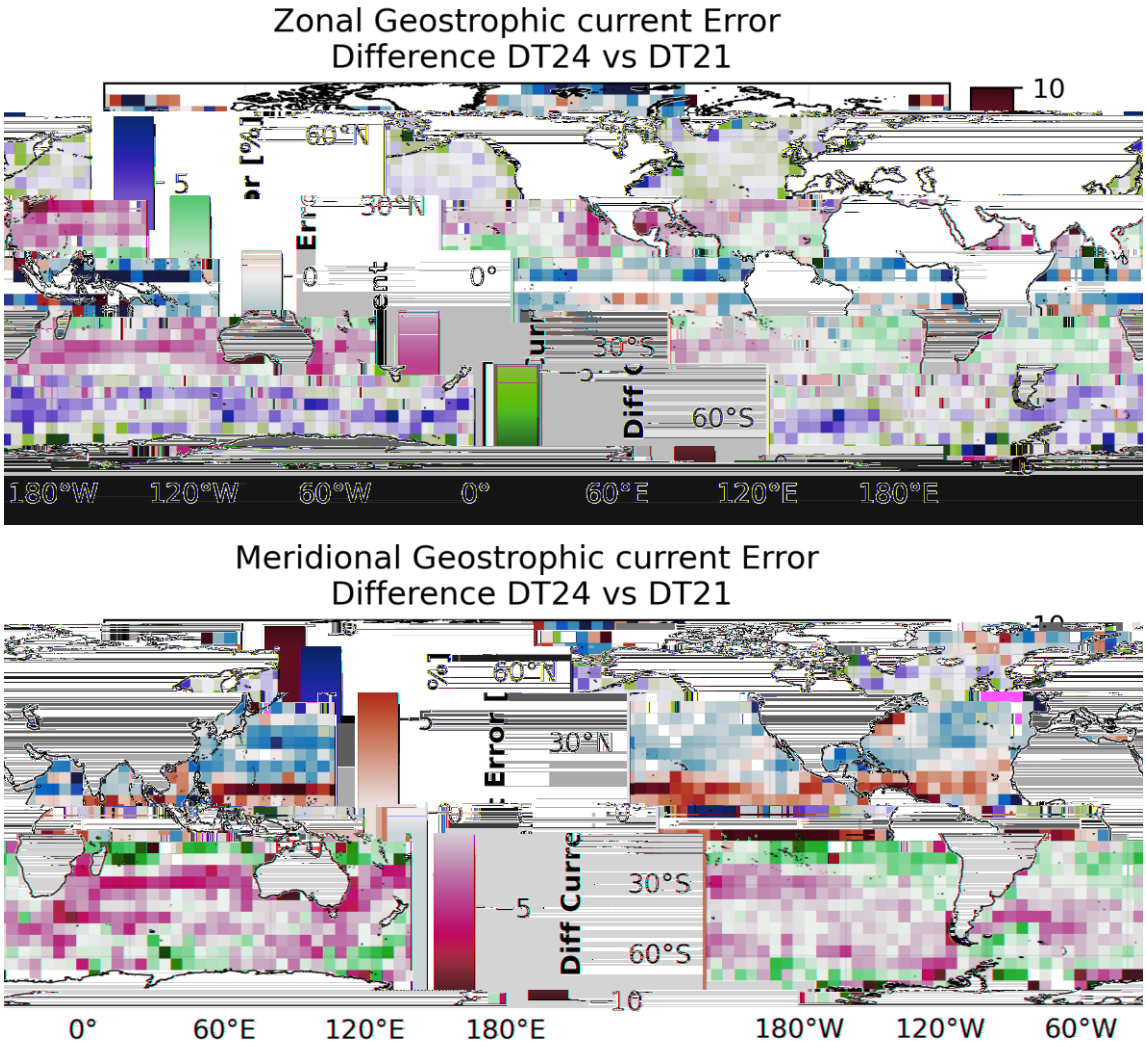

Figure 19: Zonal (top) and meridional (bottom) difference in RMSE between DUACS-DT2024 and DUACS-DT2021 gridded geostrophic current products (units: %). Negative values (i.e., blue colour) means a reduction in the error of DUACS-DT2024 products.

IV.3.2.2 NRT vs REP/DT products

As discussed in §IV.1.2.4, the quality of the NRT products is reduced in NRT conditions. The quality of the SLA and derived geostrophic current computed in NRT conditions is more sensitive to the constellation changes compared to the DT conditions. In that way, changing from two to four altimeters constellation contributes to a reduction in the RMS of the difference between altimeter NRT product and drifter current measurement by 13% (zonal component) to 19% (meridional component) in areas of high variability (equatorial band excluded) Pascual et al.,(2009).

V SYSTEM'S NOTICEABLE EVENTS, OUTAGES OR CHANGES

This section is dedicated to describe and track changes that may occur in the current operational system including changes due to outages (data gaps), upstream data (e.g., addition or loss of a sensor, inclusion/removal of in-situ platforms), reprocessing, corrections, assimilated data, boundary conditions, among others, which may impact the product quality.

V.1 NRT 1 Hz & 5 Hz sub-system version changes

Table 19: Overview of the main improvements implemented in the NRT 1 Hz and 5Hz processing.

Date	DUACS version	Posting -rate	Change description
Apr-2017	17.0	1Hz	Sentinel-3A introduced in DUACS processing
Oct-2017	17.1	1Hz	OSTM/Jason-2 Long Repeat Orbit introduced in DUACS processing
Mar-2018	18.0	1Hz	New Mean Profile for Jason-3 and updated mapping parameters
Sep-2018	18.1	1Hz	New Orbit Standards for Jason-3
Sep-2018	18.2	1Hz	New upstream products for Cryosat-2
Apr-2019	18.4	1Hz	Sentinel-3B introduced in DUACS processing Use of new Sentinel-3A Hybrid Mean Profile New Europe L4 product
Dec-2019	18.4.2	1Hz	New MDT used for Global and regional Processing
Jan-2020		1Hz	SARAL/AltiKa new GDR-F standard
Jul-2020	18.4.5	1Hz	HY-2B introduced in DUACS processing Use up-to-date standards for Ocean and Pole tide correction
Oct-2020	18.7.0	1Hz	Jason-3 GDR-F standards change Use a new MDT for regional Europe production
May-2021	18.7.1	1Hz	Use a new MDT for regional Europe production
Dec-2021	19.0.0	1Hz	DT-2021 standards uniformization: - Use new Internal-tide correction - New MSS and Mean profiles - New MDT - Use improved mapping parameters - Improved LWE correction - NetCDF format change
Apr-2022	19.1.0	1Hz	Sentinel-6A introduced & Jason-3 deactivated in DUACS processing
May-2022	19.2.0	1Hz	Jason-3 on its new interleaved orbit reintroduced in DUACS processing
Nov 2022	1.0.0	5Hz	Start of the L3 5 Hz production over the Europe area (new DUACS-NG system used)
Nov-2023	-	1Hz	The L3 1Hz production shifted on a new system (DUACS-NG), used full-rate 20Hz upstream when available (same system as for L3 5Hz production)
Nov 2023	2.0.0	5Hz	▪ Start of the L3 5 Hz production over the Global Ocean ▪ Ensure the L3 1Hz production using full-rate 20Hz upstream when available Use SWOT-Nadir measurements

Date	DUACS version	Posting -rate	Change description
Jul-2024	3.0.0	1Hz & 5Hz	Change of the altimeter standards: Ocean tide and MSS
Nov 2024	4.0.0	1Hz & 5Hz L4	Change of the mapping method change of the formal mapping error estimation; change of the geostrophic current method; change of the L4 product grid; change of the MDT

V.2 Main constellation events impacting the NRT data availability

Different events can lead to a reduction of data availability. Among these, the most common events are the following:

- A change in the altimeter constellation: either the loss or the introduction of an additional altimeter in the constellation directly impacts the number of altimeter measurements available.
- For a specific platform, a reduction in the number of altimeter measurements available as inputs of the DUACS system processing. This can be linked to an anomaly onboard the platform or on the ground segment, preventing the data reception and impacting the L0 to L2 processing. It can also be induced by a degraded acquisition of the DUACS system that can be induced by missing upstream products and/or auxiliaries (e.g., various geophysical corrections specifically updated at L3)
- An increase of invalid measurements used as inputs of the DUACS system processing. This is usually linked to specific platform events (e.g., manoeuvres), but can also be induced by L0-L2 processing anomalies or specificities. In some rare cases, degraded acquisition by the DUACS system can also lead to a bad data selection.

In December 2023, eight altimeters constitute the altimeter constellation available in NRT 1H:

- Sentinel-6A (S6A) was introduced in the DUACS system in April 2022. It is the reference mission (Jason-3 previously reference mission).
- Jason-3 was temporarily deactivated from the System in Apr 2022 (same orbit than Sentinel6A). It was reactivated on May 2022, once on its new interleaved orbit.
- Sentinel-3A (S3A).
- Sentinel-3B (S3B).
- SARAL-DP/AltiKa (AL). Since February 2019, miss-pointing anomaly leads to a significant reduction of valid measurements. Due to the risk of degradation of the DUACS production, the mission was deactivated from the system starting from 2019/02/04. The mission was reactivated in October 2019 after adding new editing procedures to remove miss-pointing anomalies.
- Cryosat-2 (C2): The last important event occurred during summer 2014, when a processing anomaly induced an important number of L2 missing measurements. These measurements were reprocessed afterward.
- HaiYang-2B (HY-2B).
- SWOT-nadir: introduced in the DUACS system in November 2023.

0 summarizes the main events affecting data availability in NRT conditions.

Table 20: Main events affecting the data availability in NRT conditions.

Date	Platform	Event
2020/01/31-2020/02/13	J3	The mission entered in safe hold mode. The Sentinel-3A mission is used as temporary anchor mission for cross-calibration processing from 2020/02/06 to 2020/03/03
2020/06/15-2020/06/23	J3	The mission entered in safe hold mode
2020/07/07	HY-2B	HY-2B is introduced in DUACS NRT processing
2020/11/30-2020/12/04	HY-2B	No upstream measurement available
2021/08/16-2021/08/17	HY-2B	No upstream measurement available
2020/07/15-2020/10/29	C2	The processing of the C2 mission was inhibited, time to manage an orbit change for this mission
2022/04/06	S6A	Sentinel6A (HR measurement) is introduced in DUACS NRT processing
2022/04/06 - 2022/05/24	J3	The processing of the mission was inhibited, time to manage an orbit change for this mission
2022/10/09-2022/10/11	HY-2B	No upstream measurement available
2022/10/11	AL	No L3 measurement available
2022/11/17-2022/12/02	S6A	Various sections of tracks are missing in upstream products.
2022/12/30- 2023/01/08	AL	
2023/04/30-2023/05/05	S3A & S3B	Data available with few days delay due to missing L0 inputs from the Marine PDGS (Payload Data Ground Segment)
2023/0731-2023/08/05	H2B	Data unavailability due to satellite manoeuvre
2023/11/30	SWON	SWOT-nadir is introduced in DUACS NRT processing
2024/05/11-2024/05/17	H2B	Data unavailability

V.3 Recent NRT 1 Hz & 5Hz sub-system evolutions overview

V.3.1 Apr 2022: DUACS 19.1.0: Sentinel-6A in DUACS processing

The Sentinel-6A mission was launched on November 21st 2020. It is designed to provide continuity to TOPEX/Poseidon, Jason-1, OSTM/Jason-2 and Jason-3 missions. The mission is based on the same orbital features and its geographic coverage is 66°S - 66°N. With the DUACS 19.1.0 version, Sentinel-6A was introduced in the SL-TAC system as the new reference mission instead of Jason-3. The introduction of Sentinel-6A is effective since April 6th 2022 (Near Real Time production). On the same day, Jason-3 was temporary deactivated from the DUACS system. This mission will be shifted in an interleaved orbit and reintroduced in the system afterwards.

Sentinel-6A is operating in two different modes:

- Low Resolution (LR) mode: based on an LRM instrument as the one used for Jason-3.
- High Resolution (HR) mode: based on SAR technology as the one used for Sentinel-3A/B.

The first year of measurement is done in the formation flight, where Sentinel-6A and Jason-3 are acquiring data using the same ground track separated by few seconds. This step allows the complete quality and validation assessment of the mission (CalVal; summary Cal/Val maturity matrix provides an overall summary of the quality assessment results).

Sentinel-6A measurement with HR mode are consistent with Jason-3 measurements. Few differences can be observed linked to the capabilities of the different instruments. With the SAR technology,

Sentinel-6A shows reduced errors at small-mesoscale level (see also section IV.1.1.2.1). The residual noise observed with Sentinel-6A HR is nearly 60% lower than the one observed on Jason-3 (estimation done on 1 Hz measurement over the Nov-Dec 2021 period) (Figure 20). Nevertheless, its capability to ensure the continuity of the MSL signal still need to be assessed. The HR mode measurement will be used in NRT L3/L4 processing.

Some SLA biases are however observed between Sentinel-6A and Jason-3. A mean global bias between STC measurements of the two missions is estimated to be 5.7 cm. Large-scale patterns are also observed at regional extent (Figure 21). They range ±1cm and vary with time. Different bias corrections are implemented at L2P and L3 processing step in order to ensure a smooth transition between Jason-3 and Sentinel-6A measurements. The global mean bias will be fully corrected. The regional biases will be progressively introduced into the NRT products.

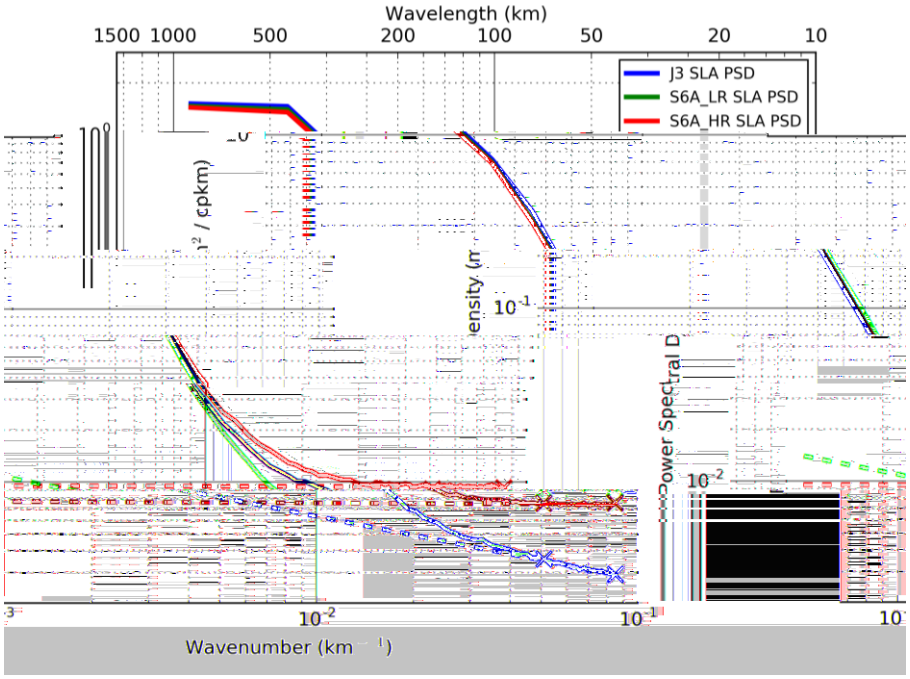

Figure 20: SLA 1 Hz Power Spectral Density (PSD) (solid lines) for Jason-3 (blue) and Sentinel-6A in LR (green) and HR mode (red). Estimated on 1 Hz measurement over the Nov-Dec 2021 period. Dashed lines underscore the white/red noise level observed on 1 Hz measurements and the crosses delimitate the fitting interval to estimate the noise level plateau/slope.

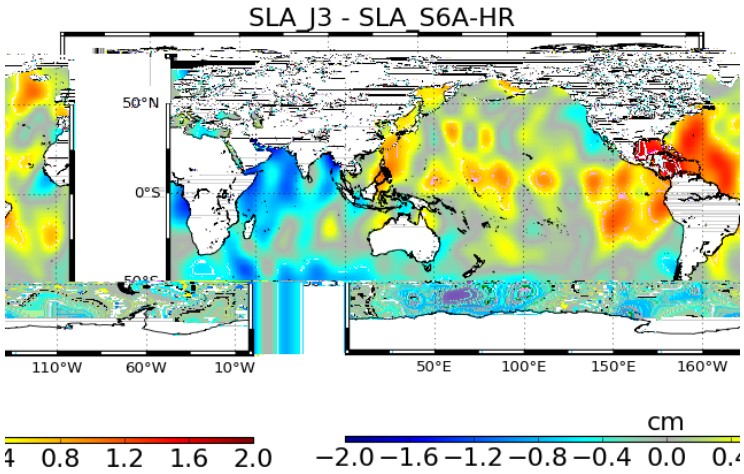

Figure 21: Regional pattern of the differences in SLA between J3 and S6A HR STC measurements. Estimation done over nearly 45 days of measurements from February 6th to March 23rd 2022. Note that this pattern will likely vary according to the temporal period considered.

V.3.2 May 2022: DUACS 19.2.0: Jason-3 orbit change

The satellite Jason-3 was moved to an interleaved orbit. The orbit manoeuvrers started on April 7th 2022, at the end of cycle 226 which was the last Jason-3 cycle on the nominal ground track. Jason-3 was slowly moved away from its successor Sentinel-6A. The final interleaved orbit was reached on April 25th 2022 and the first cycle of measurement was numbered 300.

Jason-3 was reintroduced in the SL-TAC system after the end of the orbit change manoeuvres, increasing the number of altimeters in the constellation. The impact for the users was that measurements were available from seven altimeters, with an additional dataset corresponding to the Jason-3 measurement on its interleaved orbit. The Jason-3/Sentinel-6A interleaved duo is optimized for mesoscale and circulation observation as previously discussed in Dibarboure et al., (2011) for the Jason-1/Jason-2 tandem. This improved sampling will contribute to improve the quality of the SLA gridded products (Level4 products).

The measurement errors of Jason-3 on its new orbit are expected to be the same as on its historical repeat orbit.

Due to technical issues, the Jason-3 measurements on it interleaved orbit will be first disseminated in the same dataset ("j3") as for previous measurements. From July 5th 2022, a new dataset "j3n" will be introduced to identify Jason-3 measurement on its new orbit. All historical measurements processed since the mission is on the interleaved orbit are deferred in this new dataset.

V.3.3 November 2022 - DUACS-NG 1.0.0: Start of the L3 5 Hz production over the Europe area

On November 29th 2022, new datasets will be added to the NRT catalogue. They consist in L3 along-track measurements delivered with nearly 1 km sampling resolution (i.e., 5 Hz) over Europe. These L3 5 Hz datasets allow us to resolve wavelengths from ~40 km (S6A) to ~55 km (J3) depending on the altimeter considered (10). This is a first estimation of the observable wavelengths for mesoscale signal, done over a reduced temporal period (April-June 2022) and in the North-East Atlantic part. Values obtained could thus be influenced by the seasonal variability of the signal in the area, and should be reviewed as soon as possible over a longer temporal period. Nevertheless, compared to the conventional 1 Hz processing

observing capabilities (i.e., ~65 km), these values are reduced by ~38% (S6A) to ~15% (J3). These results are induced by the relatively lower noise level obtained with the full-rate measurements compared to the conventional 1 Hz processing, visible on Figure 22 (energy level of the 1 Hz Power Spectral Density (PDS) higher than for the 20 Hz PSD at short wavelengths). In the case of Jason-3, the specific noise reduction correction applied (see Table 14) strongly contribute to this result.

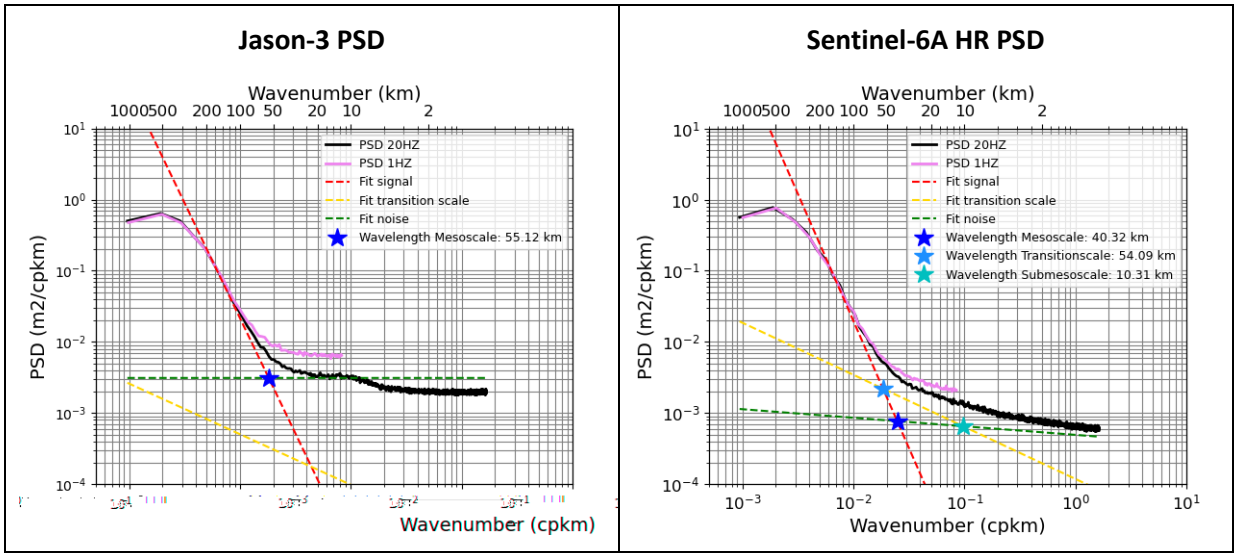

Figure 22: Power Spectral Density (PSD) of the SLA observed with the 1 Hz conventional altimeter measurement (pink) and with the full-rate (20 Hz) measurement (black) across the North-East Atlantic area, over April-June 2022. PSD for Jason-3 (left) and Sentinel-6A HR measurements (right). The dotted lines show the spectral decomposition of the 20 Hz PDS in mesoscale slope (red dashed line), small-mesoscale slope (yellow dashed line) when observable and noise slope (green dashed line). Stars show the Transition scale between mesoscale and small-mesoscale motions, and the mesoscale and small-mesoscale observable wavelengths.

The processing used for the high sampling L3 altimeter is based on the new version of the DUACS system, originally developed for processing the 1 Hz upstream altimeter measurements (Dibarboure et al., 2011; Ducet et al., 2000; Le Traon et al., 1998a; Pujol et al., 2016; Taburet et al., 2019). This new version is identified as DUACS-NG. This system has here been specifically adapted for the processing of full-rate (20 to 40 Hz) upstream products. The method is essentially the same as that for the historical 1 Hz production. It is described in section II. The main differences consist in:

- The use of high frequency (20 Hz) upstream measurements
- The use of specific empirical corrections able to reduce as much as possible the measurement noise, as it is considerably higher for 20 Hz measurements compared to 1 Hz. This step is necessary if we want to explore the small mesoscale.
- The use of a gridded MSS reference surface, rather than a mean profile (MP) defined along the tracks of the different repetitive missions. Indeed, the temporal period currently processed in 20 Hz does not allow to estimate an MP with higher accuracy than the current MSS available. Nevertheless, the position of the theoretical measurements is used to collocate the measurements for the different cycles of the mission. The theoretical location is delivered as a new variable in the dataset as described in the associated PUM[15] document.

[15] https://catalogue.marine.copernicus.eu/documents/PUM/CMEMS-SL-PUM-008-032-068.pdf

- A low-pass filtering is applied to the SLA in order to reduce the residual noise and at the same time keep as much as possible of the physical signal at small wavelengths. Two filters are considered:
  - Filtering at very short wavelength, fixing the cut-off frequency at the 5 Hz Nyquist frequency. This filter allows to subsample the signal in order to estimate a "raw" SLA with a 5 Hz sampling.
  - Filtering aiming to remove the short wavelengths for which the measurement noise dominates the signal. It applies s a cut-off frequency tailored of the observable wavelengths specific to each mission. Unlike the standard 1 Hz processing, this cut-off wavelength is not fixed but varies between altimeters, ranging from 40 to 55 km 40 and 55 km(see section IV.1.1.2.1)
  - The computation of the geostrophic current in the across-track direction is included in the processing. This processing will however not be activated from the beginning of the L3 5 Hz production, but should be activated in November 2024. Before this date, associated variables will thus be filled with Default Values (DV) values in a first time.
- A final subsampling is applied. The L3 along-track products are delivered at a 5 Hz (i.e., nearly 1 km) sampling rate.

Measurements from only few altimeters are processed with the 5 Hz sampling. Currently, the processing is applied on the different Copernicus missions (Sentinel-6A, Sentinel-3A/B) and Jason-3. It could be extended to other opportunity/collaborative missions in a near future.

V.3.4 November 2023: Use new full-rate (20Hz) upstream for L3 1Hz production

After the start of the production of the Level-3 5Hz products in 2022 (see §V.3.3), it is possible to design a L3 1Hz product using the full-rate (20Hz) upstream instead of the 1Hz version. This allows 1 Hz to benefit from the processing advances made on 20Hz/5Hz, namely:

- The noise level reduction possible with the High Frequency Adjustment (HFA) empirical correction available for some missions (see Table 144).
- The new compression (20Hz to 1Hz) methodology applied on the corrected SLA variable rather than on the range measurement, allowing to exploit the high frequency content of the different fields involved in the processing.

This contributes to improve the quality of the resulting L3 1Hz product, with an improvement rate varying according to the altimeter mission considered. An example is provided in Figure 22. It represents the PSD of the SLA deduced from the upstream 1Hz (orange line) and 20Hz (blue line). For two products/processing strictly equivalents, the two PSD should be perfectly aligned. The lower amplitude observed for the 20Hz measurements traduces the lower errors for this version. Part of the differences is also explained by the different segments available in 1Hz and 20Hz series.

The change in the L3 1Hz processing is associated with:

- a change of the production system. This may have a visible impact on the delay of processing and delay of availability of the final product for users
- a change in the products/datasets nomenclature: details are given in .
- a change of the NetCDF file nomenclature including "_1hz" for homogeneity with the nomenclature of the L3 5Hz products already available (e. g. nrt_global_s3b_phy_l3**_1hz**_20231004_20231010.nc)

See also the Product User Manual (PUM[16]) for details.

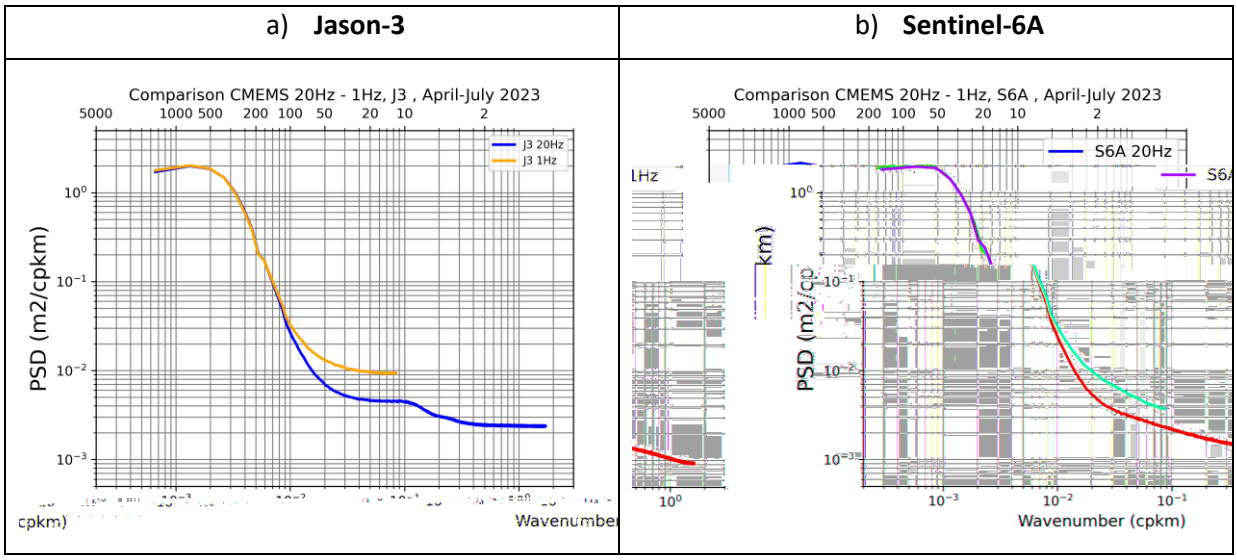

Figure 23: Power Spectral Density (PSD) of the SLA deduced from upstream 1 Hz (orange) and 20 Hz (blue) for a) Jason and b) Sentinel-6A respectively.

Table 21: Changes in L3 NRT products/dataset nomenclature implemented in November 2023.

Current product/dataset name	New product/dataset name
SEALEVEL_GLO_PHY_L3_NRT_OBSERVATIONS_008_044	SEALEVEL_GLO_PHY_L3_NRT_008_044
dataset-duacs-nrt-global-al-phy-l3	cmems_obs-sl_glo_phy-ssh_nrt_al-l3-duacs_PT1S
dataset-duacs-nrt-global-c2n-phy-l3	cmems_obs-sl_glo_phy-ssh_nrt_c2n-l3-duacs_PT1S
dataset-duacs-nrt-global-h2b-phy-l3	cmems_obs-sl_glo_phy-ssh_nrt_h2b-l3-duacs_PT1S
dataset-duacs-nrt-global-s3a-phy-l3	cmems_obs-sl_glo_phy-ssh_nrt_s3a-l3-duacs_PT1S
dataset-duacs-nrt-global-s3b-phy-l3	cmems_obs-sl_glo_phy-ssh_nrt_s3b-l3-duacs_PT1S
SEALEVEL_EUR_PHY_L3_NRT_OBSERVATIONS_008_059	SEALEVEL_EUR_PHY_L3_NRT_008_059
dataset-duacs-nrt-europe-al-phy-l3	cmems_obs-sl_eur_phy-ssh_nrt_al-l3-duacs_PT1S
dataset-duacs-nrt-europe-c2n-phy-l3	cmems_obs-sl_glo_phy-ssh_nrt_c2n-l3-duacs_PT1S
dataset-duacs-nrt-europe-h2b-phy-l3	cmems_obs-sl_glo_phy-ssh_nrt_h2b-l3-duacs_PT1S
dataset-duacs-nrt-europe-s3a-phy-l3	cmems_obs-sl_glo_phy-ssh_nrt_s3a-l3-duacs_PT1S
dataset-duacs-nrteurope-s3b-phy-l3	cmems_obs-sl_glo_phy-ssh_nrt_s3b-l3-duacs_PT1S

V.3.5 November 2023 – DUACS-NG 2.0.0: start of production over the global ocean

After the start of the production of the L3 5Hz datasets across Europe in November 2022 (see section V.3.3), the production of the L3 5Hz datasets over the global ocean has started in November 2023. The processing applied is nearly the same as for Europe. The main difference is observed in the denoising processing step. The geographical variation of the observable wavelength (Figure 7) is indeed taken into

[16] https://catalogue.marine.copernicus.eu/documents/PUM/CMEMS-SL-PUM-008-032-068.pdf

account to adjust the cut-off frequency of the low-pass filtering applied (see section II.4.6.2). The global mean observable wavelength with these L3 5 Hz datasets is nearly ~40 km (S6A) to ~57 km (J3), depending on the altimeter considered (10). Over Europe, they range 43 km (S6A) to 59 km (J3) in the Atlantic part, and 33km (S6A) to 52 km (J3) in the Mediterranean Sea and Black Sea.

An estimation of the geostrophic current in the across-track direction is also provided. It is derived from the low-pass filtered SLA. The spectral analysis of the current obtained shows a good consistency with the SQG theory of the spectral slope at mesoscale in mid-latitudes areas. Nevertheless, below ~100km wavelength and in low-latitude areas, the spectral slope is far from SQG or QG theory and may represent the signature of residual noises on the filtered SLA (see also section II.4.6.3).

V.3.6 November 2023 – DUACS-NG 2.0.0: start L3 production for SWOT-nadir measurements

The satellite Surface Water Ocean Topography (SWOT) was launched in December 2022. After a CalVal phase, which lasted until mid-July 2023, the satellite was put on its scientific orbit, defined with a 21-day repeat cycle (see 2). The satellite includes two types of altimeter measurement: a conventional nadir and a new swath measurement.

In November 2023, the SL-TAC started to use the SWOT nadir measurements in its production. The upstream 20Hz are considered and are used to compute L3 with 5Hz and 1Hz posting rate.

The CalVal analysis of the SWOT nadir measurement confirmed performances close to the Jason-3 mission.

V.3.7 July 2024: DUACS-NG 3.0.0: Use up-to-date altimeter standards for L3 1Hz & 5Hz production and H2B upstream change

The version of the altimeter standards and geophysical corrections applied on altimeter measurement continuously evolve. An update of the altimeter standards is taken into account in the NRT production with the DUACS-NG 3.0.0 version. The main changes are described below:

- the use of the new FES_2022 ocean tide correction. As reported by Carrere et al., (2023), the use of the FES_2022 model instead of FES_2014 model leads to a strong reduction in the SLA variance in the coastal band (< 100km). This reduction reaches -20 cm² (Jason-3) to -50 cm² (AltiKA & Cryosat-2) at few kilometers near the coast.
- The use of a new Mean Sea Surface corresponding to the Hybrid-2023 version. It combines the MSS SIO_2023, CNES_CLS_2022 and DTU2021, as presented in Laloue et al., (2024a). The new MSS shows lower errors than the previous MSS solution. It contributes to improve the quality of the SLA in the near coast area (error reduced by ~23% in the 0-200km coastal band compared to the CNES_CLS_2022) and in the Arctic Ocean. The change of the MSS will induces regional biases about ±5 cm in seasonal ice-covered areas, especially in the Arctic, as illustrated in the map below (Figure 24). This bias will be introduced in the DUACS products gradually as the summer ice melts in the region.

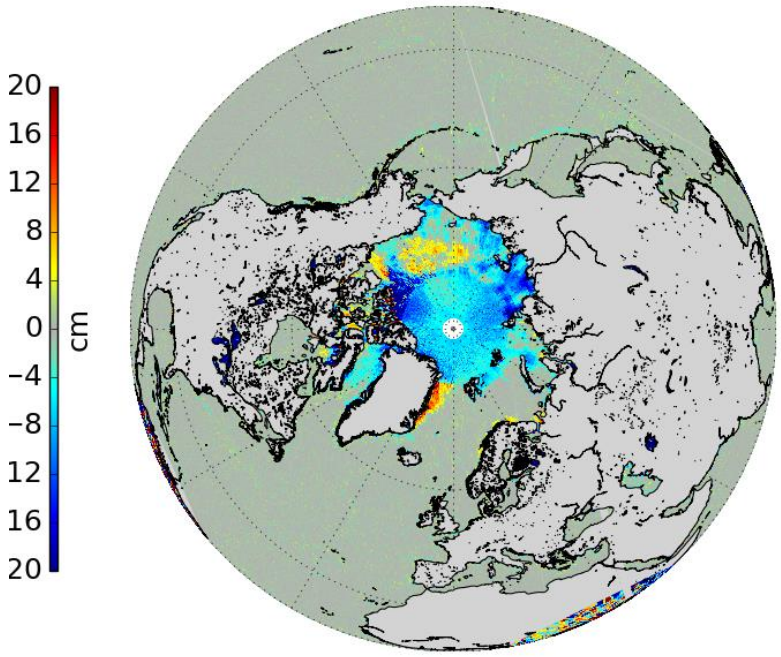

Figure 24: Regional bias introduced by the change in MSS with the DUACS-NG 3.0.0 version: differences at long wavelengths between the Hybrid_2024 (SIO_2023; CNES/CLS22; DTU21) and Hybrid_2021 (SIO; CNES/CLS15; DTU15) MSS models (Northern hemisphere).

With this version, the upstream used for the generation of L3 product for the H2B mission changes. We now benefit from the full posting-rate (20Hz) measurements, including an empirical correction to reduce the measurement noise (see Table 14). Consequently, the production of the L3 product with a 5Hz posting-rate is possible. The L3 1Hz product processing is also adapted to take into account the new 20Hz upstream. This change has low impact on the overall product quality. It however improves the data availability near the coast.

V.3.8 November 2024: DUACS-NG v4.0.0: Updated L4 products

In November 2024, the NRT product evolves in order to homogenise the NRT and MY processing. While various changes are implemented in MY series (see §V.4.3), corresponding to the DT-2024 product version, only some of them are implemented in NRT. Indeed, other changes are already implemented in NRT production (see §V.3.7). The different improvements in the NRT product are summarized in Table 22 and described below.

Table 22: Overview of the changes introduced in each DT-2024 NRT product version.

Evolution description	Description of the impact
L3 & L4: Use new MDT	Improved geostrophic current; regional biases
L3: Use new methodology for SLA, ERR and LWE correction computation	Improved LWE correction
L4: Use new methodology for geostrophic current computation	Improved mesoscale signal on L4 products
L4: Grid spatial resolution change	Finner spatial grid available
L3 & L4: CMEMS catalogue changes	Change in products/datasets names

.

V.3.8.1 New MDT

The MDT used in the DUACS is described in section II.4.5 and §V.4.3.3.

V.3.8.2 New MIOST mapping used for SLA and ERR

The methods used to process L4 gridded products from the merging of L3 along-track products have evolved from the Optimal Interpolation (OI) method, as detailed by Le Traon et al., (1998a) and Pujol et al., (2016), to the Multi-Scale Inversion of Ocean Surface Topography (MIOST) approach . While the MIOST system can also be considered a form of optimal interpolation, it's important to note that OI maps are constrained by a single-scale covariance function Arhan and De Verdiére, (1985); Le Traon et al., (1998a) and primarily focus on geostrophic circulation (processes with typical space and timescales greater than 100 km and 10 days). The multiscale approach of the MIOST method allows for the resolution of some of the surface variabilities missing in OI by incorporating covariances of various surface processes within a single inversion. In MIOST, the covariance functions are represented as wavelet modes, and inversion is performed using a variational approach Ubelmann et al., (2021b). In the new reprocessing, our focus was solely on the geostrophic component, as explored in Ubelmann et al., (2021b) and Ballarotta et al., (2023). These studies have compared the performance of the MIOST system with the current DUACS OI mapping system in DT mode, demonstrating that while MIOST is globally comparable to OI, it shows regional improvements, particularly in mid-latitudes where complex turbulent systems, such as the Gulf Stream and Kuroshio current, are better mapped by MIOST than OI.

In the context of Near Real-Time (NRT) applications, the MIOST mapping approach has been evaluated using Observing System Simulation Experiments (OSSEs). These OSSEs are designed to test new altimeter missions, different constellation scenarios, or novel types of observations and mapping systems. The OSSEs rely on models as their input; in our case, the input data come from a state-of-the-art ocean model based on primitive equations, which describes ocean dynamics. The complexity of the ocean model can vary according to the dynamics of interest, incorporating factors such as sub-grid scale parameterizations, spatial grid resolution (ranging from coarse to eddy-permitting, eddy-resolving, sub-mesoscale-resolving, and tidal-resolving regimes), and other aspects. Currently, we are using an eddy-resolving model based on the NEMO system (GLORYS12v1[17], eNATL60[18]). This model provides three-dimensional outputs, including sea surface height (SSH), temperature, salinity, and ocean currents, among others. In our study, we primarily utilize the SSH variable. Pseudo-observations, or synthetic observations, are generated by interpolating the SSH model outputs onto the theoretical tracks of the altimeter mission. To enhance realism, simulated instrumental and geophysical errors can be added to

[17] Global Ocean Physics Reanalysis | Copernicus Marine Service
[18] eNATL60/02_experiment-setup.md at master · ocean-next/eNATL60 · GitHub

these pseudo-observations. Finally, the gridded data are compared to the reference "truth," which in this context is the raw model output considered as the benchmark for validation.

The MIOST NRT mapping solution has been compared to the current operational NRT OI system. Pseudo-observations were derived from the sea surface height (SSH) field of a 1/60° North Atlantic simulation without explicit tidal forcing (eNATL60-BLB002)[19]. These pseudo-observations involve a constellation of five nadir altimeters (Jason-3, Sentinel-3A, Sentinel-3B, Sentinel-6, and HY-2B), with SSH data corrected for Dynamic Atmospheric Correction (DAC) and atmospheric tide signatures (S1 and S2). These five altimeters are then used in both the MIOST and OI mapping algorithms (in NRT mode) to reconstruct the SSH scene from the nature run. The performance of the mapping solutions is evaluated using the Root Mean Square Error (RMSE) metric. The differences in RMSE between MIOST and OI shows that the MIOST NRT mapping errors are, on average, 20% smaller than those of OI.

The MIOST NRT mapping solution has been compared to the MIOST DT mapping solution to evaluate the differences in mapping errors between DT and NRT modes using the MIOST system. This assessment was conducted using a free 1/12° global simulation from Mercator Ocean (ORCA12-TRBB36). The pseudo-observations include a constellation of five nadir altimeters (Jason-3, Sentinel-3A, Sentinel-3B, Sentinel-6, and HY-2B), with data partially corrected for Dynamic Atmospheric Correction (DAC) using only the Inverse Barometer effect. These five altimeters were then used within the MIOST system, in both DT and NRT contexts, to reconstruct the SSH scene from the nature run. As expected, the DT mapping error is more than twice as small as the NRT mapping error and exhibits greater temporal stability. Additionally, by varying the number of altimeters in the constellation, we found that the NRT reconstruction with 4-5 altimeters using MIOST is comparable to the DT reconstruction with just 2 altimeters.

The previous OI method provided an estimation of the consistency of the gridded solution using a formal mapping error indicator. However, due to the computational cost and the wavelet-based formulation of the MIOST mapping approach, the error estimation method had to be revised for MIOST to deliver a global estimation of the formal error. In the MIOST products, the formal mapping error is determined using an ensemble approach. Specifically, an ensemble of 20 gridded product members is generated, each with a perturbed covariance model and observations. The standard deviation of the sea level anomaly (SLA) estimations across these ensemble members represents the formal mapping error.

V.3.8.3 Change of the L4 grid spatial sampling

The new products are provided on a finer spatial grid compared to the previous reprocessing. The new global products have a spatial resolution of 1/8°, while the regional products offer even finer spatial sampling at 1/16°. The temporal sampling remains unchanged, with data available on a daily basis.

V.3.8.4 New geostrophic current computation methodology

See §V.4.3.5

V.3.8.5 CMEMS catalogue changes

The new NRT DT-2024 L4 “all-sat-merged” series are accessible through new datasets reflecting the change in grid spatial sampling (see §V.4.3.6). Part of previous datasets have been removed. Details are given in the following Table 23::

[19] eNATL60-BLBT02 | MEOM catalog

Table 23: Updated DT2024 of GLObal and EURopean Sea L4 NRT Product classification: Product and Dataset Identification.

Product	**Datasets for DT-2021 series (will be frozen after DT-2024 release)**	**Datasets for DT-2024 series**
SEALEVEL_EUR_PHY_L4_NRT_008_046	cmems_obs-sl_eur_phy-ssh_nrt_allsat-l4-duacs-0.125deg_P1D	cmems_obs-sl_eur_phy-ssh_nrt_allsat-l4-duacs-0.0625deg_P1D
SEALEVEL_GLO_PHY_L4_NRT_008_060	cmems_obs-sl_glo_phy-ssh_nrt_allsat-l4-duacs-0.25deg_P1D	cmems_obs-sl_glo_phy-ssh_nrt_allsat-l4-duacs-0.125deg_P1D

V.4 REP/DT sub-system version changes

Table 24: Overview of the main evolutions implemented in the DT processing. DT-2018 and DT-2021 version is no longer available.

System version	Product version	Date of change	Description of the change
6.0	*DT-2018*	*April 2018*	Full Reprocessing for REP products (1993-2017) for CMEMS v4.0: DUACS DT-2018 version
6.1	*DT-2018*	*June 2018*	Production of the -May ,2017-January, 2018 period Introduction of Jason-2 Long Repeat Orbit Phase Six satellites are used during this update in the DT processing chain (ALG, C2, H2G, J2G, J3, S3A)
6.1	*DT-2018*	*October 2018*	Production of the January 18,2018 – June 10, 2018 period. Five satellites are used during this update in the DT processing chain (ALG, C2, H2G, J3, S3A)
6.2	*DT-2018*	*April 2019*	Production of the June 11,2018 – September 23, 2018 period - Introduction of the Europe L3 products – Remove Med. and Black Sea L3 products. - L3 products vfex and vxxc are included in new phy_l3 product - E1G is introduced as a new dataset. Before it was integrated in the E1 mission. - AL and ALG begin and end dates of the temporal period processed by REP/DT system has been modified. - Use of new Sentinel-3A Hybrid Mean Profile for global and regional product. Global data have been reprocessed. - All NetCDF produced are in NetCDF-4 format
6.3	*DT-2018*	*July 2019*	Production of the September 24, 2018 – December, 2018 period. Introduction of Sentinel-3B
6.3	*DT-2018*	*December 2019*	Redelivery of the September 24, 2018 – January 12, 2019 production for correction of an anomaly of data availability near the coast Production of the January 12, 2019 – May 13, 2019 period
6.3	*DT-2018*	*July 2020*	Production of the May 14, 2019 – October 15, 2019 period Add monthly mean dataset
6.3	*DT-2018*	*December 2020*	Production of the October 16, 2019 – March 07, 2020 period Extension of the monthly mean dataset October 2019 to February 2020
6.4	*DT-2018*	*May 2021*	H2AG mission is deactivated from DUACS Production of the March 08, 2020 – June 03, 2020 period Extension of the monthly mean dataset, March 2020 to May 2020
7.0	*DT-2021*	*Dec 2021*	Full reprocessing taking into account - New altimeter standards and geophysical corrections - New MSS and MP - New mapping parameters - Improved LWE correction - NetCDF format change / product/dataset nomenclature change
7.0	*DT-2021*	*Jun-2022*	Temporal extension covering the period 2021/08/03 – 2021/12/31
7.0	*DT-2021*	*Jul-2022*	Temporal extension covering the period 2022/01/01 – 2022/02/09
7.1	*DT-2021*	*Dec-2022*	Temporal extension covering the period 2022/02/10 – 2022/06/23 Sentinel-6A introduced as new reference mission (LR measurements). Jason-3 orbit change; addition of new “j3n” dataset.
7.1	*DT-2021*	*Mar-2022*	Temporal extension covering the period 2022/06/24 – 2022/08/04
7.1	*DT-2021*	*Nov 2023*	Temporal extension covering the period 2022/08/05 – 2023/06/07
7.2	DT-2021 interim	May 2024	Temporal extension covering the period 2023/06/08 – 2023/09/08
8.0	*DT-2024*	*Dec 2024*	Full reprocessing taking into account - New altimeter standards and geophysical corrections - New MSS and MP - New MDT - New mapping method (SLA & LWE computation) - Change of the geostrophic current computation method - Change of the L4 product spatial resolution - NetCDF format change / product/dataset nomenclature change

V.4.1 January 2023: Sentinel-6A and Jason-3 interleaved orbit in DUACS processing

In January 2023, a temporal extension of the MY series was delivered. It covers the period from 2022/02/10 to 2022/06/23 and includes different changes in the constellation that are described below in this section.

First, as previously done in NRT processing (see section V.3.1), Sentinel-6A was introduced as the new altimeter reference mission and replaced Jason-3.

Sentinel-6A operates in two different modes. In MY production the Low Resolution (LR) mode, based on LRM instrument equivalent to the one used for Jason-3, is used to ensure the continuity of the MSL signal. The resulting noise level of the Sentinel-6A measurement is slightly lower than for the Jason-3 mission, with a mean 1 Hz measurement noise around 2.3 cm RMS ().

As previously observed with S6A HR measurement (see section V.3.1), CalVal analysis underscored that the S6A LR measurement shows regional biases compared to the contemporaneous Jason-3 measurement (L2 version FC007). Part of these biases are fully explained and corrected in L2P processing. This solution is in place until corrective changes are implemented in the upstream L2 processing chains (expected with L2 FC008 version). Another part of the biases however still remains to be fully understood. Figure 25 illustrates these biases observed over the Sentinel-6A/Jason-3 tandem phase. They range between ±0.5 cm. **These biases have been managed in the L3 processing step in order to ensure a smooth transition between Jason-3 and Sentinel-6A measurements.**

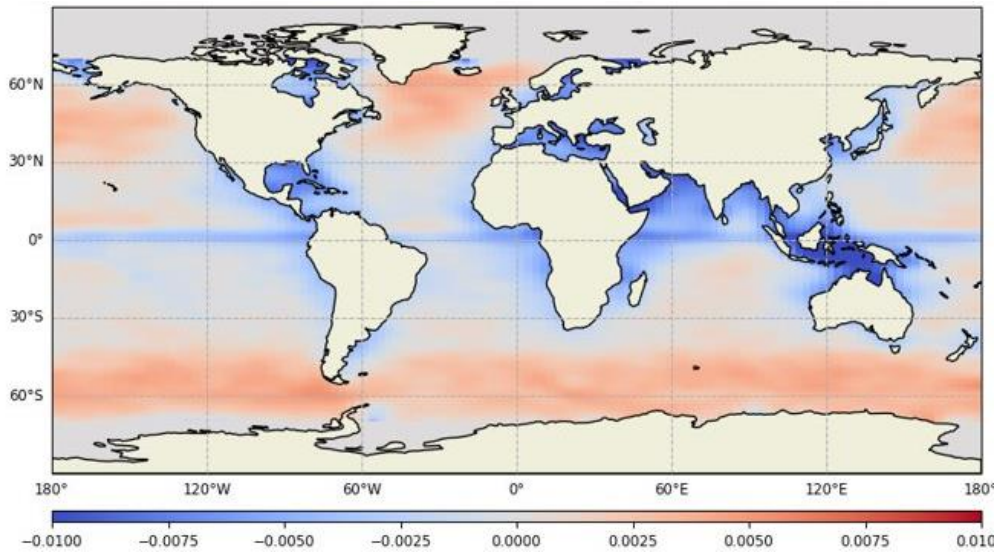

Figure 25: Residual SLA differences between Sentinel-6A LR and Jason3 measurements over the period Sep 2021-Mar 2022. Units: m.

The qualification of the L3 and L4 MY production using Sentinel-6A as reference mission showed good results, with no impact for Mean Sea Level trend continuity. Figure 26 shows the MSL trend estimation over the global ocean. It underscores a perfect continuity of the signal at the transition between Jason-3 and Sentinel-6A used as reference mission (i.e., 2022/02/10). Same result was observed for regional MSL trend estimation over the European area (not shown), and sub millimetric impact was observed in the equatorial band (latitudes comprised within ±5°) and in latitudes < -40°. Comparison with SLA measured by *in situ* tide gauge (Gloss-Clivar) also shows the continuity of the SLA. The global mean SLA

difference between altimetry and tide gauges ranges between ±1 cm over the mid-2021 to mid-2022 period tested (not shown).

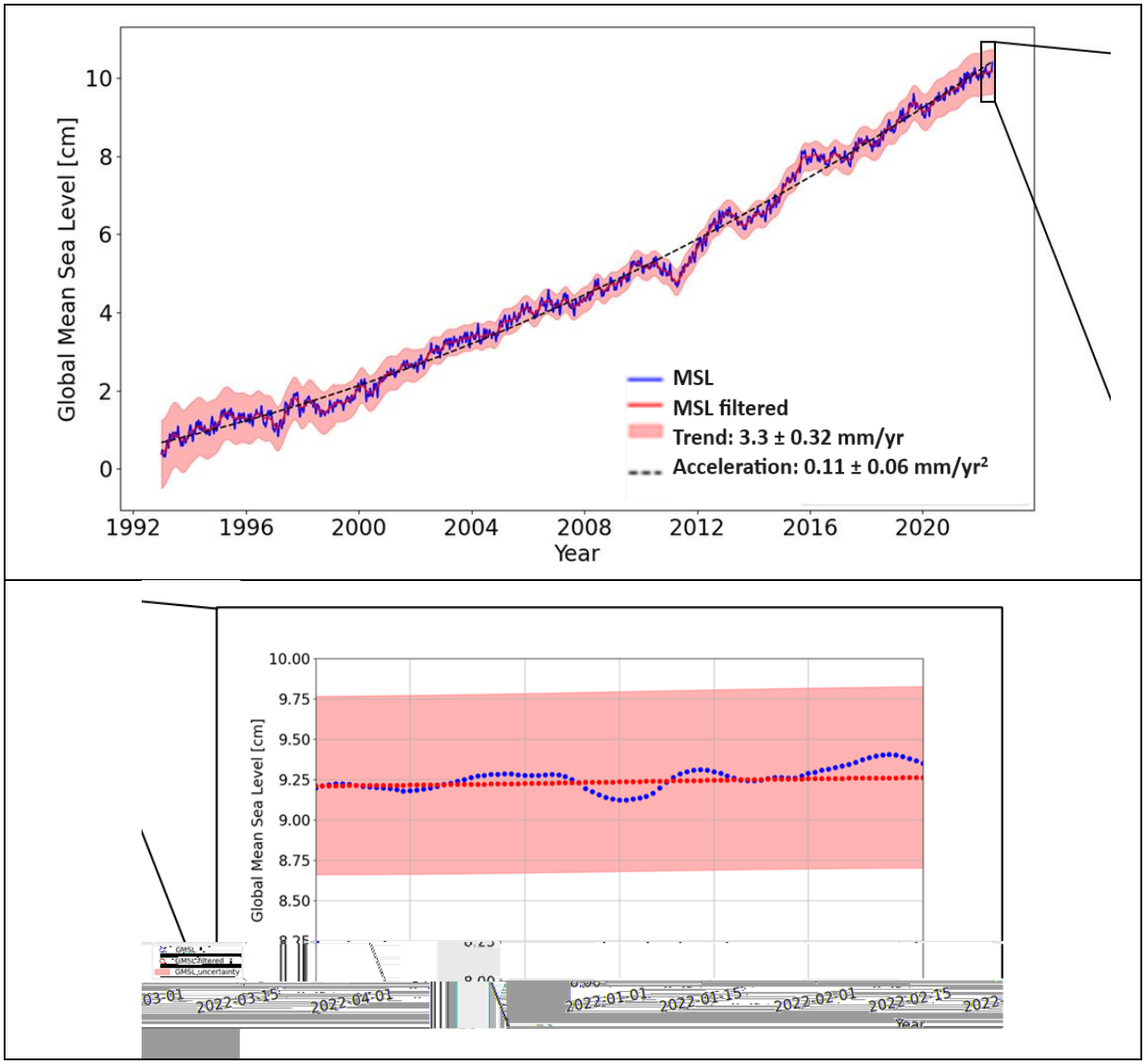

Figure 26: Mean Sea Level trend over the global ocean (deduced from L4 altimeter products) over the full altimeter temporal period available (top); and zoom centred on the transition of the reference mission from Jason-3 to Sentinel-6A (bottom). Daily mean SLA with annual and semi-annual signals removed (blue dots) and after applying a 6-months filter (red dots). Uncertainty of the MSL estimation (red envelope).

Secondly, the orbit change that occurred in April 2022 for Jason-3 (see also section V.3.2) was taken into account. Jason-3 measurements on its new interleaved orbit with Sentinel-6A are delivered in the new dataset “j3n”.

V.4.2 May 2024: temporal extension in interim mode

In May 2024, a temporary interim extension of the MY DT-2021 series was made available. It differs from previous ones by a change in the altimetric standards and geophysical corrections used in the processing. Indeed, in preparation for an upcoming complete reprocessing of the series, the upstream data are now available in the DT-2024 standards described by (Kocha et al., 2023). These changes mainly consist of:

- A new L2 product version for Jason-3 (GDR-F), Sentinel-3A (BC005) and Sentinel-6A (FC09), including improved retracking and associated Sea State bias correction.
- The use of the new ocean-tide correction FES22.
- The use of the new Mean Sea Surface combining the SIO22; CNES_CLS_22 and DTU21 versions for the geodetic missions and Sentinel-3B.

They are described in the Table 155. The use of the new standards contributes to improve the quality of the SLA field and derivates. They induce few regional biases (order of millimetre at regional scales) that will be managed in the L3/L4 processing for a seamless transition for users and ensure the continuity of the sea level at regional scales.

In order to differentiate this specific temporal extension from the historic series, the data will be delivered in specific “myint” product/datasets:

- SEALEVEL_GLO_PHY_CLIMATE_L4_MY_008_057/c3s_obs-sl_glo_phy-ssh_**myint**_twosat-l4-duacs-0.25deg_P1D
- SEALEVEL_GLO_PHY_L4_MY_008_047/cmems_obs-sl_glo_phy-ssh_**myint**_allsat-l4-duacs-0.25deg_P1D
- SEALEVEL_GLO_PHY_L4_MY_008_047/cmems_obs-sl_glo_phy-ssh_**myint**_allsat-l4-duacs-0.25deg_P1M-m
- SEALEVEL_GLO_PHY_L3_MY_008_062/cmems_obs-sl_glo_phy-ssh_**myint**_{mission}-l3-duacs_PT1S with mission bing [alg, c2n, h2b, j3n, s3a, s3b, s6a-lr]
- SEALEVEL_EUR_PHY_L4_MY_008_068/cmems_obs-sl_eur_phy-ssh_**myint**_allsat-l4-duacs-0.125deg_P1D
- SEALEVEL_EUR_PHY_L3_MY_008_061/cmems_obs-sl_eur_phy-ssh_**myint**_{mission}-l3-duacs_PT1S with mission bing [alg, c2n, h2b, j3n, s3a, s3b, s6a-lr]

V.4.3 Nov 2024: Full reprocessing of the DT products: DUACS DT-2024

In November 2024, a new version of the DUACS delayed time (MY/DT) products was delivered. This “DT-2024” version replaces the “DT-2021” available since December 2021. At the same time, the near real time (NRT) DUACS products also evolved to be consistent with the new version of the DT-2024 products. The different evolutions are implemented in the DT-2024 version, both for Level-3 (L3) and Level-4 (L4) products. They are summarized in the Table 22 and detailed in Table 25 below.

Table 25: Overview of the changes introduced with DT-2024 REP product version.

Evolution description	Description of the impact
L3 (and resulting L4): Use new altimeter standards and geophysical corrections (e.g., ocean tide, DAC, …)	Improved accuracy of SLA content; Regional biases; regional MSL trend impacted
L3 (and resulting L4): Use new Mean Sea Surface (non-repetitive missions and recent missions) or Mean Profile (repetitive missions)	Improved accuracy of SLA content; Regional biases
L3 & L4: Use new MDT	Improved geostrophic current; regional biases
L3: Use new methodology for LWE correction computation	Improved LWE correction
L4: Use new methodology for mapping and geostrophic current computation	Improved mesoscale signal on L4 products
L4: Grid spatial resolution change	Finner spatial grid available
L3 & L4: CMEMS catalogue changes	Change in products/datasets names

V.4.3.1 New altimeter standards and geophysical corrections

In the frame of the SALP[20] (Service d'Altimétrie et de Localisation Précise) project supported by CNES (Centre National d'Etudes Spatiales) and of the Sentinel Marine Altimetry L2P-L3 Service (in cooperation agreement with EUMETSAT within the Copernicus Program[21] funded by the European Union), the measurements from the different altimeter missions available since 1993 have been reprocessed taking into account the up-to-date and homogeneous altimeter standards and corrections. Regional biases also have been estimated for the reference mission series (Topex/Poseidon, Jason-1, Jason-2, Jason-3, Sentinel-6A) in order to ensure the continuity of the sea level trend at regional scale.

These changes are detailed in (Kocha et al., 2023) and summarized in Table5. They contribute to improving the quality of the L3 and resulting L4 products. Compared to previous versions (e.g. DT-2021) mesoscale improvements have been made by means of:

- Instrumental corrections (thanks to the reprocessing of Topex, Jason 3, Sentinel 3A/B and 6).
- Geophysical corrections, with impact mostly at high latitudes and along the coast with the newcorrections :
  - Ocean tide correction**:** FES 2022 (Carrere et al., 2023) which explain 70% of improvements brought by the DT-2024. The use of the FES_2022 model instead of FES_2014 model leads to a strong reduction of the SLA variance in the coastal band (< 100 km). This reduction reaches -20 cm² (Jason-3) to -50 cm² (AltiKA & Cryosat-2) at few kilometers near the coast.
  - Dynamic atmospheric correction: TUGO

[20] https://www.aviso.altimetry.fr/en/home.html
[21] https://marine.copernicus.eu/

V.4.3.2 New Mean Sea Surface and Mean Profiles

The New MSS Hybride_2023, presented by (Laloue et al., 2024b) is used in the DUACS DT-2024 product version, specifically in NRT for all missions; in MY for missions with non-repetitive orbit and new orbit missions. The MSS Hybrid_2023 combines the MSS CNES_CLS_2022, SCRIPPS_2022 and DTU21, taking advantage of their respective features. It contributes to improve the signal at small mesoscale (i.e., "at small scale" between 15 km and 100 km), especially near the coast and in high MS gradient areas).

For MY repetitive missions, specific mean profiles, estimated along the repetitive tracks are used as detailed in Table 4, Table5 and Table 166.

V.4.3.3 New MDT

The MDT used in the DUACS reprocessing is described in section II.4.5.

Improved MDTs are used in the DT-2024 product version as follows:

- For the global ocean : use of a new MDT CNES_CLS_2022 (Jousset et al., 2023), combined with CMEMS_2020 regional MDTs for Mediterranean and Black Sea (Jousset and Mulet, 2020). This hybrid MDT is available on AVISO or in the Copernicus marine Service catalogue (product 008_063[22])
- For Europe: use of the new regional Europe CMEMS_2024 MDT. This hybrid MDT is available in the Copernicus marine Service catalogue since November 2024 (product 008_070)

The main improvement of the new CNES-CLS22 MDT over the previous CNES-CLS18 MDT is in the Arctic, with better coverage, no artifacts and a more realistic solution. Global improvement of the CNES-CLS22 MDT is also remarkable, with drifter independent measurements (up to 10% of error reduction). Nevertheless, few areas appear to be degraded: south of Greenland, in the far north of the Pacific Ocean (in the Gulf of Alaska, and close to Russia) and in the southern Pacific.

Compared to the global CNES_CLS-2022 MDT, the Europe CMEMS_2024 version uses measurements from the high frequency radar in the Bay of Biscay and benefits from additional drifter measurements (year 2022), corrected with an improved estimation of the Ekman current component (Colling, 2001). It results in a higher resolution and better accuracy of this MDT in the Atlantic region compared to the global version.

The quality of the MDT fields used in the DUACS processing is fully described in MDT specific QUID document For products 008-063[17], 008-066[23] and 008-067[24].

V.4.3.4 New mapping methodology (LWE and SLA)

The methods used to process L4 gridded products from the merging of L3 along-track products have evolved from the Optimal Interpolation (OI) method, as detailed by Le Traon et al (1998) and Pujol et al., (2016) to the Multi-Scale Inversion of Ocean Surface Topography (MIOST) approach. While the MIOST system can also be considered a form of optimal interpolation, it's important to note that OI maps are constrained by a single-scale covariance function Arhan and De Verdiére, (1985); Le Traon et al.,(1998a) and primarily focus on geostrophic circulation (processes with typical space and timescales greater than 100 km and 10 days). The multiscale approach of the MIOST method allows for the

[22] Global Ocean Mean Dynamic Topography | Copernicus Marine Service
[23] Mediterranean Sea Mean Dynamic Topography | Copernicus Marine Service
[24] 17

resolution of some of the surface variabilities missing in OI, by incorporating covariances of various surface processes within a single inversion. In MIOST, the covariance functions are represented as wavelet modes, and inversion is performed using a variational approach (Ubelmann et al., 2021b). In the new reprocessing, our focus was solely on the geostrophic component and long wavelength error component, as explored in (Ubelmann et al., 2021b) and (Ballarotta et al., 2023). These studies have compared the performance of the MIOST system with the current DUACS mapping system, demonstrating that while MIOST is globally comparable to OI, it shows regional improvements, particularly in mid-latitudes, where complex turbulent systems, such as the Gulf Stream and Kuroshio current, are better mapped by MIOST than OI.

The quality of the new SLA product has been evaluated through comparisons with an independent dataset. This analysis specifically targets improvements in mapping between the MIOST and OI products by using an independent along-track dataset for performance assessment. We generated maps excluding the Saral/AltiKa altimeter to enable independent evaluation. The SSH gridded data were interpolated to the locations of the independent along-track SSH measurements. The difference between gridded SSH and along-track SSH was computed, and a statistical analysis of this SSH error was performed within 1° × 1° longitude × latitude grid cells. Before this analysis, a filtering operation was applied to isolate the spatial scales of interest, such as the 65–500 km range, which typically represents the medium mesoscale ocean signal. This filter removes noise from the reference signal (along-track) and possible large-scale biases (scales >500 km).

Figure 27 illustrates the mapping error differences between MIOST and OI for all spatial scales and, specifically, for the 65 to 500 km range. The colour scale bar indicates the reduction/increase in the mapping error with MIOST compared to OI. Overall, MIOST demonstrates smaller mapping errors than OI across all spatial scales, particularly at mid-latitudes, with an average reduction of 5%. The most significant reduction in mapping error is observed in high-variability regions. However, in intertropical and coastal regions, the MIOST product shows degradation compared to the OI product. For the 65 to 500 km range, MIOST mapping errors are reduced by approximately 8% compared to OI in high-variability mid-latitude regions. In low-variability regions, the mapping error is about 1% smaller with MIOST, although local areas such as the Argentine Sea, the Siberian plateau, and the New Zealand plateau, may exhibit larger errors with MIOST. Table 27 provides a summary of the comparison results across different regions (Global, coastal, equatorial band, low-variability, and high-variability). Overall, MIOST SSH maps align more closely with the independent SARAL/AltiKa observations than OI maps.

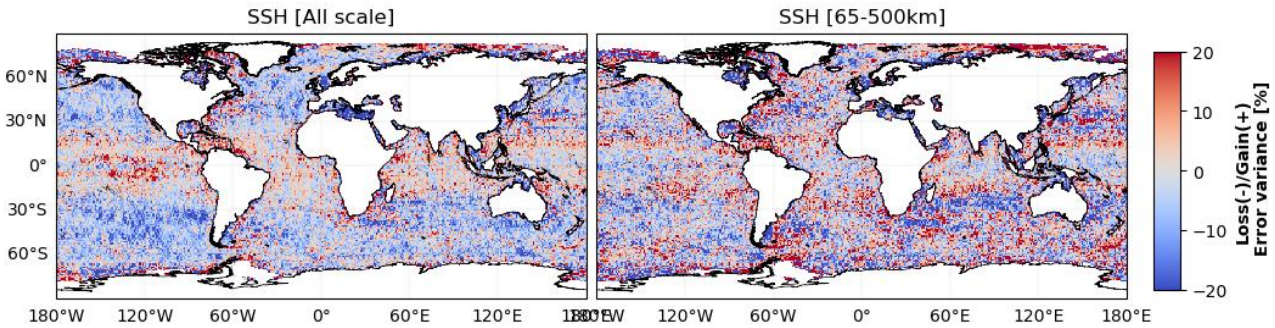

Figure 27: Gain/loss in the mapping error variance of SLA in the MIOST experiment relative to the DUACS mapping error variance for all spatial scales (left) and the scale between 65 and 500 km (right). Negative values (i.e., blue colour) means a reduction of error variance in MIOST.

Table 26: Variance of the differences between gridded (L4) DT2021 all-sat-merged products from MIOST (one altimeter was kept independent for validation) and independent SARAL-DP/AltiKa (ALG) along-track measurements over 2018 for different geographic selections. Units: cm². In parenthesis: variance reduction (in %) compared with the results obtained with the DT2021 products from DUACS. Statistics are presented for all wavelenghs (left column) and wavelengths ranging between 65-500 km (right column).

	Mapping_err_var [cm²]	**Mapping_err_filtered_var [cm²]**
global (lat between 60° and -60°)	15.49 (-2.82%)	3.39(-2.20%)
Coastal	25.29(1.08%)	5.25(-0.56%)
Offshore_highvar	30.43(-3.25%)	10.27(-7.64%)
Offshore_lowvar	12.21(-3.25%)	2.26(-1.31%)
Equatorial_band	13.70(2.01%)	2.91(0%)

The Long-Wavelength Error (LWE) correction delivered in L3 product is computed as the final step of multi-mission cross-calibration processing. It is expected to remove local SLA residual biases between neighbouring altimeter tracks: biases induced by imprecision of the different correction applied (e.g., residual ocean tide, residual DAC, residual wet-troposphere, residual ionosphere signal, etc.).

The methodology used in DUACS DT-2021 product version follows the method described by (Traon and Dibarboure, 1999). The LWE correction was estimated with higher frequency along the different tracks (100 km), and by using an Optimal Interpolation methodology to retrieve the correction on each along-track position.

The methodology employed in the MIOST product is based on the approach outlined by (Ubelmann et al., 2021b). In this method, the Long-Wavelength Error (LWE) correction is estimated through the simultaneous inversion of mesoscale variability and LWE signatures in sea surface height measurements. This inversion is conducted on a reduced-order basis, with separate decompositions for mesoscale and LWE components of the topography, and is practically implemented using a conjugate gradient method.

The spatial pattern of the LWE solution (mean, variance) shows relative similarity between the MIOST and DUACS solutions (Figure 28). The analysis of the variance of the SLA differences at multi-mission cross-over positions (Figure 28 and Figure 29) shows that the DT-2024 LWE computation methodology improves the consistency between the different missions, particularly along the European coast and in the Pacific and Indian Oceans.

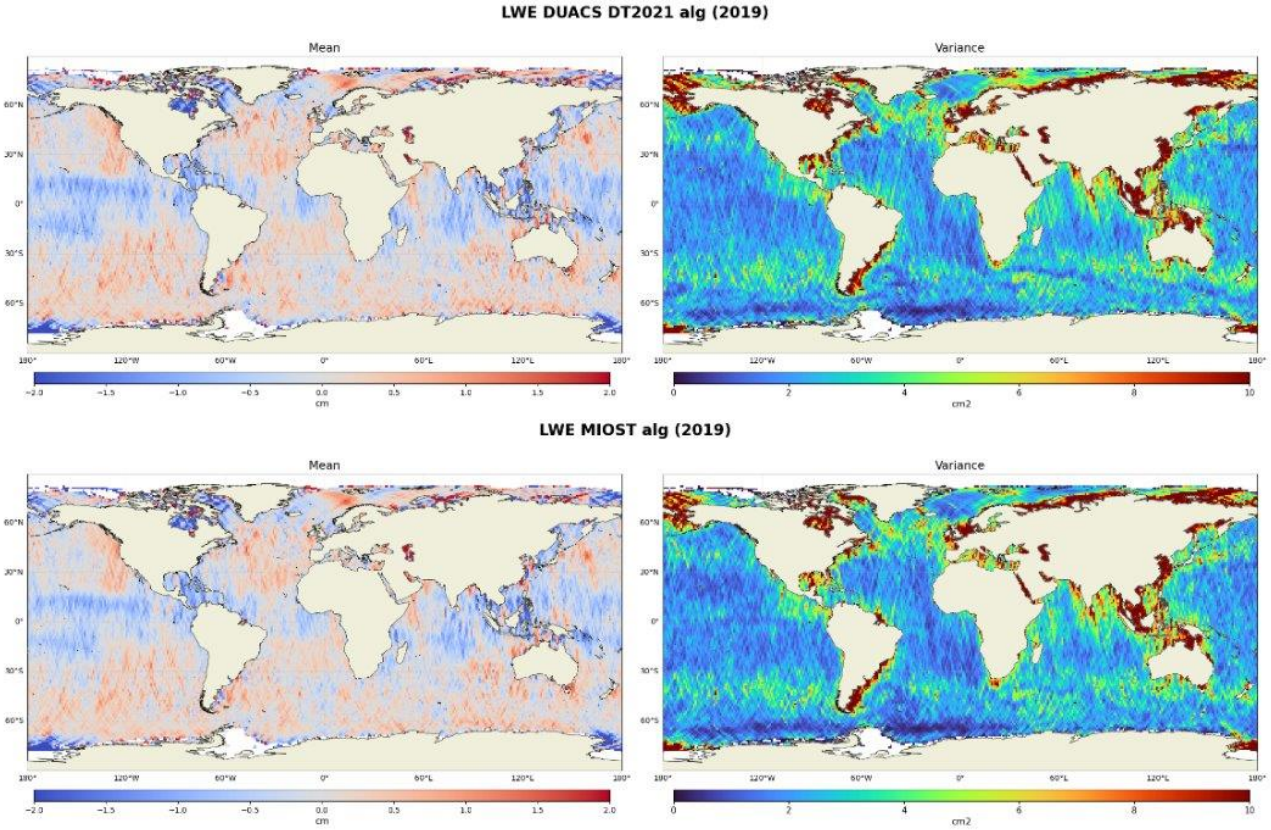

Figure 28: Mean (left) and Variance (Right) of the LWE correction for AltiKa over year 2019 using the DUACS-DT-2021 methodogy (top) and the MIOST methodology (bottom).

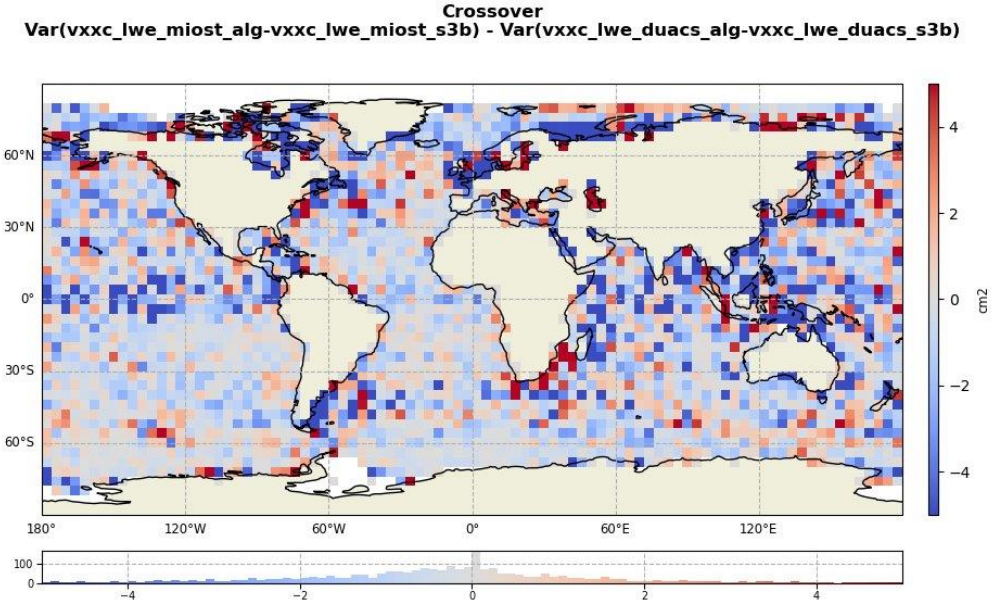

Figure 29: Variance reduction in ^{cm2} at crossover point between SARAL/Altika and Sentinel 3B. Blue indicates that L3 products (Altika vs S3B) are more coherent to each other at crossover with the MIOST LWE solution.

V.4.3.5 New geostrophic current computation methodology

The geostrophic current computation methodology has been slightly revised since the previous DUACS -DT2021 reprocessing.

The anomaly of the geostrophic current disseminated to users is derived from gridded SLA field. In the DUACS-DT2021, it is computed with the derived variable generation method described in subsection II.4.7.3

In the new DUACS-DT2024 products, geostrophic currents are calculated from the gridded SLA field using a finite-difference method (a 3-point stencil width) for latitudes beyond the ±5°N range. Within the equatorial band, the methodology remains unchanged and continues to follow the Lagerloef approach.

These evolutions in the geostrophic current computation were motivated by the fact that the refinement of the L4 spatial grid resolution was done in the new reprocessing (from ¼° grid spacing to 1/8° for global product; from 1/8° to 1/16° for regional products). Additionally, a comparison of the gridded geostrophic currents with independent drifter measurements revealed a slight improvement in consistency when using the finite difference approach compared to the 9-point stencil differentiation method (Figure 31).

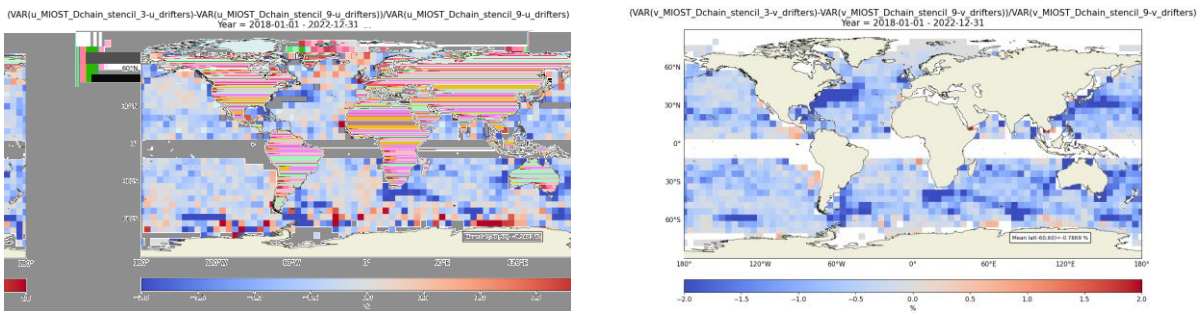

Figure 30: Error Variance Comparison of Gridded Geostrophic Velocity Fields versus Drifter Measurements (left zonal component, right meridional component). Finite Difference vs. 9-Point Stencil Differentiation. Blue means better consistency to drifter current using a finite difference approach than with a 9-point stencil differentiation

V.4.3.6 L4 grid spatial resolution change

The new products are provided on a finer spatial grid compared to the previous reprocessing. The new global products have a spatial resolution of 1/8°, while the regional products offer even finer spatial sampling at 1/16°. The temporal sampling remains unchanged, with data available on a daily basis.

V.4.3.7 Catalogue change

The new MY DT-2024 L3 series are accessible through the same datasets than previously available (except new datasets created for new altimeter missions). Nevertheless, the NetCDF files already available for the current DT-2021 series have been removed and replaced by new files containing the new DT-2024 series. Additionally, obsolete datasets have been removed.

The new MY DT-2024 L4 “all-sat-merged” series are accessible through new datasets reflecting the change in grid spatial sampling (see §V.4.3.6). Part of previous datasets have been removed. Details are given in the following Table 27:

Table 27: Updated DT-2024 of GLObal and EURopean Sea MY L4 Product classification: Product and Dataset Identifications.

Product	Datasets for DT-2021 series (will be removed after DT-2024 release)	Datasets for DT-2024 series
SEALEVEL_EUR_PHY_L4_MY_008_068	cmems_obs-sl_eur_phy-ssh_my_allsat-l4-duacs-0.125deg_P1D cmems_obs-sl_eur_phy-ssh_myint_allsat-l4-duacs-0.125deg_P1D	cmems_obs-sl_eur_phy-ssh_my_allsat-l4-duacs-0.0625deg_P1D cmems_obs-sl_eur_phy-ssh_my_allsat-l4-duacs-0.0625deg_P1M-m
SEALEVEL_GLO_PHY_L4_MY_008_047	cmems_obs-sl_glo_phy-ssh_my_allsat-l4-duacs-0.25deg_P1D cmems_obs-sl_glo_phy-ssh_my_allsat-l4-duacs-0.25deg_P1M-m cmems_obs-sl_glo_phy-ssh_myint_allsat-l4-duacs-0.25deg_P1D cmems_obs-sl_glo_phy-ssh_myint_allsat-l4-duacs-0.25deg_P1M-m	cmems_obs-sl_glo_phy-ssh_my_allsat-l4-duacs-0.125deg_P1D cmems_obs-sl_glo_phy-ssh_my_allsat-l4-duacs-0.125deg_P1M-m

The new MY DT-2024 L4 “Climate” (two-sat-merged; C3S) series are accessible through the same datasets than currently available. Nevertheless, the NetCDF files already available for the previous DT-2021 series have been removed and replaced by files containing the DT-2024 series. Additionally, obsolete datasets have been removed.

VI QUALITY CHANGES SINCE PREVIOUS VERSION

VI.1 MY processing

The newly DT-2024 reprocessed CMEMS allsat products benefit from updated altimetric standards and geophysical corrections, as well as a new mapping method. The impact of these changes on Level4 products has been assessed using independent along-track data and geostrophic current data from independent *in situ* observations (drifters). The new altimetric standards and geophysical corrections result in Level4 SLA products that are generally better than previous versions. The most significant improvements are seen in coastal regions, with up to a 10% reduction in mapping errors, mainly due to enhanced tidal corrections introduced in the new FES2022 tidal solution. The new mapping system also allows for a general refinement of Level4 products. Minor degradations are observed in coastal areas and the equatorial band. The main contribution of the new mapping system is in regions with high oceanic variability, where mapping errors are reduced by up to 7%. The improvements in L4 geostrophic currents are mainly driven by the new mapping method but remain modest, with up to a 2% reduction in errors in high variability regions compared to previous products.

VI.2 NRT processing

VI.2.1 L3 1 Hz and L4 production

With DUACS-NRT 18.6.0, a new mission is introduced in the NRT system: HaiYang-2B. Those additional measurements contribute to an improvement of the quality of the product and the sea surface sampling over all regions. Additionally, pole tide and load tide corrections have been updated to use up-to-date versions recommended by OSTST experts. This also contributes to improve the quality of the different products.

With DUACS v18.7.1, the regional Europe product was improved with the use of a new MDT solution specifically over the Mediterranean and Black Sea.

With DUACS v19.0.0, the NRT system processing parameters are updated in order to take into account the improvement made for the MY products reprocessing (DUACS DT-2021). With this version, the quality of the products is improved as discussed in the previous chapters.

With DUACS v19.1.0, the reference mission is changed to use the new Sentinel-6A measurements instead of Jason-3A. The HR (SAR) mode measurements have been selected for Sentinel-6A in NRT conditions due to its lower noise level and thus higher ability to observe the small-scale signal. The ability of this measurement to ensure the accurate Mean Sea Level continuity, at global and regional scales, still needs to be qualified, based on analysis of a long time series of measurements.

With DUACS 19.2.0, Jason-3 on its interleaved orbit missions is used in the NRT production, bringing to seven the number of altimeter missions used.

When DUACS 19.3.0, HaiYang-2C is introduced in the NRT processing, it brings to eight the number of altimeter missions used.

With the DUACS-NG 2.0.0, the L3 1Hz quality is improved thanks to the use of the full-rate (20Hz) upstream products when available. This contributes to slightly reduce the noise error at short wavelengths. With the same version, the SWOT nadir measurements are used in the system, improving the spatial and temporal sampling of the sea surface.

With the DUACS-NG 3.0.0, the L3 1Hz quality is improved thanks to the use of up-to-date altimeter standards (ocean tide correction and Mean Sea Surface). This contributes to slightly reduce the errors, especially in coastal areas.

With the DUACS-NG v4.0.0, the L4 product quality is improved thanks to the use of a multi-scale mapping methodology (MIOST). The ADT and MDT variable included in L3 and L4 products is improved thanks to the use of the up-to-date CNES_CLS_2022 global MDT, combined with regional MDT CMEMS_2020 for Mediterranean and Black Sea, and for the Europe regional product, the use of the new CMEMS_2024 regional MDT.

VI.2.2 L3 5 Hz production

In November 2022, the L3 5 Hz production starts over the European area. Only four missions are processed with this resolution: Sentinel-3A/B, Sentinel-6A, Jason-3. The L3 5 Hz products allow to observe the mesoscale signal up to 40 km with Sentinel-6A (i.e., ~38% lower than wavelengths observables with the conventional LRM 1 Hz processing).

In November 2023, the L3 5 Hz production started over the global ocean. The mean observing capability over the global ocean is nearly the same as that reported for Europe. Nevertheless, it presents regional variations. The SWOT-nadir measurements were also included in the processing, improving the spatial and temporal sampling of the sea surface.

In July 2024, the quality of the product is improved with the use of a new ocean tide model (FES2022b) and a new MSS (hybrid 2023). The improvement is higher in the coastal band. The full posting-rate measurements for the H2B mission are also used to start the production of the L3 5Hz and improve the data availability near the coast.

In November 2024, L3 product is improved thanks to the use of the up-to-date MDTs:

- For global products: a hybrid_2022 global MDT is used. It combines the global ocean CNES_CLS_2022 MDT and the regional CMEMS_2020 for Mediterranean and Black Sea MDTs.
- For Europe regional products: the CMEMS_2024 regional MDT is used.

VII REFERENCES

Ablain, M.: Validation Report: WP2500 Regional SSH Bias Corrections between Altimetry Missions, 2013.

Ablain, M. and Legeais, J. F.: SLOOP Tache 2.4 : Amélioration du filtrage de la correction ionospherique bifréquence, 2010.

Ablain, M., Larnicol, G., Faugere, Y., Cazenave, A., Meyssignac, B., Picot, N., and Benveniste, J.: Error Characterization of Altimetry Measurements at Climate Scales, in: Proceedings of the "20 Years of Progress in Radar Altimetry" Symposium, Venice, Italy, 24-29 September 2012, Benveniste, J. and Morrow, R., Eds., ESA Special Publication SP-710, https://doi.org/10.5270/esa.sp-710.altimetry2012, 2012.

Ablain, M., Meyssignac, B., Zawadzki, L., Jugier, R., Ribes, A., Spada, G., Benveniste, J., Cazenave, A., and Picot, N.: Uncertainty in satellite estimates of global mean sea-level changes, trend and acceleration, Earth Syst. Sci. Data, 11, 1189–1202, https://doi.org/10.5194/essd-11-1189-2019, 2019.

Amarouche, L., Thibaut, P., Zanife, O. Z., Dumont, J.-P., Vincent, P., and Steunou, N.: Improving the Jason-1 Ground Retracking to Better Account for Attitude Effects, Mar. Geod., 27, 171–197, https://doi.org/10.1080/01490410490465210, 2004.

Arbic, B. K., Scott, R. B., Chelton, D. B., Richman, J. G., and Shriver, J. F.: Effects of stencil width on surface ocean geostrophic velocity and vorticity estimation from gridded satellite altimeter data: OCEAN GEOSTROPHIC VELOCITY ESTIMATION, J. Geophys. Res. Oceans, 117, n/a-n/a, https://doi.org/10.1029/2011JC007367, 2012.

Arhan, M. and De Verdiére, A. C.: Dynamics of Eddy Motions in the Eastern North Atlantic, J. Phys. Oceanogr., 15, 153–170, https://doi.org/10.1175/1520-0485(1985)015<0153:DOEMIT>2.0.CO;2, 1985.

Aviso+: Along-track Level-2+ (L2P) Product Handbook for missions Jason-3, OSTM/Jason-2, Jason-1, SARAL/AltiKa, Crysoat-2, HaiYang-2A, ERS-1, ERS-2, ENVISAT, Geosat Follow On, TOPEX/Poseidon, 2020.

Aviso+: Along-track Level-2+ (L2P) Sentinel-3A, Sentinel-3B and Sentinel-6A Product Handbook, 2022.

Ballarotta, M., Ubelmann, C., Pujol, M.-I., Taburet, G., Fournier, F., Legeais, J.-F., Faugère, Y., Delepoulle, A., Chelton, D., Dibarboure, G., and Picot, N.: On the resolutions of ocean altimetry maps, Ocean Sci., 15, 1091–1109, https://doi.org/10.5194/os-15-1091-2019, 2019.

Ballarotta, M., Ubelmann, C., Veillard, P., Prandi, P., Etienne, H., Mulet, S., Faugère, Y., Dibarboure, G., Morrow, R., and Picot, N.: Improved global sea surface height and current maps from remote sensing and in situ observations, Earth Syst. Sci. Data, 15, 295–315, https://doi.org/10.5194/essd-15-295-2023, 2023.

Bignalet-Cazalet, F., Picot, N., Desai, S., Scharroo, R., and EGIDO, A.: Jason-3 Products Handbook. https://www.aviso.altimetry.fr/fileadmin/documents/data/tools/hdbk_j3.pdf, 2021.

Carrère, L. and Lyard, F.: Modeling the barotropic response of the global ocean to atmospheric wind and pressure forcing - comparisons with observations, Geophys. Res. Lett., 30, https://doi.org/10.1029/2002GL016473, 2003.

Carrere, L., Lyard, F., Cancet, M., Guillot, A., Dupuy, S., and Picot, N.: FES 2014 : a new global tidal model. OSTST 2015. https://ostst.aviso.altimetry.fr/fileadmin/user_upload/tx_ausyclsseminar/files/OSTST2015/TIDE-01-Carrere.pdf, 2015.

Carrere, L., Lyard, F., Allain, D., Cancet, M., Picot, N., Guillot, A., Faugère, Y., Dupuy, S., and Baghi, R.: Final version of the FES2014 global ocean tidal model, which includes a new loading tide solution, OSTST, La Rochelle, France, https://ostst.aviso.altimetry.fr/fileadmin/user_upload/tx_ausyclsseminar/files/Poster_FES2014b_OSTST_2016.pdf, 2016.

Carrere, L., Lyard, F., Cancet, M., Allain, D., Dabat, M.-L., Fouchet, E., Sahuc, E., Faugere, Y., Dibarboure, G., and Picot, N.: A new barotropic model for global ocean : FES2022. OSTST, https://ostst.aviso.altimetry.fr/programs/abstracts-details.html?tx_ausyclsseminar_pi2%5bobjAbstracte%5d=3287&cHash=X, 2023.

Cartwright, D. E. and Edden, A. C.: Corrected Tables of Tidal Harmonics, Geophys. J. Int., 33, 253–264, https://doi.org/10.1111/j.1365-246X.1973.tb03420.x, 1973.

Cartwright, D. E. and Tayler, R. J.: New Computations of the Tide-generating Potential, Geophys. J. Int., 23, 45–73, https://doi.org/10.1111/j.1365-246X.1971.tb01803.x, 1971.

Chelton, D. B., Schlax, M. G., and Samelson, R. M.: Global observations of nonlinear mesoscale eddies, Prog. Oceanogr., 91, 167–216, https://doi.org/10.1016/j.pocean.2011.01.002, 2011.

Chelton, D. B., Dibarboure, G., Pujol, M.-I., Taburet, G., and Schlax, M. G.: The Spatial Resolution of AVISO Gridded Sea Surface Height Fields, 2014.

Chou, M.-Y., Yue, J., Wang, J., Huba, J. D., El Alaoui, M., Kuznetsova, M. M., Rastätter, L., Shim, J. S., Fang, T.-W., Meng, X., Fuller-Rowell, D., and Retterer, J. M.: Validation of Ionospheric Modeled TEC in the Equatorial Ionosphere During the 2013 March and 2021 November Geomagnetic Storms, Space Weather, 21, e2023SW003480, https://doi.org/10.1029/2023SW003480, 2023.

Colling, A.: Ocean circulation, 2nd ed., Butterworth Heinemann, in association with the Open University, Boston, 2001.

Couhert, A., Cerri, L., Legeais, J.-F., Ablain, M., Zelensky, N. P., Haines, B. J., Lemoine, F. G., Bertiger, W. I., Desai, S. D., and Otten, M.: Towards the 1mm/y stability of the radial orbit error at regional scales, Adv. Space Res., 55, 2–23, https://doi.org/10.1016/j.asr.2014.06.041, 2015.

Desai, S., Wahr, J., and Beckley, B.: Revisiting the pole tide for and from satellite altimetry, J. Geod., 89, 1233–1243, https://doi.org/10.1007/s00190-015-0848-7, 2015.

Dibarboure, G., Pujol, M.-I., Briol, F., Traon, P. Y. L., Larnicol, G., Picot, N., Mertz, F., and Ablain, M.: Jason-2 in DUACS: Updated System Description, First Tandem Results and Impact on Processing and Products, Mar. Geod., 34, 214–241, https://doi.org/10.1080/01490419.2011.584826, 2011.

Dibarboure, G., Boy, F., Desjonqueres, J. D., Labroue, S., Lasne, Y., Picot, N., Poisson, J. C., and Thibaut, P.: Investigating Short-Wavelength Correlated Errors on Low-Resolution Mode Altimetry, J. Atmospheric Ocean. Technol., 31, 1337–1362, https://doi.org/10.1175/JTECH-D-13-00081.1, 2014.

Ducet, N., Le Traon, P. Y., and Reverdin, G.: Global high-resolution mapping of ocean circulation from TOPEX/Poseidon and ERS-1 and -2, J. Geophys. Res. Oceans, 105, 19477–19498, https://doi.org/10.1029/2000JC900063, 2000.

Dufau, C., Orsztynowicz, M., Dibarboure, G., Morrow, R., and Le Traon, P.: Mesoscale resolution capability of altimetry: Present and future, J. Geophys. Res. Oceans, 121, 4910–4927, https://doi.org/10.1002/2015JC010904, 2016.

Fernandes, M. J. and Lázaro, C.: GPD+ Wet Tropospheric Corrections for CryoSat-2 and GFO Altimetry Missions, Remote Sens., 8, 851, https://doi.org/10.3390/rs8100851, 2016.

Fernandes, M. J., Lázaro, C., Ablain, M., and Pires, N.: Improved wet path delays for all ESA and reference altimetric missions, Remote Sens. Environ., 169, 50–74, https://doi.org/10.1016/j.rse.2015.07.023, 2015.

Gaspar, P. and Ogor, F.: Estimation and analysis of the sea state bias of the ERS-1 altimeter, technical report of IFREMER contract 94/2.426016/C, 1994.

Guérou, A., Meyssignac, B., Prandi, P., Ablain, M., Ribes, A., and Bignalet-Cazalet, F.: Current observed global mean sea level rise and acceleration estimated from satellite altimetry and the associated uncertainty, EGUsphere, 1–43, https://doi.org/10.5194/egusphere-2022-330, 2022.

Guibbaud, M., Ollivier, A., and Ablain, M.: A new approach for dual-frequency ionospheric correction filtering, ENVISAT Altimetry Quality Working Group (QWG); Envisat annual activity report 2012, Chap 8.5, 2015.

Held, I. M., Pierrehumbert, R. T., Garner, S. T., and Swanson, K. L.: Surface quasi-geostrophic dynamics, J. Fluid Mech., 282, 1–20, https://doi.org/10.1017/S0022112095000012, 1995.

Iijima, B. A., Harris, I. L., Ho, C. M., Lindqwister, U. J., Mannucci, A. J., Pi, X., Reyes, M. J., Sparks, L. C., and Wilson, B. D.: Automated daily process for global ionospheric total electron content maps and satellite ocean altimeter ionospheric calibration based on Global Positioning System data, J. Atmospheric Sol.-Terr. Phys., 61, 1205–1218, https://doi.org/10.1016/S1364-6826(99)00067-X, 1999.

Jousset, S. and Mulet, S.: New Mean Dynamic Topography of the Black Sea and Mediterranean Sea from altimetry, gravity and in-situ data, 2020.

Jousset, S., Aydogdu, A., Ciliberti, S., Clementi, E., Escudier, R., Jansen, E., Lima, L., Menna, M., Mulet, S., Nigam, T., Sanchez-Roman, A., Tarry, D. R., Pascual, A., Peneva, E., Poulain, P.-M., and Taupier-Letage, I.: New Mean Dynamic Topography of the Mediterranean Sea from altimetry, gravity and in-situ data, Prep, 2022.

Jousset, S., Mulet, S., Greiner, E., Wilkin, J., Vidar, L., Dibarboure, G., and Picot, N.: New Global Mean Dynamic Topography CNES-CLS-22 Combining Drifters, Hydrological Profiles and High Frequency Radar Data, ESS Open Arch., 2023.

Kocha, C., Lievin, M., Pageot, Y., Rubin, C., Philipps, S., Dibarboure, G., Denis, I., Guinle, T., and Nogueira Loddo, C.: 30 years od sea level anomaly reprocessed to improve climate and mesoscale satellite data record. OSTST meeting., , https://doi.org/10.24400/527896/a03-2023.3804, 2023.

Lagerloef, G. S. E., Mitchum, G. T., Lukas, R. B., and Niiler, P. P.: Tropical Pacific near-surface currents estimated from altimeter, wind, and drifter data, J. Geophys. Res. Oceans, 104, 23313–23326, https://doi.org/10.1029/1999JC900197, 1999.

Laloue, A., Veillard, P., Schaeffer, P., Pujol, M.-I., Andersen, O., Sandwell, D., Delepoulle, A., Dibarboure, G., and Faugere, Y.: Merging recent Mean Sea Surface into a 2023 Hybrid model (from Scripps, DTU, CLS and CNES), 2024a.

Laloue, A., Schaeffer, P., Pujol, M.-I., Veillard, P., Andersen, O. B., Sandwell, D. T., Delepoulle, A., Dibarboure, G., and Faugère, Y.: Merging recent Mean Sea Surface into a 2023 Hybrid model (from Scripps, DTU, CLS and CNES), https://doi.org/10.22541/au.171987154.42384510/v1, 1 July 2024b.

Le Traon, P. Y., Nadal, F., and Ducet, N.: An Improved Mapping Method of Multisatellite Altimeter Data, J. Atmospheric Ocean. Technol., 15, 522–534, https://doi.org/10.1175/1520-0426(1998)015<0522:AIMMOM>2.0.CO;2, 1998a.

Le Traon, P. Y., Nadal, F., and Ducet, N.: An Improved Mapping Method of Multisatellite Altimeter Data, J. Atmospheric Ocean. Technol., 15, 522–534, https://doi.org/10.1175/1520-0426(1998)015<0522:AIMMOM>2.0.CO;2, 1998b.

Le Traon, P.-Y. and Ogor, F.: ERS-1/2 orbit improvement using TOPEX/POSEIDON: The 2 cm challenge, J. Geophys. Res. Oceans, 103, 8045–8057, https://doi.org/10.1029/97JC01917, 1998.

Legeais, J.-F., Ablain, M., and Thao, S.: Evaluation of wet troposphere path delays from atmospheric reanalyses and radiometers and their impact on the altimeter sea level, Ocean Sci., 10, 893–905, https://doi.org/10.5194/os-10-893-2014, 2014.

Lievin, M., Kocha, C., Courcol, B., Philipss, S., Denis, I., Guinle, T., Nogueira Loddo, C., Dibarboure, G., Picot, N., and Bignalet-Cazalet, F.: Reprocessing of Sea Level L2P products for 28 years of altimetry missions.
https://ostst.aviso.altimetry.fr/fileadmin/user_upload/tx_ausyclsseminar/files/OSTST2020_Reprocessing_L2P_2020.pdf, 2020.

Loren Carrère, Florend Lyard, Cancet, M., Allain, D. J., Fauchet, E., Dabat, M.-L., Tchilibou, M., Ferrari, R., and Faugère, Y.: The new FES2022 Tidal atlas. Presented at the 2023 SWOT Science Team meeting (Toulouse). Available online (last access: 19 April 2024): https://doi.org/10.24400/527896/a03-2022.3287, 2023.

Mertz, F., Mercier, F., Labroue, S., Tran, N., and Dorandeu, J.: ERS-2 OPR data quality assessment ; Long-term monitoring - particular investigation, 2005.

Moreau, T., Cadier, E., Boy, F., Aublanc, J., Rieu, P., Raynal, M., Labroue, S., Thibaut, P., Dibarboure, G., Picot, N., Phalippou, L., Demeestere, F., Borde, F., and Mavrocordatos, C.: High-performance altimeter Doppler processing for measuring sea level height under varying sea state conditions, Adv. Space Res., 67, 1870–1886, https://doi.org/10.1016/j.asr.2020.12.038, 2021.

Mulet, S., Rio, M.-H., Etienne, H., Artana, C., Cancet, M., Dibarboure, G., Feng, H., Husson, R., Picot, N., Provost, C., and Strub, P. T.: The new CNES-CLS18 global mean dynamic topography, Ocean Sci., 17, 789–808, https://doi.org/10.5194/os-17-789-2021, 2021.

Nencioli, F., Roinard, H., Bignalet-Cazalet, F., Dibarboure, G., and Picot, N.: Advantages and drawbacks of the filtered solution for dual-frequency ionospheric correction from altimetry. OSTST meeting., , https://doi.org/10.24400/527896/a03-2022.3439, 2022.

Pascual, A., Faugère, Y., Larnicol, G., and Le Traon, P.-Y.: Improved description of the ocean mesoscale variability by combining four satellite altimeters, Geophys. Res. Lett., 33, L02611, https://doi.org/10.1029/2005GL024633, 2006.

Pascual, A., Boone, C., Larnicol, G., and Traon, P.-Y. L.: On the Quality of Real-Time Altimeter Gridded Fields: Comparison with In Situ Data, J. Atmospheric Ocean. Technol., 26, 556–569, https://doi.org/10.1175/2008JTECHO556.1, 2009.

Prandi, P., Meyssignac, B., Ablain, M., Spada, G., Ribes, A., and Benveniste, J.: Local sea level trends, accelerations and uncertainties over 1993–2019, Sci. Data, 8, 1, https://doi.org/10.1038/s41597-020-00786-7, 2021.

Pujol, M., Schaeffer, P., Faugère, Y., Raynal, M., Dibarboure, G., and Picot, N.: Gauging the Improvement of Recent Mean Sea Surface Models: A New Approach for Identifying and Quantifying Their Errors, J. Geophys. Res. Oceans, 123, 5889–5911, https://doi.org/10.1029/2017JC013503, 2018.

Pujol, M.-I., Faugère, Y., Taburet, G., Dupuy, S., Pelloquin, C., Ablain, M., and Picot, N.: DUACS DT2014: the new multi-mission altimeter data set reprocessed over 20years, Ocean Sci., 12, 1067–1090, https://doi.org/10.5194/os-12-1067-2016, 2016.

Pujol, M.-I., Dupuy, S., Vergara, O., Sánchez Román, A., Faugère, Y., Prandi, P., Dabat, M.-L., Dagneaux, Q., Lievin, M., Cadier, E., Dibarboure, G., and Picot, N.: Refining the Resolution of DUACS Along-Track Level-3 Sea Level Altimetry Products, Remote Sens., 15, 793, https://doi.org/10.3390/rs15030793, 2023.

Putnam, A., Desai, S. D., and Nerem, R. S.: Estimation of the sea state bias error budget for pulse-limited satellite altimetry, Mar. Geod., 46, 460–478, https://doi.org/10.1080/01490419.2023.2224513, 2023.

Ries, J. C. and Desai, S.: Conventional model update for rotational deformation, 2017.

Scharroo, R. and Smith, W. H. F.: A global positioning system–based climatology for the total electron content in the ionosphere, J. Geophys. Res. Space Phys., 115, https://doi.org/10.1029/2009JA014719, 2010.

Scharroo, R., Lillibridge, J., Abdalla, S., and Vandemark, D.: Early look at SARAL/AltiKa data, 2013.

Taburet, G., Sanchez-Roman, A., Ballarotta, M., Pujol, M.-I., Legeais, J.-F., Fournier, F., Faugere, Y., and Dibarboure, G.: DUACS DT2018: 25 years of reprocessed sea level altimetry products, Ocean Sci., 15, 1207–1224, https://doi.org/10.5194/os-15-1207-2019, 2019.

Tran, N.: Rapport Annuel d'activité SALP - Activité SSB, 2011.

Tran, N.: Rapport Annuel d'activité SALP - Activité SSB, 2015.

Tran, N.: Envisat ESL Phase-F: Tuning activities for Envisat reprocessing baseline v3.0 (Wind, SSB, Rain and Ice), 2017.

Tran, N.: ESL Cryosat-2: Tuning activities: wind speed and SSB, 2018.

Tran, N.: Rapport Annuel d'activité SALP - Activité SSB, 2019.

Tran, N.: S3A SSB Solutions. Presented at ESL CM#8 MPC-S3; 2021, 2021.

Tran, N., Labroue, S., Philipps, S., Bronner, E., and Picot, N.: Overview and Update of the Sea State Bias Corrections for the Jason-2, Jason-1 and TOPEX Missions, Mar. Geod., 33, 348–362, https://doi.org/10.1080/01490419.2010.487788, 2010.

Tran, N., Philipps, S., Poisson, J.-C., Urien, S., Bronner, E., and Picot, N.: Impact of GDR_D standards on SSB corrections, OSTST, Venice, Italie, http://www.aviso.altimetry.fr/fileadmin/documents/OSTST/2012/oral/02_friday_28/01_instr_processing_I/01_IP1_Tran.pdf, 2012.

Tran, N., Vandemark, D., Zaron, E. D., Thibaut, P., Dibarboure, G., and Picot, N.: Assessing the effects of sea-state related errors on the precision of high-rate Jason-3 altimeter sea level data, Adv. Space Res., 68, 963–977, https://doi.org/10.1016/j.asr.2019.11.034, 2021.

Traon, P. Y. L. and Dibarboure, G.: Mesoscale Mapping Capabilities of Multiple-Satellite Altimeter Missions, J. Atmospheric Ocean. Technol., 16, 1208–1223, https://doi.org/10.1175/1520-0426(1999)016<1208:MMCOMS>2.0.CO;2, 1999.

Ubelmann, C., Dibarboure, G., Gaultier, L., Ponte, A., Ardhuin, F., Ballarotta, M., and Faugère, Y.: Reconstructing Ocean Surface Current Combining Altimetry and Future Spaceborne Doppler Data, J. Geophys. Res. Oceans, 126, e2020JC016560, https://doi.org/10.1029/2020JC016560, 2021a.

Ubelmann, C., Dibarboure, G., Gaultier, L., Ponte, A., Ardhuin, F., Ballarotta, M., and Faugère, Y.: Reconstructing Ocean Surface Current Combining Altimetry and Future Spaceborne Doppler Data, J. Geophys. Res. Oceans, 126, e2020JC016560, https://doi.org/10.1029/2020JC016560, 2021b.

Ubelmann, C., Carrere, L., Durand, C., Dibarboure, G., Faugère, Y., Ballarotta, M., Briol, F., and Lyard, F.: Simultaneous estimation of ocean mesoscale and coherent internal tide sea surface height signatures from the global altimetry record, Ocean Sci., 18, 469–481, https://doi.org/10.5194/os-18-469-2022, 2022.

Vergara, O., Morrow, R., Pujol, I., Dibarboure, G., and Ubelmann, C.: Revised Global Wave Number Spectra From Recent Altimeter Observations, J. Geophys. Res. Oceans, 124, 3523–3537, https://doi.org/10.1029/2018JC014844, 2019.

Vergara, O., Morrow, R., Pujol, M.-I., Dibarboure, G., and Ubelmann, C.: Global submesoscale Transition Scale estimation using alongtrack satellite altimetry, Prep, 2022.

Wahr, J. M.: Deformation induced by polar motion, J. Geophys. Res. Solid Earth, 90, 9363–9368, https://doi.org/10.1029/JB090iB11p09363, 1985.

Zaron, E. D.: Baroclinic Tidal Sea Level from Exact-Repeat Mission Altimetry, J. Phys. Oceanogr., 49, 193–210, https://doi.org/10.1175/JPO-D-18-0127.1, 2019.

Zawadzki, L. and Ablain, M.: Accuracy of the mean sea level continuous record with future altimetric missions: Jason-3 vs. Sentinel-3a, Ocean Sci., 12, 9–18, https://doi.org/10.5194/os-12-9-2016, 2016.